On the Study of Analogues in Cosmic Magnetism

Thesis presented in fulfillment of the requirements for the degree of Doctor of Philosophy in Applied Mathematics

Patrick William Adams
B.Sc. (IT), M.Sc.

October 2017

Supervisor:
Dr B. Osano

University of Cape Town
Faculty of Science
Department of Mathematics and Applied Mathematics

The financial assistance of the National Research Foundation (NRF) and the University of Cape Town towards this research are hereby acknowledged. Opinions expressed and conclusions arrived at, are those of the author and are not necessarily to be attributed to the NRF nor the University of Cape Town.

Abstract

The dynamo process, by which the strength of the magnetic field is amplified, is still not well-understood and, in part, requires an understanding of the behaviour of the plasma fluid (i.e. a charged fluid) in different conditions. It has long been known that charged and non-charged fluids display similar behaviour to each other, with key quantities such as the magnetic field, $\mathbf{B}$, and fluid vorticity, $\boldsymbol{\omega}$, being both structurally-similar and playing similar roles to each other in their respective evolution equations.

This thesis addresses the long-standing problem of Analogue Magnetism by using numerical magnetohydrodynamical simulations to study the behaviour of charged and non-charged fluids in the presence of non-negligible magnetic diffusion and kinematic viscosity by comparing the behaviour of the root-mean squares magnetic field, B_{rms}, from a charged fluid, to that of the rms vorticity, ω_{rms} , from a non-charged fluid. Simulations are done together with and without the presence of source terms in their respective evolution equations. Similar behaviour between the two fluids is confirmed for the case of equal values of dissipation, both with and without the presence of source terms in the evolution equations, thus indicative of an analogy. The condition on similar behaviour between B_{rms} and ω_{rms} requires that there be strong dissipation when source terms are present in the equations. Evidence of a battery-aided dynamo in the temporal evolution of B_{rms} is also observed in the presence of source terms. Fine-tuning of the values of the magnetic diffusivity and kinematic viscosity of the non-charged fluid to establish an empirical range over which non-charged fluids may be used to study the behaviour of charged fluids is also considered.

The second- and third-order terms in the Taylor expansion of the mean electromotive force are also studied in Mean Field Magnetohydrodynamics, and integral forms for the tensors corresponding these higher-order terms are derived and expressed. The mean-field Induction equations incorporating these new tensors are also derived, with the effects of these new tensors on the evolution of the mean- and fluctuating magnetic fields being considered briefly. We end off with a brief discussion regarding the possible application of Analogue Magnetism to better study

the Reynolds stress tensor, which is known to be the fluid analogue of the mean electromotive force in Magnetohydrodynamics .

DECLARATION

I know the meaning of plagiarism and declare that all of the work in the dissertation, save for that which is properly acknowledged, is my own.

PATRICK WILLIAM ADAMS

In loving memory of:

Miss Magdalene Mathilda Rachael Adams, Mrs Maria Anna Adams, Mr Ohlson October, Miss Bianca Vaneli Kleinsmith and Ms Olivia Barron

The great labour is done.

★

Foreword

At last, I am come to the end of the Great Labour. As I write this, things seem slightly surreal, but I am content. Here, I must give my thanks to the many people who have undertaken this journey with me by giving to me their unconditional love, guidance and support.

To my parents, Sybil and Patrick Adams, I give my thanks for putting up with my highs and lows during this final phase of my studies. To my mother, thank-you for helping me around the house with food and maintenance, and for sitting behind me with your Bible late at nights as I typed away at this work. To my father, thank-you for pulling in my car at nights when I was often passed-out on my bed, fast asleep. To the rest of my family, I also give my thanks for the support, thoughts and prayers – Mum, and Aunties Cynthia and Kathleen in particular!

To my friends (in no particular order), Miss Maryanne Kamunya, Miss Mpheng Magome, Miss Nikki Peceur, and Mr Theo Naicker: thank-you for your unconditional support and conversations, and also putting up with listening to me talk for hours about my studies. It is most truly appreciated! To the remainder of my friends and acquaintances, I also give my thanks for the helpful conversations, votes of support and words of wisdom that often came at a time when I'd needed them most.

My thanks also goes to Dr Andrew Young of the UCT Student Wellness Service for his guidance and mentoring during the last phases of my studies. It has gone a long way and is much appreciated.

To my classical voice teacher, Prof. Sidwill Hartman, I also give my unreserved thanks for his understanding, advice, and patience with me often making many mistakes during our lessons. It has not gone unnoticed, and I am eternally grateful for it. Now, I can continue working towards my goal of being a performer! To my vocal coaches, Mr Victor Trichardt and Mr Danie Theron, I also give my unreserved thanks for the advice, patience and occasional chastising when I make the same mistakes over and over and over again. :-)

Last, but most certainly not least, I wish to thank my Ph.D. supervisor, Dr Bob Osano for his patience, mentoring, guidance and open door whenever I needed to discuss anything with him. I

am truly grateful for all you've done for me and will treasure it forever.

And now, on to the business of this work. . .

It's always about timing. If it's too soon, no one understands. If it's too late, everyone's forgotten.

— Anna Wintour (1949 –)

★

Contents

Chapter 1

Introduction

Magnetic fields exist everywhere in the universe. In our day-to-day lives, they have found applications in fields such as medicine, building construction and computing. Scientifically, our first interactions with magnetic fields occur in Geomagnetism and Heliomagnetism: the studies of the Earth's and Sun's own magnetic fields respectively.

We find that the Earth's magnetic field is critical in protecting the planet from hazardous high-energy radiation that is emitted by the sun and incoming in the form of cosmic rays from deep space. In addition to this, the Earth's magnetic field is also responsible for the maintenance and continued presence of the atmosphere, without which, life as we know it would not be able to exist. In the context of Heliomagnetism, it is known that the Sun's own magnetic field is responsible for the various prominences and plasma loops that are observed on the its surface, as well as for the presence of sun spots and their associated 11-year cycle.

Outside of our solar system, magnetic fields are also studied in large astrophysical objects such as galaxies, particularly those that possess active nuclei where jets of radiation emanating from the galactic cores can be observed. On the cosmological scale, magnetic fields are also studied in clusters and super-clusters of galaxies. It is thought that the understanding of the behaviour of magnetic fields in these types of contexts is critical in understanding the formation and long-term evolution of these objects.

The origin of magnetic fields in the universe is not well understood, and it is not certain whether

the universe originally came into being in a magnetized state [24]. Many theories regarding the origin of magnetic fields have been put forward. One such theory describes the formation of seed magnetic fields due ionization currents, with a temperature gradient not normal to the current itself, sweeping across areas in the universe with arbitrary density fluctuations [105,106,108]. This results in the generation of a time-varying thermal electric field that possesses a non-vanishing curl, thus leading to a weak thermal seed magnetic field from a zero initial magnetic field. Another well-known theory is that of the thermal or Biermann battery, which is a cosmic battery and is the simplest battery to be proposed [12]. A different type of battery, arising from a component of the mean electromotive force (EMF) in mean-field Magnetohydrodynamics (MHD) is also briefly discussed in [74] and is thought to be able to seed a small-scale, fluctuating magnetic field if there is no initial small-scale field present in the system. Other battery mechanisms have also been discussed in [24, 26, 66, 105, 108, 113] and others, but all of these batteries, including the Biermann battery, lead to magnetic fields whose strengths are significantly weaker than those that are observed today.

The study of the amplification of magnetic fields is known as *dynamo theory*, and the mechanism that amplifies the magnetic field's strength is called a dynamo. One of the reasons concerning the theory's shortfall when it comes to predicting the strength of magnetic field observed today is due to the fact that the processes involved in the amplification of the magnetic field's strength are not well-understood. In the case of the Earth's magnetic field, the geophysical dynamo arises as a consequence of the Earth's rotation, causing the magnetized liquid within the mantle to move, causing the seed magnetic field present within the planet's core to be amplified [67]. In the case of the sun, the dynamo is thought to originate from deep within the convection zone and, as a consequence, is responsible for the 11-year sunspot cycle and all of its associated phenomena [24].

Many theoretical dynamos have been proposed thus far, but the most well-known of these is called the Vainshtein-Zel'dovich Stretch-Twist-Fold (STF) dynamo, and was proposed by Vainshtein and Zel'dovich in 1972 [112]. This simple model outlines the amplification of the magnetic field by describing how a ring of magnetic flux present within the plasma is first stretched, twisted around into a figure-of-eight and then finally folded. The end result is that after the STF process is complete, the magnetic field strength would be increased by a factor of 2^n, for the process being done n times.

Before the proposal of the STF dynamo, earlier dynamo models based on phenomenological observations were proposed by authors such as Parker [69], Babcock [6], and Leighton [58], while the first formal mathematical description of a dynamo was made by Herzenberg [39] which also complemented the existing phenomenological dynamo models of the time [24].

In order to better understand the dynamo process, there is a need to understand the behaviour of the plasma fluid in which the magnetic field itself is present. This conducting fluid has long been thought to behave in a manner that is analogous to a non-conducting fluid. In an attempt to better understand the behaviour of the conducting fluid, based on what was understood of the behaviours of non-charged fluids at the time, the field of *analogue magnetism* was established. Analogue magnetism is one of the prime focusses of this work, and we use it to study the behaviour of a conducting fluid, compared to that of a non-conducting fluid, in different contexts. A brief history of analogue magnetism now follows.

1.1 Literature Review: Analogue Magnetism

Analogies are able to provide an often unconventional but effective way of studying various physical phenomena that are observed around us. Using knowledge from an existing field, analogies allow us to relate key quantities and governing equations from one field or physical setup to another and, by doing so, explain any phenomena observed in the other field or physical setup through what is known from the original case. One such example is the analogy that exists between the behaviour observed in the LRC circuit and the behaviour observed in the damped, driven pendulum, which is its analogous system. In this case, the pendulum's angular displacement and the electrical charge on the capacitor, moving about the circuit, are analogous to each other; the pendulum's angular velocity and the electrical current moving through the circuit are also analogues of each other.

Since the discovery of magnetism, analogues have been sought between Electromagnetism and Fluid Dynamics in order to more easily explain different phenomena, such as magnetic and electrical forces observed during experiments, in terms of the theories and models that existed at the time. In the following, we present a brief history of the origins of the problem of Analogue Magnetism, and discuss some work done in more recent years.

The discovery of the magnetic effects of electrical currents by Ørsted in 1820 gave rise to two distinct schools of thought regarding the origins of these effects, as well as the unification of electricity and magnetism. These schools chose to focus on either: a) the magnetic effects of a moving current were due to some sort of "action at a distance", mediated essentially though the assumed existence of some type of "æther", or, b) the magnetic effects of a moving current were due to forces originating from within the spaces between current-carrying wires and magnets. The work of Ampère gave rise to the former school of thought, while the work of Faraday gave rise to the latter school of thought [93].

One of the important claims made by Ampère was the existence of an imaginary "electrical fluid" that circulated about molecules (producing some type of "molecular current"), in which the circular forces proposed by Ørsted existed. Faraday himself could not accept this proposal, as there was no satisfactory way of explaining how such a fluid could exist in the first place, nor how the proposed circular forces could exist within the fluid itself. According to Faraday, the spaces observed between the circular field lines produced by current-carrying wires would provide a better explanation in unifying electricity and magnetism [93].

In their 1861 work, Maxwell studied Ampère's "electrical fluid" and "molecular vortices" alongside Faraday's interpretation Ørsted's results in great detail by trying to explain the proposed phenomena though an analogy between normal fluids studied in hydrodynamics and the magnetic field lines. Through this work, Maxwell suggested that the magnetic vector potential, $\mathbf{A}$, characteristically mimicked the fluid velocity field, $\mathbf{u}$, that engulfed some magnetic field within it [65, 93].

Maxwell's original idea has since formed the basis of many a foray into the field of Analogue Magnetism, where phenomena observed in magnetic fluids such as plasmas, were attempted to be explained through current knowledge of the physics and phenomena observed in Fluid Dynamics. Some examples of this include work the analogy between Aharonov-Bohm effect [3] and Fizeau's Experiment (1851), where the fluid velocity and vorticity fields mimic the magnetic vector potential and magnetic flux density fields [27], the establishment of a successful analogy between turbulent hydrodynamics and electromagnetism, which was used to describe the dynamical behaviour of averaged flow quantities of an incompressible fluid at high fluid Reynolds numbers [62], as well as a methodological approach focussing on finding analogies between physical magnitudes and establishing isomorphisms between systems of equations, specifically geared to

Fluid dynamics	Electromagnetism
Fluid Velocity, $\mathbf{u}$	Magnetic Vector Potential, $\mathbf{A}$
Fluid Vorticity, $\boldsymbol{\omega}$	Magnetic Flux Density, $\mathbf{B}$
Fluid Acceleration	Electric Field Intensity, $\mathbf{E}$
Fluid Mass	Electric Charge
Fluid Density	Charge Density

Table 1.1: Matching of key quantities in Fluid Dynamics to their corresponding quantities in Electromagnetism. A more comprehensive listing may be found in [64].

find an analogy between the equations Fluid Dynamics and Electromagnetism, termed "fluidic electrodynamics" [64]. Siegel also further explores Maxwell's original ideas of the analogy in their work, *Innovation in Maxwells electromagnetic theory: Molecular vortices, displacement current, and light* (2002) [93].

Unfortunately, more work needs to be done through experimentation and modelling in order to properly grasp the consequences of Maxwell's original idea, thus properly establishing a robust theory of Analogue Magnetism. As of now, many of the results still remain to be seen as a convenient or even coincidental theoretical analogy between the governing equations of Fluid Dynamics and Electromagnetism. Based on work done until today, we know that the matching between some of the key quantities of Fluid Dynamics and Electromagnetism listed in table 1.1 holds. A more comprehensive listing may be found in [64].

Other important work in Analogue Magnetism has involved the analysis of physical behaviours of forces and other quantities in Fluid Dynamics and Electrodynamics in order to advance the possibility of a robust theory. The author of [63] investigated the known inertial forces of Fluid Dynamics and Electromagnetism. In particular, the inertial properties of matter in Electromagnetism were investigated in conjunction with hydrodynamic drag in potential flows, and a parallel between the two was found.

The author of [5] derives hydrodynamical equations from Maxwell's equations and, through relating what they term a "hydro-electric field" to the local acceleration of a fluid, and the Lorentz gauge to the incompressible fluid condition, proposes analogous Lorentz gauge in hydrodynam-

ics. In addition to this, a parallel between the Lorentz Force in electrodynamics and the Euler Force in fluid dynamics is also proposed.

In [61], the author proposes an analogy between the inhomogeneous Maxwell equations and two equations found in turbulent hydrodynamics. A mechanical analogue to the Poynting vector of Electromagnetism is then proposed, while a claim that Electromagnetism may be interpreted as a turbulent flow field is also made.

While running magnetogenesis simulations of cosmic magnetic fields using a Biermann Battery term, the authors of [56] discuss the analogy between the magnetic flux density and vorticity fields, noting that their root mean square (rms) strengths appear to saturate around the same time, as well as with the same strength in the case for a turbulent dynamo acting on the magnetic field.

As an application of cosmic magnetism to the amplification of primordial magnetic fields, the authors of [18] show how magnetic structures can form at large scales. Considering a three-dimensional model, it is found that primordial magnetic fields at large scales are much stronger than expected if the effects of MHD turbulence and the inverse-cascade effect are taken into account.

Together with understanding the behaviour of the conducting fluid in which the magnetic field resides, the dynamo process itself also needs to be understood. When studying dynamo theory in astrophysical and cosmological contexts, the idea of large- and small-scale magnetic fields must be addressed. We expand on this in the next section.

1.2 Literature Review: Mean-Field Electrodynamics

When studying turbulence (more properly, velocity-dominant turbulence) in Fluid Dynamics, the ideas of large- and small-scale velocity fields become important. Here, the total velocity field, $\mathbf{U}$ is decomposed into two parts: the mean velocity field, $\overline{\mathbf{U}}$, and the fluctuating velocity field, $\mathbf{u}$. The fluctuating velocity field is often assumed to take on the form of some sort of turbulence such as that studied by Richardson [82], who introduced the idea of turbulent eddies, and Kolmogorov [49–52], who studied the decay of energy spectra in turbulence.

Mean-field Electrodynamics (MFEM) was developed as an application of mean-field theory to Electrodynamics. Following the decomposition of the velocity field into its mean and fluctuating components as is done when studying turbulence in Fluid Dynamics, the total magnetic flux density, $\mathbf{B}$, is also decomposed into its mean and fluctuating components, $\overline{\mathbf{B}}$ and $\mathbf{b}$ respectively. Using this decomposition of $\mathbf{B}$, it is then possible to study both large- and small-scale magnetic fields, as well as the dynamos that operate on these fields. The study of the conducting fluid in the context of MFEM is called mean-field MHD (MFMHD). In the case of MHD, it is primarily magnetically-dominant turbulence that is studied.

The study of large- and small-scale dynamos in MFMHD is of great relevance in astrophysical and cosmological contexts. The distinction between large- and small-scale dynamos is often seen to be immaterial [24], as it can often be seen that small-scale dynamos (i.e. those dynamos that work on the scales of the fluctuating magnetic and velocity fields) produce large magnetic fields that are coherent over an entire computational domain. It should be noted, however, that the orientation of these structures is still random [24]. This is in stark contrast to the large-scale dynamo, which produces magnetic fields whose structures are coherent in both space and time, an example of this being the structures observed in the Sun's magnetic field [24]. Further work on the solar magnetic field also includes studies of the solar magnetic flux, active regions of helicity in the magnetic field, the flux of the solar magnetic helicity and regions of magnetic activity on the sun's surface and are discussed in [2, 25, 30, 34, 36, 95, 97, 98].

The motivation for the study of the large-scale dynamo stems in part from observations of the Sun's own magnetic field [24] and has been studied in great detail. In the context of the solar magnetic field, works such as [97, 98], have established the presence of the large-scale solar dynamo due to the spatio-temporal coherence of the large-scale magnetic structures observed in the solar magnetic field itself. The solar magnetic field's helicity has also been a subject of keen interest together with the study of the large-scale solar dynamo, with measurements of the helicity flux being measured, estimated and discussed in works such as [7, 70, 71, 92]. Other aspects of the solar dynamo are also discussed in [45].

The motivation for study of the small-scale dynamo arises from the study of magnetically-dominant turbulence [24], and were first studied by Kazantsev [42] who modelled the velocity field associated with these dynamos using the statistical properties of turbulence. This led to the Kazantsev equation, whose solutions can indicate small-scale dynamo action, and have been

studied in detail in works such as [47, 84, 86, 102, 103] and others. The small-scale dynamo is particularly important in many astrophysical and cosmological contexts due to it being able to function in both fully-isotropic flows, as well as in random flows in sufficiently-conducting plasmas [23]. These dynamos are again also studied in the context of the solar magnetic field, where they are used to describe the small-scale magnetic field that is observed at the solar surface [1, 4, 14, 23].

Along with the study of the large-scale dynamo and large-scale magnetic field comes their associated phenomena. The most well-known of these is called the α-effect, which is known to generate poloidal magnetic fields from toroidal magnetic fields in rotating fluids [24, 69]. This α-effect is now known to arise from the mean electromotive force (EMF), $\mathcal{E}$ that itself arises naturally from the Induction equations for $\overline{\mathbf{B}}$ and $\mathbf{b}$ as an interaction between the the fields $\mathbf{u}$ and $\mathbf{b}$. It is found that this mean EMF is an average quantity, being written as: $\mathcal{E} = \overline{\mathbf{u} \times \mathbf{b}}$, with the overbar denoting an ensemble average. The exact averaging procedure employed here is discussed further in section 3.1.

One of the central problems in MFMHD is to determine a functional form for the mean EMF. As mentioned before, the α-effect studied by Parker [69] proposed that the mean EMF should take on the form $\mathcal{E} = \alpha\overline{\mathbf{B}}$. Later on, a more extensive study of the mean EMF was done by Steenbeck *et al.* [83, 96], and a Taylor expansion of the mean EMF in derivatives of $\overline{\mathbf{B}}$ given by:

$$\mathcal{E}_i = \alpha_{ij}\overline{B}_j + \beta_{ijk}\frac{\partial \overline{B}_j}{\partial x_k} + \dots \tag{1.1}$$

was proposed. The problem of determining a functional form for the mean EMF now focussed on finding forms for the new tensors α_{ij} and β_{ijk}. The tensor α_{ij} is the well-known α-effect and the tensor β_{ijk} is an additional effect involving turbulent magnetic diffusion [23, 24, 74, 78, 83]. Methods for analytically determining the forms of α_{ij} and β_{ijk} are studied extensively in works such as [24, 55, 67, 74, 78, 83, 96] and others.

It is known that the mean EMF has a fluid analogue, the Reynolds stress tensor, that is given by $R_{ij} = \overline{u_i u_j}$ [67], which is also known as the two-point, second-order velocity correlation tensor. In the work by Frisch [32], a fluid analogue to the MHD α-effect, called the anisotropic kinetic alpha effect (AKA) is derived and is shown to exist for very specific cases of the mean velocity field, $\overline{\mathbf{U}}$. Further work on this analogous fluid α-effect has also been discussed in the

works [33, 44, 48, 109]. This is discussed further in section 3.3.

1.3 Literature Review: Magnetohydrodynamical Simulation

Now that we have discussed some of the work done in literature in Analogue Magnetism and mean-field MHD, we must address the field of numerical simulation. Together with the analytical methods employed in Chapters 2 and 3, the use of direct numerical MHD simulation is one of the tools used in order to obtain and discuss the results presented in this work.

For many years, work in MHD, Dynamo Theory, Turbulence, and Fluid Dynamics in general could only be done through theoretical analysis or direct experimentation. It is known that the governing equations that are studied in these fields are often highly complex, often also possessing many non-linear terms that may not always be neglected in analysis. Due to the complexity of these governing equations, analytical solutions to these equations are often impossible to obtain. Thus, a new mode of scientific enquiry had to be developed: that of computer simulation. Although indirect at times, it is a powerful mode of enquiry, allowing complicated governing equations to be solved quickly, thus also allowing the development of more sophisticated modelling techniques of physical phenomena and a better understanding of the system(s) being analysed. This is particularly true in MHD, Dynamo Theory, Turbulence, and Fluid Dynamics. With the gradual improvement of technology, and the coming-of-age of high-performance computing, many problems in these areas that were previously deemed intractable have now become tractable, with more time being spend on developing increasingly-efficient computer codes for specialised applications in these fields.

Many computer codes developed for numerical simulation are specially designed to run on a variety of computer architectures, ranging from a single machine possibly possessing a multi-core CPU or several GPUs, to larger, more complicated architectures such as those found in cluster- or supercomputers which typically possess thousands of CPU cores in addition to possibly thousands of GPU units. Many of these codes are freely available, for example the popular ZEUS code which was presented in a series of test problems considered the works by Stone *et al.* [99–101]. Another example of a popular computer code for running MHD simulations is the PENCIL CODE, which is the code that is used to obtain the results presented in this work. Its

design rationale is described in [15–17]. The advent of general-purpose computing on graphics processing units (GPGPU) has seen many codes similar to ZEUS and PENCIL come into use. Such codes include GPUPEGAS, which is used to simulate interacting galaxies through MHD [41], FARGO3D [9], which is used mainly for applications planetary-disk interactions in forming stellar systems, and RAMSES-GPU [43] which is related to the popular RAMSES MHD code [111], being ported for use on the GPU.

Hydromagnetic turbulence, among others, is an example of an area that has benefitted greatly from advances in computing. The study of turbulence by Kolmogorov [31, 53, 54] and others and its application in turbulent dynamo theory is another. The gradients of the various slopes observed in the energy spectrum of a magnetic field amplified by a turbulent dynamo has been the subject of study for many authors (e.g. [15, 16, 24, 37, 38] and others). In particular, in [37], discussed the importance of a fine enough mesh resolution in order to correctly capture important features in the magnetic energy spectrum. Even though turbulence is not always considered in some simulations, the discussion of mesh resolution is key when assessing the quality of solutions obtained so as to avoid any artifacts that are solely due to a mesh that is possibly too coarse.

Simulation of turbulent dynamos is also of key importance in MHD simulation. In the works [90, 91] the tensors α_{ij} and β_{ijk} from the mean EMF are calculated through simulation in the case of a rotating spherical shell filled with electrically-conducting fluid. The authors of [110] show through simulation of isotropic helical turbulence that α_{ij} and β_{ijk} can also be calculated and their effects observed up to a value of ~ 220 for the magnetic Reynolds number, $\mathrm{Re_M}$, even observing the emergence of a small-scale turbulent dynamo for $\mathrm{Re_M} \sim 30$. Using helical turbulence simulations once more, the large- and small-scale dynamos studied in the work [10] are found to operate in unison during the kinematic phase, after which, as the Lorentz force becomes more important, the large-scale dynamo continues to operate as the small-scale dynamo saturates and stops working. The initial result found in [10] is in agreement with the simulations done in [107], which also observes the unified operation of the large- and small-scale dynamos during the kinematic phase. The dependence of the magnetic Prandtl number on small-scale dynamo action has also been studied in works by [46, 72, 85, 87–89], with simulations done showing evidence for this hypothesis.

The search for a robust theory of Analogue Magnetism is currently entering a new phase that

stands to benefit from advances already made in computing and computer technology. Such a theory would allow the indirect study of many more complicated aspects of Electromagnetism than what is currently possible. Now that we have discussed some of the key results obtained in literature, we move on to the formal statement of this work.

1.4 Statement of the Research Problem and Thesis Layout

This thesis addresses problems in the fields of Analogue Magnetism and Mean-Field Electrodynamics. In all cases, we first develop and, where necessary, recall relevant results from the theory, after which the relevant simulation work is done. Results are discussed in terms of both the physics observed, as well as from a technical viewpoint. Our research questions are as follows:

1. In Analogue Magnetism, we study the effects of both a non-negligible viscosity and a non-negligible diffusivity in an proposed analogous system consisting of the Induction equations for the magnetic field present in a conducting fluid, $\mathbf{B}$, and the equations for the evolution of vorticity of a non-conducting fluid, $\boldsymbol{\omega}$, both containing no source terms. From a technical standpoint, we determine empirical ranges for which analogous behaviour can be observed between the charged and non-charged fluids (thus also indicating an analogy between the magnetic field and the vorticity) such a system in the presence of non-negligible viscosity and diffusivity.

   We then introduce source terms into the analogous system and repeat the numerical simulation for different values of viscosity and diffusivity. Again, we consider cases where the values of the viscosity and diffusivity are equal to each other, as well as cases where they are not equal to each other. In these simulations we wish to determine whether a given seed field of small magnitude would be amplified in strength, and whether its amplification is aided by the presence of the battery term in the Induction equations. We also wish to determine whether analogous behaviour between the charged and non-conducting fluid (and hence an analogy between the magnetic field and the vorticity) can still be observed in the presence of the source terms now included in the system.

   To perform our numerical simulations, we make use of an open-source, high-order finite

difference MHD code, the PENCIL CODE.

All of the above will be covered in Chapter 2.

2. In Mean-Field Electrodynamics, we focus our study on the mean EMF. Bearing in mind the two well-studied second- and third-order tensors α_{ij} and β_{ijk} occurring in front of the zeroth- and first-order spatial derivatives of $\overline{\mathbf{B}}$ in its Taylor series expansion, we consider the fourth- and fifth-order tensors occurring in front of the terms in the second- and third-order spatial derivatives of $\overline{\mathbf{B}}$. Using the methods of [74], we seek an integral representation of these two higher-order tensors. Assuming that these tensors are also isotropic and homogeneous, we seek to represent them in simple forms and, using these, re-derive Ohm's Law and the Induction equations for $\overline{\mathbf{B}}$ and $\mathbf{b}$ in order to determine the type of terms that these tensors would introduce into the equations.

   Making use of a scale analysis of both Induction equations, lower limits on these new terms are also sought, above which, their effects would become comparable to those of the inductive and magnetic-diffusive terms in the equations.

   Finally, we seek to discuss the purported analogy between the mean EMF and Reynolds stress tensor from Fluid Dynamics, proposing the use of a theory of analogies to possibly study how the form of the Reynolds stress tensor may be obtained.

   All of the above will be covered in Chapter 3.

Finally, in chapter 4, we re-iterate some of the important findings that were made in this work and discuss future extensions to the work that has been done, in light of the findings that were made.

Chapter 2

Analogue Magnetism

Having posed our research question regarding the existence of a possible analogy between charged and non-charged fluids, we now set out in an attempt to answer it. In this chapter we review the governing equations of MHD as well as the key equations of Fluid Dynamics in order to establish a mathematical basis for exploring the possibility of analogous behaviour between charged and non-charged fluids. After discussing some key points in the modelling of a conducting fluid, we develop the system of equations that will be used in our comparative study. The inclusion of source-terms in the system of equations to be studied are also motivated and discussed.

In order to solve the analogous system, we motivate the need for the use of direct numerical simulation as a tool to aid in our investigation. We develop the idea of using high-order finite difference methods to approximate spatial derivatives in partial differential equations, as well as the use of Runge-Kutta schemes for time integration. Based on our findings, we motivate the need for using a high-order finite differences code in order to perform our numerical simulations.

Using direct numerical MHD simulations, we investigate the possibility of similar behaviour between charged and non-charged fluids as evidence for the existence of an analogy between them. Particular attention is paid to the case where both the charged and non-charged fluids have comparable values of magnetic diffusivity and kinetic viscosity in order to determine whether any similar behaviour between the two fluids can be observed. This is done for both the cases in which source terms are present in the system, as well as when they are not present. We

also investigate whether any similar behaviour between the two fluids could still be observed in the case of unequal values of magnetic diffusivity and kinetic viscosity for both the cases of source terms in the equations being absent and present. Results from these simulations are then discussed in detail.

In order to guide our investigation into Analogue Magnetism, we also seek to address the following guiding questions:

1. Using MHD simulation as a tool, could we find a non-conducting fluid that exhibits properties that are similar to those of a conducting fluid?
2. How well would such a non-conducting fluid approximate the behaviour observed in a conducting fluid, and hence magnetic fields, given the chosen conditions?
3. If such a non-conducting fluid is found to exist, could we use it to study the behaviour of magnetic fields in extreme environments?

2.1 The Equations of Magnetohydrodynamics

The full equations governing the flow of a conducting fluid, also called the equations of MHD, are given by:

$$\frac{\mathrm{D}\rho}{\mathrm{D}t} = -\rho\left(\nabla\cdot\mathbf{u}\right) \tag{2.1a}$$

$$\frac{\mathrm{D}\mathbf{u}}{\mathrm{D}t} = -\frac{\nabla p}{\rho} - \nabla\Phi_{\mathrm{grav}} + \frac{\mathbf{J}\times\mathbf{B}}{\rho\mu_0} + \nu\left[\nabla^2\mathbf{u} + \frac{1}{3}\nabla\left(\nabla\cdot\mathbf{u}\right)\right] + \frac{\mathbf{f}}{\rho} \tag{2.1b}$$

$$\frac{\partial\mathbf{B}}{\partial t} = \nabla\times\left(\mathbf{u}\times\mathbf{B} - \mu_0\eta\mathbf{J}\right) \tag{2.1c}$$

$$\frac{\mathrm{D}e}{\mathrm{D}t} = \frac{\eta}{\rho}\mathbf{J}^2 - (\gamma-1)e\cdot\mathbf{u} \tag{2.1d}$$

$$pV = Nk_BT \tag{2.1e}$$

$$\nabla\cdot\mathbf{B} = 0 \tag{2.1f}$$

$$\mathbf{J} = \sigma\left(\mathbf{E} + \mathbf{u}\times\mathbf{B}\right). \tag{2.1g}$$

They are, in order, the Continuity equation (2.1a), the Navier-Stokes or Momentum equations (2.1b), the Induction equations (2.1c) and the equation for Internal Energy (2.1d); this latter equation is often replaced with an equation describing the time evolution of Entropy instead when considering problems where convection is important. Here, ρ is the fluid density, $\mathbf{u}$ the fluid velocity field, $\mathbf{B}$ the magnetic flux density, hereafter simply called the magnetic field, p the scalar fluid pressure, and the internal energy, e, (defined as $e \equiv (\gamma - 1)^{-1}(p/\rho)$). Other important quantities appearing in these equations include the current density, $\mathbf{J}$, the ratio of specific heats, γ, permeability of free space, μ_0, the gravitational potential, Φ_{grav}, and the fluid kinematic viscosity, ν, hereafter simply referred to as the (fluid) viscosity. The final term, $\mathbf{f}/\rho$, in the Navier-Stokes equations represents all additional body forces that may be acting on the fluid.

In addition to the evolution equations, we also require an equation of state, here given by the ideal gas law (2.1e), in order to relate the scalar fluid pressure to the fluid density, as well as Gauss' Law for Magnetism (2.1f), in order to ensure that the magnetic field remains divergence-less. Ohm's Law (2.1g) is also included in this set of equations for completeness and relates the Lorentz force $\mathbf{u} \times \mathbf{B}$ and electric field $\mathbf{E}$ to the current density; σ here is the electrical conductivity of the conducting fluid. It should be noted that the result of Ohm's Law is used in the Induction Equations' derivation to obtain their form given here. In eqn (2.1e), V is the volume, N the particle number density, k_B the Boltzmann constant and T the temperature.

2.1.1 The Kinetic Particle Approximation

All of the simulations presented in this work rely on the equations of MHD to describe the flows under consideration. MHD, like Fluid Dynamics, is a macroscopic theory, dependent on the assumption that a plasma may in fact be considered as a conducting fluid rather than a collection of many particles (viz. an N-body problem). There are conditions under which this fluid approximation of the plasma is no longer valid; we briefly comment on some of the conditions under which this fluid approximation holds.

The governing equations of MHD are derived from expanding moments of the Boltzmann Equations (2.2) as a set of equations describing the dynamics of a multi-fluid plasma (i.e. an ion-electron fluid) on a microscopic scale. The Boltzmann Equations are given by:

$$\frac{\partial f_\alpha}{\partial t} + \mathbf{v} \cdot \frac{\partial f_\alpha}{\partial \mathbf{r}} + \frac{q_\alpha}{m_\alpha}(\mathbf{E} + \mathbf{v} \times \mathbf{B}) \cdot \frac{\partial f_\alpha}{\partial \mathbf{v}} = C_\alpha, \tag{2.2}$$

where $f_\alpha = f_\alpha(\mathbf{r}, \mathbf{v}, t)$ is the distribution function, $\mathbf{r}$ the spatial distance from the origin in the co-ordinate system, m_α the mass of a particular species of particle, subscript α denotes the particle species (e.g. ions or electrons), and C_α represents the time rate-of-change of the distribution function due to particle collisions [35].

Consider a typical length scale, a, together with a representative plasma magnetic field strength, B, and plasma fluid density, ρ. In order to ensure that the MHD fluid approximation remains valid, we have to observe the following conditions [35]:

- The MHD length scale, λ_{MHD}, must be much longer than the ion cyclotron radius, R_i: $\lambda_{\text{MHD}} \sim a \gg R_i$.
- The MHD time scale, τ_{MHD}, must be much longer than the reciprocal of the ion cyclotron frequency, Ω_i: $\tau_{\text{MHD}} \sim a/v_A \gg \Omega_i^{-1}$.

Here, v_A is the Alfvén velocity which is defined using the quantities above as:

$$v_A = \frac{B}{\sqrt{\mu_0 \rho}}. \tag{2.3}$$

If we continue to operate on these length and time scales, we may treat the plasma as a fluid and be assured that the MHD approximation will hold.

2.1.2 From the Particle Approximation to the Fluid Approximation

2.1.2.1 Magnetic Fluids

In the previous section, we was that that MHD assumes the conducting fluid to be composed of many positively- and negatively-charged particles moving in the presence of a magnetic field. The particles' behaviour is of course described through the use of the equations of Kinetic Theory and Thermodynamics. From a macroscopic point of view, the properties of the particles

may be averaged over volumes that are small in comparison to the macroscopic scale, but also much larger than the actual distance between the particles themselves (again, observing the MHD approximation).

Fully-ionized plasma consists of charged particles (point charges) that are in constant motion. Here, the charge density, q, and current density, $\mathbf{J}$, may both be regarded as functions of both position and time: $q = q(\mathbf{r}, t)$ and $\mathbf{J} = \mathbf{J}(\mathbf{r}, t)$. If the charges are assumed to be free and the magnetic effects due to the particles' orbital and spin angular momenta may be regarded as negligible, then the electromagnetic field within the medium may be wholly described by only the electric and magnetic field vectors, $\mathbf{E}$ and $\mathbf{B}$.

Going down to the scale of the individual particles, however, one finds that both the charge and current densities exhibit δ-distribution-type behaviour in that at the position of the particle, these quantities are non-zero whilst they are identically zero everywhere else; a result that is to be expected at these scales.

For a single particle, the volume charge density may be expressed as:

$$\rho_q(\mathbf{r}) = q\delta^3(\mathbf{r}), \tag{2.4}$$

while if the charge is located in some volume, V, the expression turns into the volume integral for the total charge given by:

$$Q = \int_V \rho_q(\mathbf{r}) \mathrm{d}V. \tag{2.5}$$

From here it is possible to calculate the average charge contained within the volume by taking a volumetric average:

$$\langle Q \rangle = \frac{1}{V} \int_V \rho_q(\mathbf{r}) \mathrm{d}V. \tag{2.6}$$

It is also possible to determine the average current density, $\langle \mathbf{J} \rangle$ using this method. Once more, it can be seen from the above that the fluid approximation will hold as long as the volume, V, is made small in the limit on the macroscopic scale, but still larger than the inter-particle distances

themselves. Considering any volume smaller than this will cause the fluid approximation will break down.

2.2 Establishing the Equations to be Investigated

2.2.1 The Induction Equations and Viscous Fluids

The Induction Equations, which govern the time evolution of the magnetic field, $\mathbf{B}$, are given by:

$$\frac{\partial \mathbf{B}}{\partial t} = \nabla \times (\mathbf{u}_{\mathrm{PF}} \times \mathbf{B}) + \eta \nabla^2 \mathbf{B}, \tag{2.7}$$

where $\mathbf{u}_{\mathrm{PF}}$ is the velocity of the *conducting fluid* (i.e. the plasma or *plasma fluid*) and η is the magnetic diffusivity. Using the results from sections 2.1.2, and recalling that we are operating on the MHD time- and length scales, it is possible to derive the Induction Equations by combining Faraday's Law with the Ampère-Maxwell Law and Ohm's Law. This formulation also brings about a term describing the Faraday displacement current, which itself may be neglected as long as the time scales under consideration over which the electric field varies are much greater than the Faraday time [24].

It is important to note that $\mathbf{B} = \mathbf{0}$ is a solution to eqns (2.7), meaning that if the magnetic field itself is initially zero, then no magnetic field will grow nor develop – some "seed field" is required in order for there to be a growth. We shall address this problem of generating a magnetic field from zero initial conditions in section 2.2.3.

The magnetic field $\mathbf{B}$ is most usually written as the curl of some other vector field, $\mathbf{A}$: $\mathbf{B} = \nabla \times \mathbf{A}$, where $\mathbf{A}$ is the magnetic vector potential. The Induction Equations may then be written in terms of the magnetic vector potential as:

$$\frac{\partial \mathbf{A}}{\partial t} = \mathbf{u}_{\mathrm{PF}} \times (\nabla \times \mathbf{A}) + \eta \nabla^2 \mathbf{A} - \nabla \varphi, \tag{2.8}$$

where φ is a scalar potential that arises from the definition of the electric field, $\mathbf{E}$, in Electrodynamics, which is defined as:

$$\mathbf{E} = -\nabla\varphi - \frac{\partial \mathbf{A}}{\partial t}. \tag{2.9}$$

We have also assumed that $\nabla \cdot \mathbf{A} = 0$, using the Coulomb gauge. Note that taking the curl of both sides of eqns (2.8) returns us to eqns (2.7). One of the consequences of using the definition of $\mathbf{B} = \nabla \times \mathbf{A}$ allows us to do the following:

$$\begin{aligned} \nabla \cdot \mathbf{B} &= \nabla \cdot (\nabla \times \mathbf{A}) \\ \Rightarrow \nabla \cdot \mathbf{B} &= 0, \end{aligned}$$

due to the divergence of a curl being identically zero, recovering the result given in expression (2.1f). This allows us to then solve eqns (2.8) instead of eqns (2.7) in order to ensure the divergenceless condition on $\mathbf{B}$. This is advantageous from the numerical point of view, since if eqns (2.7) were solved instead, an additional scheme would need to be implemented in the code in order to ensure that $\nabla \cdot \mathbf{B}$ remains negligible within some small error.

Often when solving eqns (2.7), it is useful to know whether the magnetic field will grow. This is especially important when studying the onset of dynamo action, when a growing solution to eqns (2.7) is sought, requiring one to know the relative contributions of the two terms in the equations. For a growing solution to be obtained, it would be required that the contribution from the first term on the RHS of eqns (2.7), also called the induction term, exceeds that of the second term on the RHS of the same equations, also called the diffusive term. In light of this, it is possible to define a dimensionless quantity called the magnetic Reynolds number, which is taken as the ratio of the inductive term to the diffusive term in eqns (2.7):

$$\mathrm{Re_M} := \frac{u_{\mathrm{PF}} L}{\eta}, \tag{2.10}$$

where u_{PF} is the typical velocity scale of the plasma fluid flow and L is the typical length scale of the plasma fluid flow. The magnetic Reynolds number characterises the importance of diffusion in the flow, and can thus tell us whether dynamo action (i.e. growth of the magnetic field) would be able to take place or not. For $\mathrm{Re_M} < 1$ we would expect to observe decaying magnetic fields, and for $\mathrm{Re_M} > 1$ we would expect to see growing fields. The case of $\mathrm{Re_M} = 1$

tells us that the growth of magnetic fields from the dynamo effect is balanced out by the effects of diffusion in the flow, effectively cancelling each other out. For example, in the context of astrophysical plasmas, the magnetic Reynolds number is very large ($\mathrm{Re_M} \sim 10^9$ for the lower part of the solar convection zone [24]) due to the magnetic diffusivity often being very small. From the point of view of MHD, these types of plasmas are often seeing as being close to the ideal plasmas that are described in Ideal MHD. In Ideal MHD, the diffusive terms from eqns (2.7) and consequently (2.8) are often dropped.

The value of the magnetic Reynolds number, depending on the problem being considered, can also tell us if it is possible to drop the diffusive term when solving eqns (2.7) in a particular context. For example, in the context of astrophysical plasmas, the magnetic diffusivity is often negligibly small due to the magnetic Reynolds number being very large ($\mathrm{Re_M} \sim 10^9$ for the lower part of the solar convection zone [24]), meaning that these types of plasmas are often close to the ideal plasma of MHD. In this case, the diffusive terms from eqns (2.7) and consequently (2.8) are often dropped.

For non-charged (or simply *viscous*) fluids the flow is governed by the Navier-Stokes Equations, given by:

$$\frac{\mathrm{D}\mathbf{u}_{\mathrm{VF}}}{\mathrm{D}t} = -\frac{\nabla p_{\mathrm{VF}}}{\rho_{\mathrm{VF}}} + \nu_{\mathrm{VF}}\nabla^2\mathbf{u}_{\mathrm{VF}}, \tag{2.11}$$

where the subscript VF now refers to the non-conducting fluid (viz. the velocity field $\mathbf{u}$, pressure p and density ρ), ν_{VF}[1] is the kinematic viscosity of this fluid and $\mathrm{D}/\mathrm{D}t$ is the usual Lagrangian derivative from before; all other symbols introduced retain their usual meanings. As with the conducting fluid possessing a magnetic Reynolds number, the non-conducting fluid also possesses a fluid Reynolds number which is defined similarly to its magnetic counterpart by:

$$\mathrm{Re} := \frac{u_{\mathrm{VF}}L}{\nu_{\mathrm{VF}}}, \tag{2.12}$$

where u_{VF} is the typical velocity scale of the viscous fluid flow, ν_{VF} the kinematic viscosity of

[1] We note here that both the charged and non-charged fluids would have the same values of ν for our considerations. However, as we are considering two distinct fluids, it is important to note that each as its own kinematic viscosity, which we then denote as ν_{PF} and ν_{VF} respectively.

the viscous fluid, and L is the typical length scale of the viscous fluid flow. The diffusive term in eqns (2.11) is also often neglected when considering ideal (i.e. non-viscous) fluids. For real fluids that possess properties that are close to ideal fluids, the fluid Reynolds number is typically also very large, corresponding to a small kinematic viscosity. When solving eqns (2.11) when considering fluids for which the kinematic viscosity is small, the diffusive term is often dropped.

In practice, the fluid Reynolds number characterises the transition of a fluid flow from being non-turbulent to becoming fully turbulent. For large values of Re, fluid flow is typically expected to be turbulent.

Another quantity of interest to us in this work is the vorticity of the velocity field, $\mathbf{u}_{\mathrm{VF}}$, which is defined as $\boldsymbol{\omega}_{\mathrm{VF}} = \nabla \times \mathbf{u}_{\mathrm{VF}}$. As with the velocity field, the vorticity field also has a governing evolution equation, which is obtained by taking the curl of eqns (2.11). Here, we first expand the time derivative term on the LHS as:

$$\frac{\mathrm{D}\mathbf{u}_{\mathrm{VF}}}{\mathrm{D}t} = \frac{\partial \mathbf{u}_{\mathrm{VF}}}{\partial t} + \mathbf{u}_{\mathrm{VF}} \cdot \nabla \mathbf{u}_{\mathrm{VF}}, \tag{2.13}$$

which now leaves eqns (2.11) as:

$$\frac{\partial \mathbf{u}_{\mathrm{VF}}}{\partial t} + \mathbf{u}_{\mathrm{VF}} \cdot \nabla \mathbf{u}_{\mathrm{VF}} = -\frac{\nabla p_{\mathrm{VF}}}{\rho_{\mathrm{VF}}} + \nu_{\mathrm{VF}} \nabla^2 \mathbf{u}_{\mathrm{VF}}. \tag{2.14}$$

Recalling the Vector Calculus identity for $\nabla(\mathbf{X} \cdot \mathbf{Y})$, where $\mathbf{X}$ and $\mathbf{Y}$ are two vector quantities, the term $\mathbf{u}_{\mathrm{VF}} \cdot \nabla \mathbf{u}_{\mathrm{VF}}$ may be expressed as:

$$\mathbf{u}_{\mathrm{VF}} \cdot \nabla \mathbf{u}_{\mathrm{VF}} = \frac{1}{2} \nabla {\mathbf{u}_{\mathrm{VF}}}^2 - \mathbf{u}_{\mathrm{VF}} \times \boldsymbol{\omega}_{\mathrm{VF}}, \tag{2.15}$$

where ${\mathbf{u}_{\mathrm{VF}}}^2 \equiv \mathbf{u}_{\mathrm{VF}} \cdot \mathbf{u}_{\mathrm{VF}}$ is a pure scalar quantity and $\boldsymbol{\omega}_{\mathrm{VF}}$ is the vorticity defined above. Noting the fact that the curl and Laplacian operators commute with each other, we may now take the curl of eqns (2.14) to yield the time evolution equations for the vorticity field:

$$\frac{\partial \boldsymbol{\omega}_{\mathrm{VF}}}{\partial t} = \nabla \times (\mathbf{u}_{\mathrm{VF}} \times \boldsymbol{\omega}_{\mathrm{VF}}) + \nu_{\mathrm{VF}} \nabla^2 \boldsymbol{\omega}_{\mathrm{VF}} - \nabla \times \left(\frac{\nabla p_{\mathrm{VF}}}{\rho_{\mathrm{VF}}} \right). \tag{2.16}$$

For a pressureless fluid, or where the fluid pressure is constant in space so that $\nabla p_{\mathrm{VF}} = 0$, these equations reduce to the simpler form:

$$\frac{\partial \boldsymbol{\omega}_{\mathrm{VF}}}{\partial t} = \nabla \times (\mathbf{u}_{\mathrm{VF}} \times \boldsymbol{\omega}_{\mathrm{VF}}) + \nu_{\mathrm{VF}} \nabla^2 \boldsymbol{\omega}_{\mathrm{VF}}. \tag{2.17}$$

The case $\nabla p_{\mathrm{VF}} \neq 0$ will be deferred to section 2.2.3.

2.2.2 The Analogous System

Collecting eqns (2.7), (2.8), (2.11), and (2.16) from the previous section, we may now establish the analogous systems of equations that we wish to study. The Navier-Stokes and magnetic vector potential evolution equations form one system:

$$\frac{\partial \mathbf{u}_{\mathrm{VF}}}{\partial t} = \mathbf{u}_{\mathrm{VF}} \times \boldsymbol{\omega}_{\mathrm{VF}} + \nu_{\mathrm{VF}} \nabla^2 \mathbf{u}_{\mathrm{VF}} - \frac{1}{2} \nabla {\mathbf{u}_{\mathrm{VF}}}^2 \tag{2.18a}$$

$$\frac{\partial \mathbf{A}}{\partial t} = \mathbf{u}_{\mathrm{PF}} \times (\nabla \times \mathbf{A}) + \eta \nabla^2 \mathbf{A} - \nabla \varphi, \tag{2.18b}$$

while the vorticity evolution and Induction equations form the other:

$$\frac{\partial \boldsymbol{\omega}_{\mathrm{VF}}}{\partial t} = \nabla \times (\mathbf{u}_{\mathrm{VF}} \times \boldsymbol{\omega}_{\mathrm{VF}}) + \nu_{\mathrm{VF}} \nabla^2 \boldsymbol{\omega}_{\mathrm{VF}} \tag{2.19a}$$

$$\frac{\partial \mathbf{B}}{\partial t} = \nabla \times (\mathbf{u}_{\mathrm{PF}} \times \mathbf{B}) + \eta \nabla^2 \mathbf{B}. \tag{2.19b}$$

System (2.19) will be the primary subject of study in this work, as we are interested in exploring the possible analogy between charged (or *plasma fluid*) (PF) and non-charged (or *viscous fluids*) fluids (VF). As mentioned in the previous section, we note that the pressure term from the Navier-Stokes equations is not included for the present study; the viscous fluid in this case is assumed to have constant pressure in space so that $\nabla p_{\mathrm{VF}} \neq 0$.

The last two terms in system (2.18) should also be mentioned briefly: these terms appear as "integration constants" when going from system (2.19) to system (2.18) and automatically go to

zero once the curl of the equations of system (2.18) is taken (viz. $\nabla \times \nabla\phi = \mathbf{0}$). For this reason, we shall usually leave out these two terms when writing system (2.18), but include these terms here for the sake of completeness.

From the point of view of governing equations, the first step in trying to find a suitable analogy between two physical systems requires that there be similarity in their governing equations. Examining systems (2.18) and (2.19), we see that each of the equations do indeed share similar terms. Both the Navier-Stokes and vorticity evolution equations share an inductive-like term, such as what is seen in the Induction Equations, as well as a diffusive term which is multiplied by the kinematic viscosity (in the case of the viscous fluid) or the diffusivity (in the case of the plasma fluid). We also note that the quantities of interest to us are $\mathbf{B}$ and $\boldsymbol{\omega}_{\mathrm{VF}}$. When the viscosity and diffusivities are set to zero in both systems, one recovers the Induction Equations for Ideal MHD and the Euler momentum equation for ideal fluids.

We note that in other studies such as [8, 56], $\mathbf{B}$ is often compared to $\boldsymbol{\omega}_{\mathrm{PF}}$, the vorticity of the plasma fluid itself, in order to investigate possible similarity behaviour between the two quantities. Those studies attempt to investigate the effects of the properties of the plasma fluid (e.g. different kinematic viscosities etc.) itself on the evolution of the magnetic field rather than trying to investigate possible analogous behaviour between a viscous and plasma fluid.

Searching for a possible analogue between the plasma and viscous fluids involves solving system (2.19) together with different values of the viscosity and diffusion, and to observe the individual temporal growth and decay rates of these fields (i.e. comparing the temporal growth or decay rate of $\mathbf{B}$ to that of $\boldsymbol{\omega}_{\mathrm{VF}}$), and saturation levels where relevant. In order to establish whether a viable analogue may exist between the two fluids in question requires that all of the aforementioned at least show similar behaviour.

2.2.3 Including the Source Terms

While we have stated the analogous systems that will be the subjects of our study in this work, the issue of the pressure term that is present in the Navier-Stokes equations has not yet been addressed. The pressure term in question, appearing as $\nabla p_{\mathrm{VF}}/\rho_{\mathrm{VF}}$ in the Navier-Stokes equations (2.11), plays an important role in the vorticity evolution equations. The pressure term itself arises

from the divergence of the stress tensor, $\tilde{\boldsymbol{\sigma}}_{ij}$, with the stress tensor itself being isotropic and having only three non-zero, equal, on-diagonal components, $\sigma_{xx} = \sigma_{yy} = \sigma_{zz} = p$, permitting us to write $\nabla \cdot \tilde{\boldsymbol{\sigma}} = \nabla p$. As we saw in the previous section, when we took the curl of the Navier-Stokes equations (2.11) in order to derive the vorticity equations (2.17), we were left with:

$$\frac{\partial \boldsymbol{\omega}_{\mathrm{VF}}}{\partial t} - \nabla \times (\mathbf{u}_{\mathrm{VF}} \times \boldsymbol{\omega}_{\mathrm{VF}}) - \nu_{\mathrm{VF}} \nabla^2 \boldsymbol{\omega}_{\mathrm{VF}} = -\frac{\nabla p_{\mathrm{VF}} \times \nabla \rho_{\mathrm{VF}}}{{\rho_{\mathrm{VF}}}^2}, \tag{2.20}$$

where we have chosen to isolate the curled pressure term on the RHS (we'll refer to this term as a source term), while taking all the other terms to the LHS. Note that the conducting fluid also obeys a structurally-similar equation for its own vorticity; since we are looking to compare the behaviour of charged and non-charged fluids, however, we do not consider the vorticity equation for the conducting fluid here. It is important to note here that while $\boldsymbol{\omega}_{\mathrm{VF}} = \mathbf{0}$ is a solution of the homogeneous counterpart of eqns (2.20), eqns (2.19a), a solution to eqns (2.20) would be comprised of the solution to eqns (2.19a), plus the corresponding particular solution that takes into account the source term of eqns (2.20). A Green's function could, for example, be used to find this particular solution.

Our reason for choosing to write eqns (2.20) in the form given is to illustrate the behaviour of the source term in the presence of vorticity: the source term may be seen as acting together with the diffusive term in decreasing any vorticity that may already be present within the fluid itself.

The presence of the source term in eqns (2.20) means that the equations posed in system (2.19) will no longer share structural similarities. As was mentioned before, the source term in eqns (2.20) arises from taking the curl of the pressure term in eqns (2.11), which itself arises from the presence of stresses within the fluid flow. In order to regain structural similarity between the equations in system (2.19) in the presence of eqns (2.20)'s source term, we need to revisit our formulation of the conducting fluid, paying particular attention to its constituents: ions and electrons. We expand on this in the next section.

2.2.3.1 The Biermann Battery and the Two-fluid Approximation

A conducting fluid consisting of ions and electrons is a type of multi-fluid, with each of the fluid's constituents obeying its own equation of motion. Due to the masses of the ions being vastly greater than that of the electrons, exchange of momentum between the two particle species is inevitable, meaning that the consideration of stresses within the conducting fluid are important.

The simplest way of finding a matching term from the Induction Equations to the pressure term in the Navier-Stokes and vorticity evolution equations is to recall the composition of our plasma fluid: it consists of both ions and electrons. In essence, we have proposed to work with a multi-fluid. Considering both particle species, it is possible to write down equations of motion in a unified manner as:

$$\frac{\mathrm{D}\mathbf{u}_\mathrm{k}}{\mathrm{D}t} = \frac{Ze}{m_\mathrm{k}c}\left(\mathbf{E} + \mathbf{u}_\mathrm{k} \times \mathbf{B}\right) - \frac{\nabla p_\mathrm{k}}{n_\mathrm{k} m_\mathrm{k}} - \nabla\Phi_\mathrm{grav} + \frac{\mathbf{P}_{\mathrm{kk}'}}{n_\mathrm{k} m_\mathrm{k}}, \tag{2.21}$$

where the subscript k may be replaced with either of the subscripts e or i, representing ions or electrons respectively, and the subscript k' denoting the other particle species. The particles in this case carry a charge of Ze/c, where c is the speed of light, e the standard charge on a proton in Electron Standard Units (ESU), and Z the particle charge in units of the proton charge [94]. The term $\mathbf{P}$ represents the total momentum transfer from one particle species to another through collisions, per unit volume and per unit time. In this case, a simplifying assumption has also been made on the stress tensor, $\tilde{\boldsymbol{\sigma}}$, which appears in the equations of motion for both particle species. Assuming that the plasma's random velocity distribution is isotropic, the stress tensor is left with only three equal on-diagonal components that are also equal to the fluid scalar pressure (i.e. $\sigma_{xx} = \sigma_{yy} = \sigma_{zz} = p$), admitting the simple form of ∇p in eqns (2.21) [94]. Taking the difference between $n_\mathrm{e}\mathrm{D}\mathbf{u}_\mathrm{e}/\mathrm{D}t$ and $n_\mathrm{i}Z\mathrm{D}\mathbf{u}_\mathrm{i}/\mathrm{D}t$ and changing to units of $c = 1$, we are then left with:

$$\frac{m_\mathrm{e}}{n_\mathrm{e}e^2}\frac{\partial \mathbf{J}}{\partial t} = \mathbf{E} + \mathbf{u}_\mathrm{i} \times \mathbf{B} + \frac{\nabla p_\mathrm{e}}{e n_\mathrm{e}} - \frac{\mathbf{J} \times \mathbf{B}}{e n_\mathrm{e}} - \eta\mathbf{J}, \tag{2.22}$$

where $\eta = P_\mathrm{ei}/en_\mathrm{e}J$ may be recognised as the magnetic diffusivity. Expression (2.22) is the General Ohm's Law [24, 94]. The time derivative term in $\mathbf{J}$ is an inertial term which may be neglected for time scales larger than the plasma oscillation period, whilst the term in $\mathbf{J} \times \mathbf{B}$

is the usual Hall term arising due to a non-vanishing Lorentz Force and may also be neglected. $\nabla p_{\rm e}/en_{\rm e}$ is the Biermann battery term [12,24,94]. This term represents the effects of the electron pressure gradient on the fluid flow, and is key in the generation of magnetic fields from a zero initial condition. If this term is written as the sum of both a non-conservative vector field and the gradient of a scalar function, then a magnetic field will be produced when the curl is taken.

The General Ohm's Law can be used to re-derive the Induction Equations (see for example [24]). For the purposes of this work, we neglect the Hall's effect due to our assumption of a negligible Lorentz force, as well as the displacement current due to the time scales of our simulations being longer than 10^{-20}s [24], and keep only the battery and Ohmic terms from the expression. Expression (2.22) is rewritten for the electric field, $\mathbf{E}$, and substituted into Faraday's Law, $\nabla \times \mathbf{E} = -\partial \mathbf{B}/\partial t$. Using Ampère-Maxwell Law, a substitution for the current density $\mathbf{J}$ may be made as well. After some algebra, the Induction Equations with the Biermann battery term are given by:

$$\frac{\partial \mathbf{B}}{\partial t} = \nabla \times (\mathbf{u}_{\rm i} \times \mathbf{B} - \eta \mathbf{J}) + \nabla \times \left(\frac{\nabla p_{\rm e}}{e n_{\rm e}} \right), \tag{2.23}$$

where $n_{\rm e}$ is the electron number density. Assuming that the conducting fluid consists of only Hydrogen, having a plasma ionization fraction of χ that is constant in space, and has both electrons and protons at the same temperature, we may use the Ideal Gas Law, $p_{\rm e} = n_{\rm e} k_{\rm B} T$, where $k_{\rm B}$ is the Boltzmann constant and T is the temperature, as well as the identifications $p_{\rm e} = \chi p_{\rm PF}/(1+\chi)$ and $n_{\rm e} = \chi \rho_{\rm PF}/m_{\rm p}$, where χ is the plasma ionization factor and $m_{\rm p}$ is the standard mass of the proton in order to rewrite the battery term in terms of the pressure and density. Eqns (2.23) then read as:

$$\frac{\partial \mathbf{B}}{\partial t} - \nabla \times (\mathbf{u}_{\rm PF} \times \mathbf{B}) - \eta \nabla^2 \mathbf{B} = \frac{m_{\rm p}}{e(1+\chi)} \left(\frac{\nabla p_{\rm PF} \times \nabla \rho_{\rm PF}}{{\rho_{\rm PF}}^2} \right). \tag{2.24}$$

This is the form of the Induction Equations with the Biermann battery term that we shall consider in our work. With the appearance of the Biermann term, eqns (2.24) and (2.20) are once more structurally similar.

As with eqns (2.20), we have also written eqns (2.24) in the form of the homogeneous equation on the LHS equalling the source term on the RHS. In this form, we note once more that while

$\mathbf{B} = \mathbf{0}$ is a solution to the homogeneous Induction equations (2.7), a solution to eqns (2.24) would also consist of the solution to (2.7), plus the corresponding particular solution that takes into account the source term of eqns (2.24) which would normally be found using a Green's function.

In the given form above, it can be seen that the source term aids the induction term in growing magnetic fields by providing a weak initial seed field that the induction term can then pick up and begin amplifying. Again, in the case of a barotropic flow, the source term can evaluate to zero due to $\nabla p \times \nabla \rho$ vanishing, and will also occur if the pressure gradients of the fluid density and fluid pressure are parallel to each other.

Taking into account the new source term in the Induction Equations and still working in units of $c = 1$, our analogous systems may now be written as:

$$\frac{\partial \mathbf{u}_{\mathrm{VF}}}{\partial t} = \mathbf{u}_{\mathrm{VF}} \times \boldsymbol{\omega}_{\mathrm{VF}} + \nu_{\mathrm{VF}} \nabla^2 \mathbf{u}_{\mathrm{VF}} - \frac{1}{2} \nabla {\mathbf{u}_{\mathrm{VF}}}^2 - \frac{\nabla p_{\mathrm{VF}}}{\rho_{\mathrm{VF}}} \tag{2.25a}$$

$$\frac{\partial \mathbf{A}}{\partial t} = \mathbf{u}_{\mathrm{PF}} \times (\nabla \times \mathbf{A}) + \eta \nabla^2 \mathbf{A} - \nabla \varphi + \frac{m_{\mathrm{p}}}{e(1+\chi)} \frac{\nabla p_{\mathrm{PF}}}{\rho_{\mathrm{PF}}}, \tag{2.25b}$$

for the Navier-Stokes and vector potential evolution equations, while the vorticity evolution and new Induction Equations now appear as:

$$\frac{\partial \boldsymbol{\omega}_{\mathrm{VF}}}{\partial t} = \nabla \times (\mathbf{u}_{\mathrm{VF}} \times \boldsymbol{\omega}_{\mathrm{VF}}) + \nu_{\mathrm{VF}} \nabla^2 \boldsymbol{\omega}_{\mathrm{VF}} - \frac{\nabla p_{\mathrm{VF}} \times \nabla \rho_{\mathrm{VF}}}{{\rho_{\mathrm{VF}}}^2} \tag{2.26a}$$

$$\frac{\partial \mathbf{B}}{\partial t} = \nabla \times (\mathbf{u}_{\mathrm{PF}} \times \mathbf{B}) + \eta \nabla^2 \mathbf{B} + \frac{m_{\mathrm{p}}}{e(1+\chi)} \frac{\nabla p_{\mathrm{PF}} \times \nabla \rho_{\mathrm{PF}}}{{\rho_{\mathrm{PF}}}^2}. \tag{2.26b}$$

With the exception of the differing signs in the new source terms, we once more see that all of the terms in the equations of systems (2.25) and (2.26) match. Note that if we set $\tilde{\boldsymbol{\omega}}_{\mathrm{VF}} \equiv -\boldsymbol{\omega}_{\mathrm{VF}}$, then system (2.26) may be written as:

$$\frac{\partial \tilde{\boldsymbol{\omega}}_{\mathrm{VF}}}{\partial t} = \nabla \times (\mathbf{u}_{\mathrm{VF}} \times \tilde{\boldsymbol{\omega}}_{\mathrm{VF}}) + \nu_{\mathrm{VF}} \nabla^2 \tilde{\boldsymbol{\omega}}_{\mathrm{VF}} + \frac{\nabla p_{\mathrm{VF}} \times \nabla \rho_{\mathrm{VF}}}{{\rho_{\mathrm{VF}}}^2} \tag{2.27a}$$

$$\frac{\partial \mathbf{B}}{\partial t} = \nabla \times (\mathbf{u}_{\mathrm{PF}} \times \mathbf{B}) + \eta \nabla^2 \mathbf{B} + \frac{m_{\mathrm{p}}}{e(1+\chi)} \frac{\nabla p_{\mathrm{PF}} \times \nabla \rho_{\mathrm{PF}}}{{\rho_{\mathrm{PF}}}^2}. \tag{2.27b}$$

It should be noted that taking the curl of the pressure term $\dfrac{\nabla p_{\star\mathrm{F}}}{\rho_{\star\mathrm{F}}}$, where the $\star\mathrm{F}$ means either VF or PF, we are left with the following:

$$\begin{aligned}\frac{\nabla p_{\star\mathrm{F}}}{\rho_{\star\mathrm{F}}} &= \frac{\rho_{\star\mathrm{F}}\nabla\times\nabla p_{\star\mathrm{F}} - \nabla\rho_{\star\mathrm{F}}\times\nabla p_{\star\mathrm{F}}}{{\rho_{\star\mathrm{F}}}^2} \\ &= \frac{-\nabla\rho_{\star\mathrm{F}}\times\nabla p_{\star\mathrm{F}}}{{\rho_{\star\mathrm{F}}}^2} \\ &= \frac{\nabla p_{\star\mathrm{F}}\times\nabla\rho_{\star\mathrm{F}}}{{\rho_{\star\mathrm{F}}}^2},\end{aligned}$$

which leads to the sign difference in the source terms in system (2.27).

System (2.27) will form the basis of our analysis. The Induction and vorticity evolution equations are now identical, save for the multiplicative term in front of the battery term in the former equations. Making the identification using $\tilde{\boldsymbol{\omega}}_{\mathrm{VF}} \equiv -\boldsymbol{\omega}_{\mathrm{VF}}$ in order to arrive at system (2.27) also suggests that while magnetic fields may grow in a plasma fluid, we should observe vorticity decaying within a viscous fluid, if an analogy indeed exists. This is due to the gradient of fluid pressure, ∇p: in the conducting fluid, it aids in helping magnetic fields grow, whilst in the non-conducting fluid it contributes to the decay of vorticity.

Using the identification $\tilde{\mathbf{u}}_{\mathrm{VF}} \equiv -\mathbf{u}_{\mathrm{VF}}$, system (2.25) may be written in a similar way as:

$$\frac{\partial\tilde{\mathbf{u}}_{\mathrm{VF}}}{\partial t} = \tilde{\mathbf{u}}_{\mathrm{VF}}\times(\nabla\times\mathbf{u}_{\mathrm{VF}}) + \nu_{\mathrm{VF}}\nabla^2\tilde{\mathbf{u}}_{\mathrm{VF}} - \frac{1}{2}\nabla\tilde{\mathbf{u}}_{\mathrm{VF}}^2 + \frac{\nabla p_{\mathrm{VF}}}{\rho_{\mathrm{VF}}} \tag{2.28a}$$

$$\frac{\partial\mathbf{A}}{\partial t} = \mathbf{u}_{\mathrm{PF}}\times(\nabla\times\mathbf{A}) + \eta\nabla^2\mathbf{A} - \nabla\varphi + \frac{m_{\mathrm{p}}}{e(1+\chi)}\frac{\nabla p_{\mathrm{PF}}}{\rho_{\mathrm{PF}}}. \tag{2.28b}$$

Our search for a possible analogue between plasma and viscous fluids would now also have to extend to the case of non-zero source terms in the equations. Again, the temporal growth and decay rates of the magnetic and vorticity fields, as well as their saturation levels and possibly energy spectra would have to be investigated.

2.2.3.2 The Source Numbers

We also propose here two new quantities called the source numbers, denoted as $\mathrm{S_M}$ and $\mathrm{S_V}$ respectively, and consider their derivations here. We first consider the case of the source number for the Induction Equations (occasionally referring to this particular quantity also as the *battery number*), and then finally consider the source number for the vorticity evolution equations.

When generating magnetic fields from a zero initial condition, one of the primary concerns is that of the amount of diffusion in the system. If the diffusion is set too high, any magnetic fields produced via the battery term will effectively be diffused out of the system. Thus, the battery term, like the induction term, has to compete with the diffusive term in order for a significant field to be observed. Similarly to how the magnetic Reynolds number is defined as the ratio of the induction term to the diffusive term, the battery number is defined as the ratio of the battery term to the diffusive term. As with $\mathrm{Re_M}$, should $\mathrm{S_M} < 1$, we would expect no magnetic field produced by the battery term to grow, whilst if $\mathrm{S_M} > 1$, a growing field should be expected to be observed. If $\mathrm{S_M} = 1$, the diffusion and battery terms have balanced each other out and no change should be observed in the magnetic field strength. From the dimensional analysis point of view,

$$\begin{aligned}\mathrm{S_M} &= \frac{\text{battery term}}{\text{diffusive term}} \\ &= \frac{m_\mathrm{p}}{e(1+\chi)} \cdot \left|\frac{\nabla p \times \nabla \rho}{\rho^2}\right| \cdot \left|\frac{1}{\eta \nabla^2 \mathbf{B}}\right| \\ &= \frac{m_\mathrm{p}}{e(1+\chi)\eta} \cdot \frac{p_0}{L^3 B_0 \rho_0},\end{aligned}$$

which defines how the battery number is calculated in terms of the typical scales of the variables in the equations. Here, p_0 is the typical pressure scale of the fluid, ρ_0 the typical density scale of the fluid, and B_0 the scale of the magnetic field and L is once more the typical length scale of the fluid; all other symbols retain their usual meanings. We finally write the definition of the battery number as:

$$\mathrm{S_M} = \frac{m_\mathrm{p}}{e(1+\chi)\eta} \cdot \frac{p_0}{L^3 B_0 \rho_0}. \tag{2.29}$$

Furthermore, we are required to know the dimensions of the battery number. We should expect

that like the magnetic Reynolds number, the battery number should also be dimensionless. In order to demonstrate this, we would require that the battery number have the same dimensions as the diffusive term in the Induction Equations. It can be shown that the dimensions of the diffusive term (denoted using the standard square brackets) in the Induction Equations are given by:

$$\left[\eta\nabla^2\mathbf{B}\right] = M_\star {L_\star}^2 {T_\star}^{-3} {I_\star}^{-1}, \tag{2.30}$$

where we use subscript stars to denote that we are working with dimensions. Taking the battery term and now including the fundamental constant c, we are left with:

$$\begin{aligned}\left[\frac{cm_\mathrm{p}}{e(1+\chi)}\cdot\frac{\nabla p\times\nabla\rho}{\rho^2}\right] &= \frac{L_\star {T_\star}^{-1} M_\star}{I_\star {L_\star}^{-1}}\frac{M_\star {L_\star}^{-2} {T_\star}^{-2} M_\star {L_\star}^{-4}}{{M_\star}^2 {L_\star}^{-6}} \\ &= M_\star {L_\star}^2 {T_\star}^{-3} {I_\star}^{-1},\end{aligned} \tag{2.31}$$

which are the same dimensions of the diffusive term. Thus, we may conclude that the battery number is indeed a dimensionless quantity.

Though the exact numerical values of the battery numbers for our simulations done are not considered in this work, we shall investigate the relationship between the battery number and the observance of a growing magnetic field generated by the battery term. Using the battery number, we shall be able to determine whether the battery term is indeed in operation during a given simulation, as well as how its effect stacks up against that of the diffusive term in the Induction Equations.

Similarly, we may compute the vorticity source number as:

$$\begin{aligned}\mathrm{S_V} &= \frac{\text{source term}}{\text{diffusive term}} \\ &= \left|\frac{\nabla p\times\nabla\rho}{\rho^2}\right|\cdot\left|\frac{1}{\nu\nabla^2\boldsymbol{\omega}}\right| \\ &= \frac{p_0}{\nu_{\star\mathrm{F}} L^3\omega_0\rho_0},\end{aligned}$$

which defines now how the vorticity source number is calculated in terms of the typical scales of the variables in eqns (2.27a). Here, ω_0 the scale of the vorticity field, while all other symbols

retain their meanings from above. We finally write the definition of the vorticity source number as:

$$\mathrm{S_V} = \frac{p_0}{\nu_{\star\mathrm{F}} L^3 \omega_0 \rho_0}. \tag{2.32}$$

As before, we take $\star$F to mean either VF or PF, referring to the kinematic viscosity that is present in either the non-charged or conducting fluid.

2.3 Numerical Implementation

Having now laid out the evolution equations which we shall use in order to investigate the possible analogue between magnetic and viscous fluids, we are in a position to begin answering our research question. To this end, we look at numerical solutions to the systems (2.27) and (2.28) that were given in the previous section.

It should be noted that the equations comprising the systems which will be investigated are themselves extremely complex and almost impossible to solve analytically. This is especially true for the Navier-Stokes and Induction Equations with their respective pressure and source terms present. The need thus arises for us to perform our investigation through the use of direct numerical simulation of the fluids in question, thus solving the relevant systems of governing equations numerically. As we are considering a subset of the MHD equations in our work, it is appropriate to make use of an MHD code that is specialised in simulating charged fluids, along with other types of MHD phenomena.

The PENCIL CODE[2] is a publicly-available high-order finite differences MHD code that is well-suited to the study of various problems in MHD, including forced MHD turbulence, studies of dynamos, weakly-compressible flows and convection problems [17]. High-order finite difference codes such as this one are becoming increasingly popular due to their ease of implementation, parallelization and suitability for the study of a larger number of MHD problems. The PENCIL CODE is itself also modular in the sense that different variables and physical processes are consolidated into modules which can be included or excluded from any particular run as the need

[2] http://pencil-code.nordita.org

arises [17]. As an example: it is possible to simulate both MHD and normal hydrodynamics by including or excluding the code's `Magnetic` module which what we have done in this study.

It should be noted that the code solves the MHD equations in their so-called non-conservative form, making it a non-conservative code [16, 17]. The quality of solutions can thus be checked by monitoring how well certain conserved quantities (such as entropy, mass and momentum) are conserved for the duration of a particular run. These conserved quantities are thus only conserved up to the discretisation error of the numerical scheme, rather than up to machine accuracy [17]. More details on the code's technical aspects are covered in [15, 17].

2.3.1 The PENCIL CODE Equations

A short description, adapted from the code's accompanying manual [17], of the standard equations solved by the PENCIL CODE now follows.

2.3.1.1 The Continuity Equation

Equation (2.33) is the Continuity Equation, given in terms of the logarithm of the fluid density, $\ln \rho$:

$$\frac{\mathrm{D} \ln \rho}{\mathrm{D}t} = -\nabla \cdot \mathbf{u}. \tag{2.33}$$

For the types of problems that the PENCIL CODE is specialised in solving (viz. convection problems), it is numerically advantageous to solve for the logarithm of the density, $\ln \rho$, rather than for ρ itself, due to the fact that there may be extremely large variations in the ranges of both temperature and density in some applications [17].

2.3.1.2 The Navier-Stokes Equations

Equations (2.34) are the Navier-Stokes Equations, describing the temporal evolution of the fluid velocity field, $\mathbf{u}$:

$$\frac{\mathrm{D}\mathbf{u}}{\mathrm{D}t} = -c_s^2\gamma\nabla\left(\frac{s}{c_p} + \ln\rho\right) - \nabla\Phi_{\mathrm{grav}} + \frac{\mathbf{J}\times\mathbf{B}}{\rho} + \nu\left(\nabla^2\mathbf{u} + \frac{1}{3}\nabla\nabla\cdot\mathbf{u} + 2\mathbb{S}\cdot\nabla\ln\rho\right) + \zeta(\nabla\nabla\cdot\mathbf{u}) + \mathbf{f}, \tag{2.34}$$

which are also referred to as the Momentum Equations for the fluid. Here, $\mathbb{S}$ is the traceless rate-of-strain tensor, given as

$$\mathbb{S}_{ij} = \frac{1}{2}\left(\frac{\partial v_i}{\partial x_j} + \frac{\partial v_j}{\partial x_i} - \frac{2}{3}\delta_{ij}\nabla\cdot\mathbf{v}\right) \tag{2.35}$$

in Cartesian co-ordinates. The constant $\gamma = c_p/c_v$ is the ratio of specific heats, with c_p being the specific heat at constant pressure and c_v the specific heat at constant volume; s is the quantity denoting entropy. Additionally, ν describes the fluid's kinematic viscosity, ζ its shock viscosity, Φ_{grav} some gravitational potential, and c_s^2 is the squared sound-speed that is calculated using the equation of state for a perfect gas as:

$$c_s^2 = \gamma\frac{p}{\rho} = c_{s_0}^2\exp\left[\frac{s\gamma}{c_p} + (\gamma-1)\ln\frac{\rho}{\rho_0}\right], \tag{2.36}$$

where c_{s_0} and ρ_0 are some reference values of the speed of sound and density respectively at some reference height[3] [17]. All other forces that have possibly been unaccounted for (e.g. other body and surface forces) are contained in the final term, $\mathbf{f}$ in eqns (2.34).

2.3.1.3 The Induction Equations

Equations (2.37) are the Induction Equations solved by the code, describing the temporal evolution of the magnetic vector potential field, $\mathbf{A}$:

$$\frac{\partial\mathbf{A}}{\partial t} = \mathbf{u}\times\mathbf{B} - \eta\mu_0\mathbf{J}. \tag{2.37}$$

[3] As the code is mainly used for solving convection-related problems, the use of these reference values at some reference height is important due to these quantities being able to vary with height in a convective system.

This form arises from the divergenceless condition on $\mathbf{B}$, and allows the expression $\mathbf{B} = \nabla \times \mathbf{A}$. Thus, $\mathbf{B}$ can always be easily recovered from $\mathbf{A}$ after a simulation is complete with no additional need to implement any routine to ensure that $\mathbf{B}$ remains divergenceless to within an acceptable error.

2.3.1.4 The Entropy Equation

Equation (2.38) is the Entropy Equation, describing the temporal evolution of the entropy, s:

$$\rho T \frac{\mathrm{D}s}{\mathrm{D}t} = \mathcal{H} - \mathcal{C} + \nabla \cdot (K \nabla T) + \nu \mu_0 \mathbf{J}^2 + 2\rho\nu \mathbb{S} \otimes \mathbb{S} + \zeta \rho (\nabla \cdot \mathbf{u})^2. \tag{2.38}$$

Again, due to the PENCIL CODE's specialist application in convection problems, it is more useful to solve for the entropy than the internal energy, as is normally given in the MHD governing equations. Here, $\mathbb{S} \otimes \mathbb{S} := \mathbb{S}_{ij}\mathbb{S}_{ij}$ is a tensor product. The PENCIL CODE chooses to solve this instead of the internal energy evolution equation for the internal energy e. This implies that $\ln \rho$ and s are seen as the two fundamental thermodynamical variables. When considering different convection processes, it is natural to rather track the evolution of the entropy as a physical variable [17]. Here, $\mathcal{H}$ and $\mathcal{C}$ represent explicit heating and cooling terms respectively, T the temperature and K the radiative thermal conductivity [17]. All other symbols seen here retain their original meanings as described previously.

It should be noted that this equation is only listed for completeness and does not form part of our investigation for this work.

2.3.2 Finite Differences and Time Integration

Finite difference methods (FDM) are of paramount importance in the numerical solution of partial differential equations, including those that form the basis of study in this work. Using a set of discrete points called a stencil (see figure 2.1), an arbitrary function $f(x, t)$, along with its space and time derivatives, are turned into discrete approximations. The resulting partial difference equation is solved on a mesh of arbitrary size, which represents a discrete set of points on the partial differential equation's solution domain.

Due to the fact that the FDM solution seeks to approximate the function and its governing partial differential equation, errors in the approximation itself become an important point to consider.

The first of these errors is the truncation error, which is described by the next-highest-order derivative term in the Taylor Series expansion when it is truncated to form an approximation to a function's derivative. In this way, a sixth-order FDM scheme (the default used by the PENCIL CODE) would have a truncation error that is proportional to h^6, where h is the distance between two points on the solution mesh. In practice, the truncation error is defined as the difference between the function's partial derivative and its finite differences representation, thus giving an idea of how good the approximation is.

Generally, an n-th order FDM scheme will always possess an h^n-order truncation error which is multiplied by the $f^{(n+1)}(x)$'th derivative term in the series. In the case of the sixth-order scheme, the derivative term multiplying h^6 is $f^{(7)(x)}/7!$. Depending on whether the derivative multiplying the truncation error is an odd or even derivative, the truncation error itself may be referred to as a dispersive error (if the derivative is even) or a diffusive error (if the derivative is odd) [15]. Using a high-order FDM scheme is important in ensuring that an accurate numerical solution is obtained.

The PENCIL CODE is able to make use of various FDM approximations for the spatial derivatives in the MHD equations, including second-, sixth- and tenth-order approximations. Though the default is sixth-order, the user may change this before compile-time by specifying in the makefile that the code use a different order to approximate the spatial derivatives.

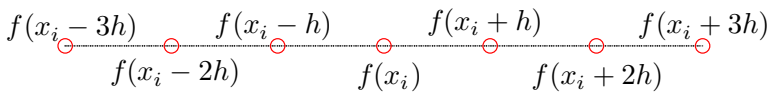

Figure 2.1: A typical one-dimensional stencil for the sixth-order, centered-difference approximation to the first- and second derivatives to a function, $f(x)$. Nodes here are equally-spaced with spacing h.

In order to understand how the FDM is implemented in the PENCIL CODE, we briefly re-

view the derivation of the sixth-order, centered-difference approximation to the first- and second derivatives of a function, $f(x)$. A similar procedure to what is presented below may be followed in the case of a multi-variable function, $g(x_1, x_2, x_3, \ldots)$, where partial derivatives are taken with respect to one particular spatial variable while holding the others constant. Vector functions of the form $\mathbf{F}(\mathbf{x}, t)$ are handled in a similar way to the case of scalar multi-variable functions.

Consider now a sufficiently differentiable function, $f(x)$, that is defined on some domain $[-L, L]$ which has been discretised into equally-spaced nodes, $x_i = -L + ih$, where h is the spacing between the nodes and $i \in \mathbb{Z}$. We denote the value of $f(x)$ at a discrete point, x_i, on the domain as $f(x_i) \equiv f_i$. We wish to approximate the first derivative, $f'(x)$, via the use of the discrete points as shown in Figure 2.1. Dropping the notation for the discrete points for the moment, we assume that we may approximate $f'(x)$ at the point $f(x)$ using six equally-spaced "sample" points as [15]:

$$\begin{aligned} f'(x) \approx\ & Af(x+3h) + Bf(x+2h) + Cf(x+h) + Df(x-h) \\ & + Ef(x-2h) + Ff(x-3h), \end{aligned} \tag{2.39}$$

where the coefficients A to F are as yet undetermined. This situation corresponds to Figure 2.1, in which the first derivative at the middle point, $f(x_i)$, is approximated by the sample points surrounding it. The Taylor Series expansions around each of these sample points may be written in a unified manner as:

$$\begin{aligned} f(x \pm nh) =\ & f(x) \pm nhf'(x) + \frac{n^2h^2}{2}f''(x) \pm \frac{n^3h^3}{3!}f'''(x) + \frac{n^4h^4}{4!}f^{(4)}(x) \\ & \pm \frac{n^5h^5}{5!}f^{(5)}(x) + \mathcal{O}\left(h^6\right). \end{aligned} \tag{2.40}$$

By substituting each of the Taylor expansions of the sample points back into Expression (2.39) and regrouping all coefficients multiplying to a like derivative, the linear system of equations

$$\begin{pmatrix} 1 & 1 & 1 & 1 & 1 & 1 \\ 3 & 2 & 1 & -1 & -2 & -3 \\ 9 & 4 & 1 & 1 & 4 & 9 \\ 27 & 8 & 1 & -1 & -8 & -27 \\ 81 & 16 & 1 & 1 & 16 & 81 \\ 243 & 32 & 1 & -1 & -32 & -243 \end{pmatrix} \begin{pmatrix} A \\ B \\ C \\ D \\ E \\ F \end{pmatrix} = \begin{pmatrix} 0 \\ 1/h \\ 0 \\ 0 \\ 0 \\ 0 \end{pmatrix}, \tag{2.41}$$

is obtained. Since we wish to obtain an approximation to $f'(x)$, each of the other remaining coefficient groups multiplying the function and derivative terms have been set to zero. This system has a unique solution given by:

$$\begin{pmatrix} A \\ B \\ C \\ D \\ E \\ F \end{pmatrix} = \frac{1}{h} \begin{pmatrix} 1/60 \\ -3/20 \\ 3/4 \\ -3/4 \\ 3/20 \\ -1/60 \end{pmatrix}, \tag{2.42}$$

which yields the coefficients needed to approximate $f'(x)$ in Expression (2.39). If we choose to revert to the discrete notation as described before, the sixth-order, central finite difference approximation to the first derivative is written as [15]:

$$f'(x) \approx \frac{\frac{1}{60}f_{i+3} - \frac{3}{20}f_{i+2} + \frac{3}{4}f_{i+1} - \frac{3}{4}f_{i-1} + \frac{3}{20}f_{i-2} - \frac{1}{60}f_{i-3}}{h}. \tag{2.43}$$

Similarly, the second derivative, $f''(x)$, may be approximated by the form:

$$\begin{aligned} f''(x) \approx\ & Af(x+3h) + Bf(x+2h) + Cf(x+h) + Df(x) + Ef(x-h) \\ & + Ff(x-2h) + Gf(x-3h), \end{aligned} \tag{2.44}$$

where the coefficients A to G again need to be determined. This situation again corresponds to Figure 2.1, in which the second derivative at the middle point, $f(x_i)$, is now being approximated

by it *and* the sample points surrounding it. Again, the Taylor Series expansions around each of these sample points (excluding $f(x_i)$) may be written in a unified manner as:

$$\begin{aligned} f(x \pm nh) &= f(x) \pm nhf'(x) + \frac{n^2h^2}{2}f''(x) \pm \frac{n^3h^3}{3!}f'''(x) + \frac{n^4h^4}{4!}f^{(4)}(x) \\ &\pm \frac{n^5h^5}{5!}f^{(5)}(x) + \frac{n^6h^6}{6!}f^{(6)}(x) \pm \mathcal{O}\left(h^7\right), \end{aligned} \tag{2.45}$$

where we have expanded to an extra term in the Taylor Series due to the inclusion of the extra point, $f(x_i)$. Substituting back into Expression (2.44) and regrouping coefficients that are multiplying a common derivative leads to the linear system given by:

$$\begin{pmatrix} 1 & 1 & 1 & 1 & 1 & 1 & 1 \\ 3 & 2 & 1 & 0 & -1 & -2 & -3 \\ 9 & 4 & 1 & 0 & 1 & 4 & 9 \\ 27 & 8 & 1 & 0 & -1 & -8 & -27 \\ 81 & 16 & 1 & 0 & 1 & 16 & 81 \\ 243 & 32 & 1 & 0 & -1 & -32 & -243 \\ 729 & 64 & 1 & 0 & 1 & 64 & 729 \end{pmatrix} \begin{pmatrix} A \\ B \\ C \\ D \\ E \\ F \\ G \end{pmatrix} = \begin{pmatrix} 0 \\ 0 \\ 2/h^2 \\ 0 \\ 0 \\ 0 \\ 0 \end{pmatrix}, \tag{2.46}$$

which has the unique solution,

$$\begin{pmatrix} A \\ B \\ C \\ D \\ E \\ F \\ G \end{pmatrix} = \frac{1}{h^2} \begin{pmatrix} 1/90 \\ -3/20 \\ 3/2 \\ -49/18 \\ 3/2 \\ -3/20 \\ 1/90 \end{pmatrix}. \tag{2.47}$$

These are the coefficients needed to approximate $f''(x)$ in Expression (2.44). Adopting the notation described before, the sixth-order, central finite difference approximation to the second derivative is written as:

$$f''(x) \approx \frac{\frac{1}{90}f_{i+3} - \frac{3}{20}f_{i+2} + \frac{3}{2}f_{i+1} - \frac{49}{18}f_i + \frac{3}{2}f_{i-1} - \frac{3}{20}f_{i-2} + \frac{1}{90}f_{i-3}}{h^2}. \tag{2.48}$$

The finite difference approximations for the second-, fourth- and tenth-orders are all derived in a similar fashion, using less sample points than the sixth-order (in the case of the second- and fourth-order approximations) or more sample points (in the case of the tenth-order approximation). High-order FDM schemes are always deemed favourable due to their versatility and the fact that they can offer truncation error orders that can almost match those of the spectral methods [15]. Despite this, they do suffer a major drawback: high-order FDM schemes require more sample points in the stencil in order to form an approximation to the function that is to be discretised.

In practical terms, this poses a problem near the boundaries of the mesh, as larger ghost zones are required for points on the stencil that lie outside of the mesh. Thus, more storage space is required to store the mesh and ghost zones. This can be partially overcome by the use of so-called compact finite difference schemes, such as those proposed by Lele (1992) [59], which also offer much better truncation errors [15], though these schemes are somewhat impractical to use in parallel computations due to their compact nature. Coefficients for the approximation of the derivative also become more difficult to calculate due to the fact that more and more terms are taken into account from the resulting Taylor Series. This is trivial, though, as the coefficients for the derivative approximation are only calculated once and hard-coded into a module (in the case of the PENCIL CODE or function that deals with the numerical differentiation. Thus, when choosing an FDM scheme, one has to take all of the above factors into account and make a trade-off. In the case of the PENCIL CODE, the sixth-order (explicit) finite difference approximation to the derivatives is the most appealing in light of the above factors.

Another factor that plays a critical role in the proper functioning of any FDM code is that of time integration. In essence, time integration allows the numerical solution to the partial differential equation being solved to advance in time, making it important to pay careful attention to how this integration is implemented in a code.

The simplest method of time integration is accomplished once more by approximating the temporal derivative term in a partial differential equation via a simple forward finite difference approximation. This first-order approximation is derived trivially from the Taylor Series expansion of the function $f(t)$ and involves approximating the function's first derivative, $f'(t)$, by making

use of the sample point $f(t+\tau)$, where τ is the temporal step size. Expanding around the point $f(t+\tau)$ and discarding all terms like $\mathcal{O}(\tau^2)$, the approximation is written as:

$$f'(t) \approx \frac{f(t+\tau) - f(t)}{\tau} + \frac{\tau}{2} f''(t), \tag{2.49}$$

where the trailing second-derivative term represents the truncation error. As this term is proportional to τ only, it has a first-order truncation error, from where the approximation gets its name. Due to the low-order truncation error, this approximation is not very good. In the PENCIL CODE it is used mainly for testing purposes. Other FDM approximation schemes for the time integration exist. Examples of these are the central difference scheme as used for approximation of the spatial derivatives above, as well as the backward difference approximation, which involves approximating the first derivative using the sample point $f(t-\tau)$ instead of the point $f(t+\tau)$ in a first-order Taylor Series expansion.

While these FDM time integration methods are all easily implemented, they all require potentially massive amounts of storage space to compute the numerical solution at subsequent time steps (both the central and forward FDM time integration schemes need to access values of the numerical solution at previous time levels) and can also be potentially expensive to calculate at each time step (in the case of the backward FDM scheme, which requires solving a potentially large system of equations in order to obtain the value of the numerical solution at subsequent time steps). For this reason, more sophisticated time-integration techniques are employed. One such time-integration technique that is used by the PENCIL CODE is a specialised version of the third-order Runge-Kutta method.

In order to apply the Runge-Kutta scheme to a set of partial differential equations, the set of equations must be converted into a set of ordinary differential equations (ODEs) via the Method of Lines. This involves replacing the spatial derivatives in the partial differential equations by their finite-difference approximations, leaving a system of partial differential equations that is still spatially-coupled, but now only dependent on the time variable.

As an illustrative example, applying this method to the partial differential equation $u_t = -\alpha u_x$ [15], for a function $u = u(x,t)$ and using a first-order FDM approximation for the spatial derivative, one will arrive at the set of ODEs given by:

$$\frac{\mathrm{d}u_i}{\mathrm{d}t} = -\alpha \frac{u_{i+1} - u_i}{h}, \tag{2.50}$$

where α is some arbitrary constant. A set of initial and boundary conditions are needed to close the system. The original partial differential equation is now approximated by a system of ODEs instead. Time-integration of the system may now either be done via Euler's Method or any one of the high-order Runge-Kutta schemes. It is in this that the power of the MoL is now realised: instead of having to develop new time-integration schemes for sets of partial differential equations, they may simply be reduced to a set of ODEs and then time-integrated using an already well-established scheme.

For the PENCIL CODE, even though the the resulting system of ODEs is vastly complex due to the implementation being done on vector functions, the same time-integration idea applies and time-integration is done through the use of a specialised third-order Runge-Kutta (RK3) scheme. The RK3 scheme in use is from a family of RK methods known as RK-2N schemes which were proposed in Williamson (1980) [114], the N in the name referring to the amount of variables that need to be updated at every time step. This means that only $2 \times N$ variables need to be stored in the computer's memory at any given time [15]. It should be noted, however, that not all RK schemes can be reformulated as RK-2N schemes [15, 114].

If we take as a prototype, the ODE system

$$\frac{\mathrm{d}u}{\mathrm{d}t} = F(u, t), \tag{2.51}$$

which is to be time-integrated via the RK-2N scheme in use by the PENCIL CODE, we may express its iteration as [15]:

$$w_i = \alpha_i w_{i-1} + \tau F(u_{i-1}, t_{i-1}) \tag{2.52}$$

$$u_i = u_{i-1} + \beta_i w_i, \tag{2.53}$$

where $i = 1 \ldots 3$ (corresponding to a third-order RK-2N scheme [15]), w_i are weights that need to be determined at every step in the iteration and τ is the adaptive time step size that is determined according to the Courant-Friedrich-Levy condition (CFL) at every iteration. In order

to move from the current approximation to the numerical solution, $u^{(n)} \equiv u(t_n)$, to the next approximation, $u^{(n+1)} \equiv u(t_n + \tau)$ (i.e. to go from time t_n to time $t_n + \tau$), three time steps (two intermediate; the third step being counted as the time $t + \tau$) need to be taken according to the iteration described by Equations (2.52) and (2.53). This involves determining the values of the coefficients α_i and β_i, as well as the values of the intermediate time steps, t_i. Fortunately, these are only calculated once via a detailed analysis of the iteration itself [15, 114] and then coded into the code's default time stepping routine.

The CFL timestep selection condition used by the code is given by [17]:

$$\delta t = \min\left(c_{\delta t}\frac{\delta x_{\min}}{U_{\max}}, c_{\delta t,\mathrm{v}}\frac{\delta x_{\min}^2}{D_{\max}}, c_{\delta t,\mathrm{s}}\frac{1}{H_{\max}}\right), \tag{2.54}$$

where

$$\delta x_{\min} \equiv \min(\delta x, \delta y, \delta z), \tag{2.55}$$

where δx, δy and δz are calculated as the length of the simulation box, divided by the mesh resolution, and

$$U_{\max} \equiv \max\left(|\mathbf{u}| + \sqrt{{c_s}^2 + {v_A}^2}\right), \tag{2.56}$$

with c_s and v_A denoting sound speed and Alfvén speed, respectively;

$$D_{\max} = \max(\nu, \gamma\tilde{\chi}, \eta, D), \tag{2.57}$$

where ν is the fluid kinematic viscosity, $\tilde{\chi} = K/(c_p\rho)$ the thermal diffusivity, η the magnetic diffusivity and D the passive scalar diffusivity, and

$$H_{max} = \max\left(\frac{2\nu\mathbb{S}^2 + \zeta(\nabla\cdot\mathbf{u})^2 + ...}{c_v T}\right), \tag{2.58}$$

where, once more, $\mathbb{S}$ is the rate-of-strain tensor, c_v the specific heat at constant volume, and ζ the fluid shock viscosity. The quantities $c_{\delta t}$, $c_{\delta t,\mathrm{v}}$ and $c_{\delta t,\mathrm{s}}$ represent the Courant coefficients for

the advective, diffusive and entropic time-steps respectively. The presence of additional terms on the RHS of the entropy equation is denoted by the ellipses.

The code uses this condition by default in order to select the new time-step for the next iteration. It is possible to change this by specifying a fixed time-step in the simulation parameter input file, though this time-step should ideally be smaller than the viscous time-step. If not, time-integration issues may arise during the simulation, though this can be largely dependent on the problem that is being studied. The numerical solutions can be investigated for any issues relating to manually-specified time-steps that are possibly too large.

Introducing too much or too little diffusion or viscosity into the system can also affect the time-step size, as given by condition (2.54), particularly if a run is done with either one or both of the kinematic viscosity or magnetic diffusivities set to zero. If the code determines that the time-step has become too small in this case, the simulation will stop of its own accord and report to the user that the time-step has become too short. Results produced from such runs are not necessarily incorrect, and can be checked by the user for any possible errors due to the numerical setup of the problem that is being investigated.

Any issues relating to the values of diffusivity or viscosity are typically be remedied by either using a finer mesh, adjusting the initial conditions (particularly the starting amplitudes of quantities such as the velocity field or magnetic field), using a fixed time-step (not recommended, unless the user wishes to investigate particular phenomena) or having the code output a mesh Reynolds number that can be monitored at every iteration to ensure that the numerical solution remains consistent.

2.3.3 Tracked Simulation Quantities

As we noted previously, the PENCIL CODE solves the Induction Equations in terms of the vector potential, $\mathbf{A}$, automatically implementing the divergenceless condition, along with the Navier-Stokes equations for the velocity field, $\mathbf{u}$. We had noted before, however, that for the purposes of our study, we are interested in solving the Induction Equations for the magnetic flux density, $\mathbf{B}$ and the vorticity evolution equations for the vorticity field, $\boldsymbol{\omega}$.

When simulating the viscous and magnetic fluids, it is possible to monitor the growth of both

Diagnostic Quantity	Description	PENCIL CODE Notation
$B_{\rm rms}$	rms Magnetic Flux Density	$\langle \mathbf{B}^2 \rangle^{1/2}$
$A_{\rm rms}$	rms Magnetic Vector Potential	$\langle \mathbf{A}^2 \rangle^{1/2}$
$u_{\rm rms}$	rms Velocity Field	$\langle \mathbf{u}^2 \rangle^{1/2}$
$\omega_{\rm rms}$	rms Fluid Vorticity	$\langle \boldsymbol{\omega}^2 \rangle^{1/2}$
t	Simulation Time	t

Table 2.1: A listing of the diagnostic quantities used in our simulations. Here, $\langle \cdot \rangle$ indicates a volume-averaged quantity

the magnetic field and its corresponding vector potential, as well as that of the vorticity field and the corresponding velocity field, via the use of diagnostic quantities that are printed out during a simulation run. The user is able to choose from a wide range of diagnostic quantities, which include, among others, the simulation time value, root-mean-square (rms) magnetic field strength, rms velocity field strength, kinetic helicity, magnetic helicity and so forth. A more extensive list of these quantities is presented in [17].

The quantities required for our purposes are the magnetic field strength, vorticity field strength, velocity field strength, magnetic potential field strength and the simulation time value. All of the relevant field strengths are calculated by the code during simulation as root-mean-square, volume-averaged quantities and output to a file for plotting and other visualisation purposes as required by the user. Other quantities, such as those for mass conservation, fluid pressure and magnetic helicity and so forth are not always calculated as rms quantities, but are still volume-averaged. A list of the quantities that are investigated for our work is presented in table 2.1.

So even though the PENCIL CODE does not directly solve the equations for the problem we are considering, it is still possible for us to obtain the relevant simulation quantities we seek without much further post-processing. It should be noted, however, that the code itself does not compute quantities such as the magnetic and fluid Reynolds numbers, nor does it do so for the magnetic and fluid Prandtl numbers. Together with the battery number that we had proposed, these quantities are calculated by the user during post-processing of the simulation data.

2.3.3.1 Physical Units in the PENCIL CODE

Before moving on to present the results of this work, we briefly discuss the topic of physical units in the PENCIL CODE.

All simulation results that are obtained from the PENCIL CODE are independent of the physical unit system used to interpret them. This is due to the unit-agnostic nature of many of the calculations performed [17]. The following example is taken from the manual to illustrate this:

> "*... if you simulate a simple hydrodynamical flow in a box of length* $L = 1$. *and get a maximum velocity of* $u_{\max} = 0.5$ *after* $t = 3$ *time units, then you may interpret this as* $L = 1$m, $u_{\max} = 0.5$m/s, $t = 3$s, *or as* $L = 1$pc, $u_{\max} = 0.5$pc/Myr, $t = 3$Myr, *depending on the physical system you have in mind. The units you are using must of course be consistent, thus in the second example above, the units for diffusivities would be* pc^2/Myr, *etc.*"
>
> — PENCIL CODE Manual [17], pg. 33

The code itself, of course, makes use of an internal unit system which we refer to as *code units* or, more simply, as *units*.

To illustrate the code units, we determine the units of the magnetic flux density, $[B]$. Note that the code makes use of the internal value $\mu_0 = 1$. Now using the definition of the Alfvén velocity, the units of the magnetic flux density are determined by

$$[B] = \sqrt{\mu_0 [\varrho]}[v], \tag{2.59}$$

where we have assumed that our chosen units for density and velocity are $[\varrho]$ and $[v]$ respectively[4].

The units of length, $[L]$, velocity, $[v]$, and density, $[\varrho]$, may chosen by the user and are typically appropriate to the problem that is to be considered. However, special care must be taken when choosing the units of velocity and density. The PENCIL CODE makes use of the value c_{s_0} in order

[4] Here, we use $[\cdot]$ to denote only the units of a particular quantity and not a dimensional analysis

to set the unit of velocity. In particular, when c_{s_0} is set to unity, the unit of velocity is measured in units of the chosen sound speed relevant to the problem at hand. Similarly, if $\varrho_0 = 1$, then units of density are also measured in units of density applicable to the problem at hand. Once these are chosen, units of temperature and magnetic flux density are obtained via the means outlined above. Similarly, units of time, $[t]$, are obtained by noting that $[t] = [L]/[v]$.

In the context of computation, the subject with physical units, their choice and calculation can quickly become out-of-hand. We refer the interested reader to the PENCIL CODE manual [17], as well as relevant related threads[5] on the PENCIL CODE discussion group for further information regarding the interpretation of simulation results in terms of physical units. The user may specify the desired units in the relevant input file before runtime. In order to ease the rescaling of the numerical results obtained after a run, post-processing scripts written for the commercial data visualization programming language, Interpreted Data Language, or IDL, are provided. Should one not have access to an IDL package, the correct physical units obtained via the same calculations above may simply be multiplied into the output manually.

The simulation results presented in this work do not take any physical units into account, and thus, quantities are always quoted in code units.

2.4 Simulation Results and Discussion

In our discussion of analogous system in section 2.2, we proposed the procedure through which the possible analogy between magnetic and viscous fluids would be investigated. Our investigation will thus be twofold: we first investigate, through simulation, the analogous system with no source terms, and then only consider the system including the source terms afterwards. In all of our simulations, we track the diagnostic quantities B_{rms}, A_{rms}, u_{rms} and ω_{rms}, as outlined in table 2.1. These diagnostics will be compared to both the simulation time in order to monitor their temporal evolution, as well as to each other, in order to investigate whether any similar behaviour between the charged and non-charged fluids can be observed as evidence for a possible analogy between the two in their respective systems.

[5] Our questions relating to the issue with physical units in the code may be found at the following URL: http://bit.ly/WyMd2o.

According to systems (2.27) and (2.28), the diagnostics will be compared to each other in the following ways: B_{rms} versus ω_{rms} and A_{rms} versus u_{rms}. Note that unlike what is established from system (2.27), it would not make sense to compare, for example, $-B_{rms}$ to ω_{rms}, as the rms quantities are themselves, by definition, positive.

We first present the results of our test simulations in which we study the effect of the mesh size on the quality of solutions obtained to systems (2.27) and (2.28) with no source terms in order to select a mesh size that would be the most efficient (in terms of computation time and quality of the numerical solution obtained) for our needs. Here, values of the viscosity and diffusivity are varied in order to observe their effects on the numerical solution obtained as the mesh size is varied. Once a suitable mesh size is chosen, the values of the magnetic diffusion, η, and the kinetic viscosity, ν_{VF}, are set to a value equal to that of water at 20°C (see table 2.2 for a list of common fluids and their viscosities at 20°C) in order to investigate whether any similar behaviour between the charged and non-charged fluids could be observed, which would be indicative of the possibility of an analogy between the known viscous fluid (in this case, water), and the conducting fluid with its magnetic diffusion set to the corresponding value. Different combinations of the diffusivity and viscosity are investigated next in order to establish whether a) similar behaviour indicative of an analogy between two fluids having different values of viscosity and diffusivity could be established and, if so, b) over how wide a range of values of these two fluid parameters could the observed similar behaviour between the two fluids exist. To this end, an effective Prandtl number (which will be defined in section 2.4.2) is computed for each of the runs presented here and results are discussed in terms of this quantity.

The source terms in systems (2.27) and (2.28) are then included in our numerical simulations. As before, we investigate the parameter space of magnetic diffusivity and kinetic viscosity in order to determine whether any similar behaviour between the charged and non-charged fluids can be observed once more. In particular, runs taking into account the presence of source terms are done with weak seed fields present in order to determine whether the source terms in the systems (2.27) and (2.28) could aid in the amplification of these fields' strengths. The results pertaining to the amplification of seed fields aided by the presence of the source terms are discussed in terms of the newly-defined source numbers, which are taken to be the ratio of the magnitudes of the respective source terms to that of the respective diffusive terms in systems (2.27) and (2.28).

Note that we do not consider the effects of temperature, and thus also the effects of entropy,

Fluid	ν_{VF} (cm^2/s)
Water	1.0×10^{-2}
Air	1.5×10^{-1}
Alcohol	2.2×10^{-2}
Mercury	1.2×10^{-3}

Table 2.2: Kinematic viscosities of some common fluids at 20°C. Adapted from [57].

in the simulations presented and discussed in this work. It should be noted, however, that temperature is another important factor in determining whether a charged and non-conducting fluid would exhibit similar behaviour to each other due to both the magnetic diffusivity and kinetic viscosity being dependent on temperature. In line with not considering the effects of temperature and entropy, the entropy module in the PENCIL CODE is set to `NOENTROPY`.

The Lorentz force in the Navier-Stokes equations is also assumed to be vanishing, thus eliminating the possibility of a back-reaction from the magnetic field, and hence also Hall's effect. As the magnetic field itself can only interact with the fluid field via the Lorentz force, the fluid is effectively isolated from the effects of the growing magnetic field. From the point-of-view of the simulations, any simulation run with the magnetic fields turned off (i.e. by specifying `NOMAGNETIC` in the simulation Makefile), or with the Lorentz force explicitly turned off in the Navier-Stokes equations within the presence of a magnetic field, will see the velocity field exhibit the same behaviour regardless of whether there is a magnetic field or not.

As many of the simulations conducted here produce similar results, only a selection of the results obtained will be discussed in this work. All results presented here are done in a simulation box of dimensions $2\pi \times 2\pi \times 2\pi$ together with periodic boundary conditions. All field initial conditions are set to Gaussian noise of small initial amplitude. For our purposes, the PENCIL CODE will be solving eqns (2.33), (2.34) and (2.37).

2.4.1 Mesh Size Selection

For the simulations presented here, we consider a non-conducting fluid which evolves according to a simplified system consisting only of eqns (2.33) and (2.34), having different values of $\nu_{\rm VF}$. We consider simulation boxes of sizes 32^3, 64^3 and 128^3 respectively, and the temporal evolution of u_{rms} and ω_{rms} are observed. A summary of simulation parameters for these runs are listed in table 2.3. Results obtained for all of these runs are similar, and hence we only present those of runs 1 and 3 in this section for illustrative purposes. Our objective for these runs is to determine which of the simulation boxes is the most cost-effective to use in terms of data storage, as well as actual time taken to run the simulation itself, without losing any of the initial information given by the propagation equations.

ν	32^3	64^3	128^3
0	Run 1	Run 5	Run 9
10^{-5}	Run 2	Run 6	Run 10
10^{-3}	Run 3	Run 7	Run 11
10^{-1}	Run 4	Run 8	Run 12

Table 2.3: *The simulation parameters used to obtain the results for mesh selection. Rows in grey indicate run results presented in this section.*

In run 1 we set $\nu = 0$, corresponding to an inviscid fluid (thereby eliminating the diffusive term in eqn (2.34)). The evolutions of u_{rms} and ω_{rms} are presented in figures 2.2 and 2.3. All three of the considered meshes indicate that u_{rms} experiences marginal decay, which could be approximated using a straight flat line (consistent with a constant term) for larger values of t. The magnitude of ω_{rms}, on the other hand, appears to show a marginal growth over the duration of the run; we present the case of the evolution of ω_{rms} for the 32^3 box in figure 2.3, the results for the other two boxes being similar. If the growth of ω_{rms} for all three simulation boxes are presented together on one set of axes, the result appears to show that this quantity does not grow,

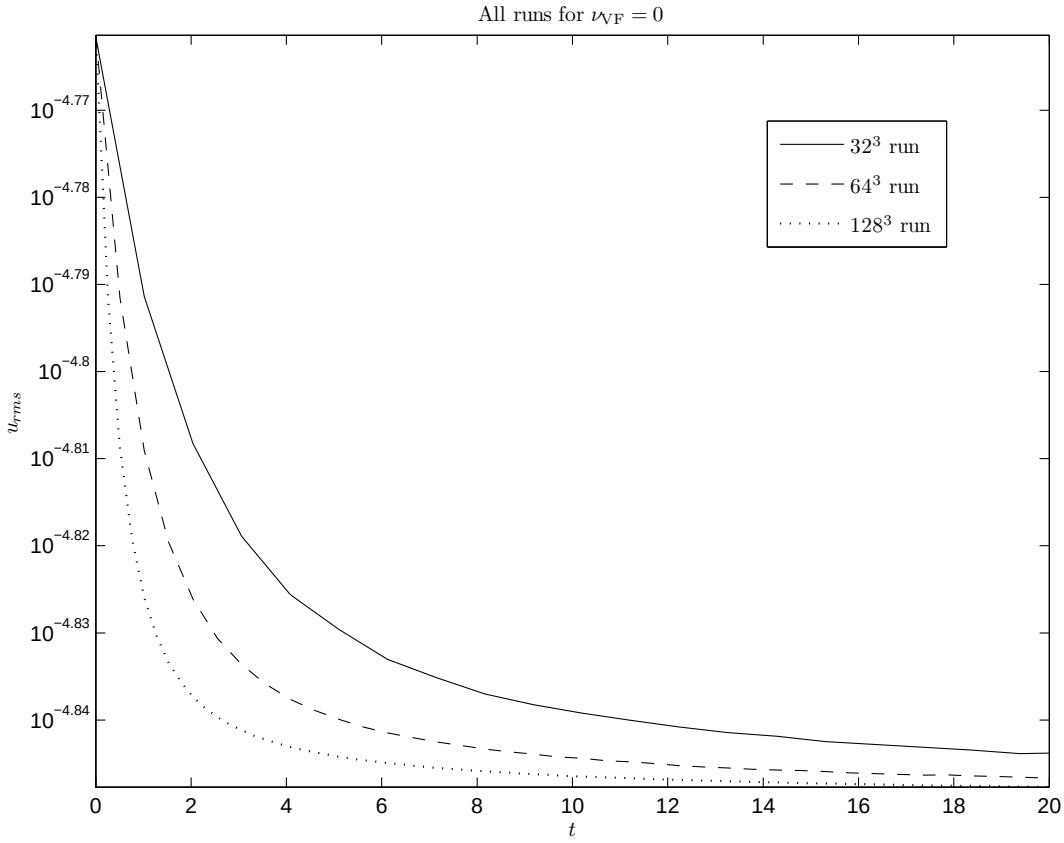

Figure 2.2: *Plots of u_{rms} versus time for all the 32^3, 64^3 and 128^3 boxes. Results for all boxes show a monotonically decaying solution, with the decay becoming gradually more pronounced for a finer mesh.*

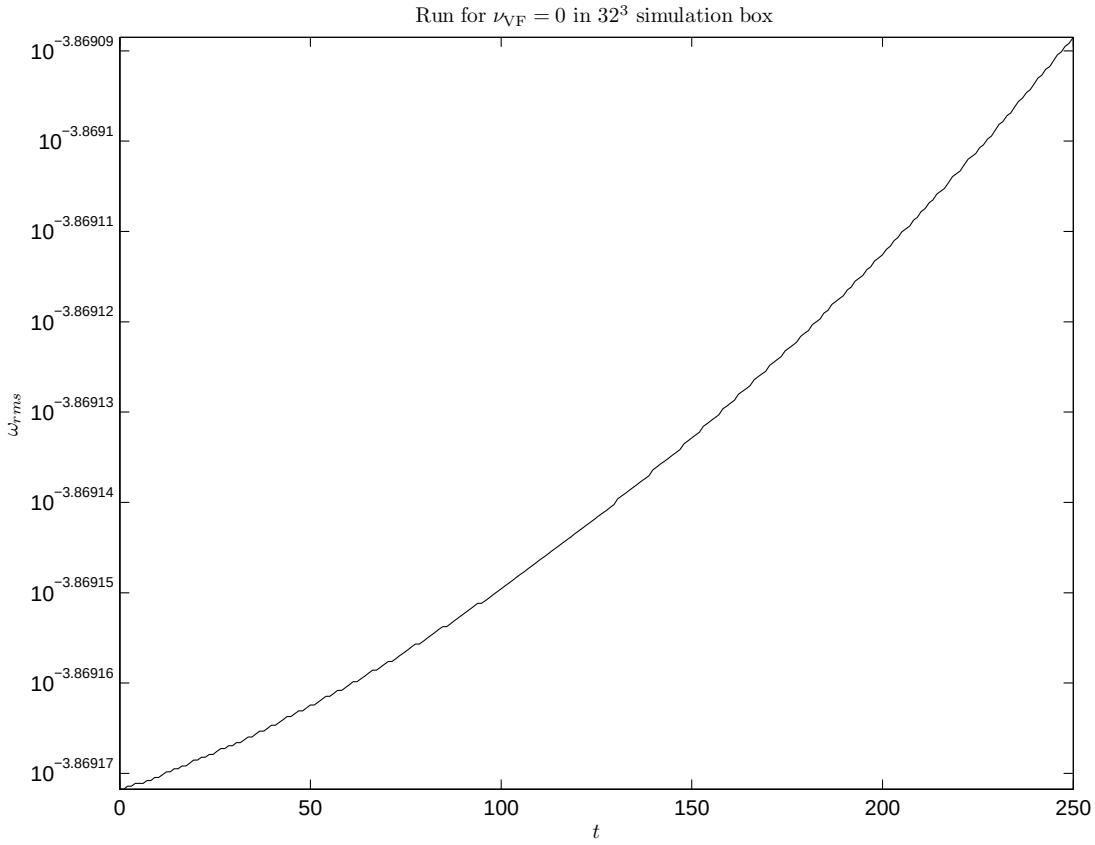

Figure 2.3: *The plots of ω_{rms} versus time for the 32^3 box. As can be seen, there is a very slow growth in ω_{rms} over the entire run, corresponding to the slow decay of u_{rms}. Results for the other meshes are similar to the 32^3 case, displaying very slow growth for ω_{rms} as well.*

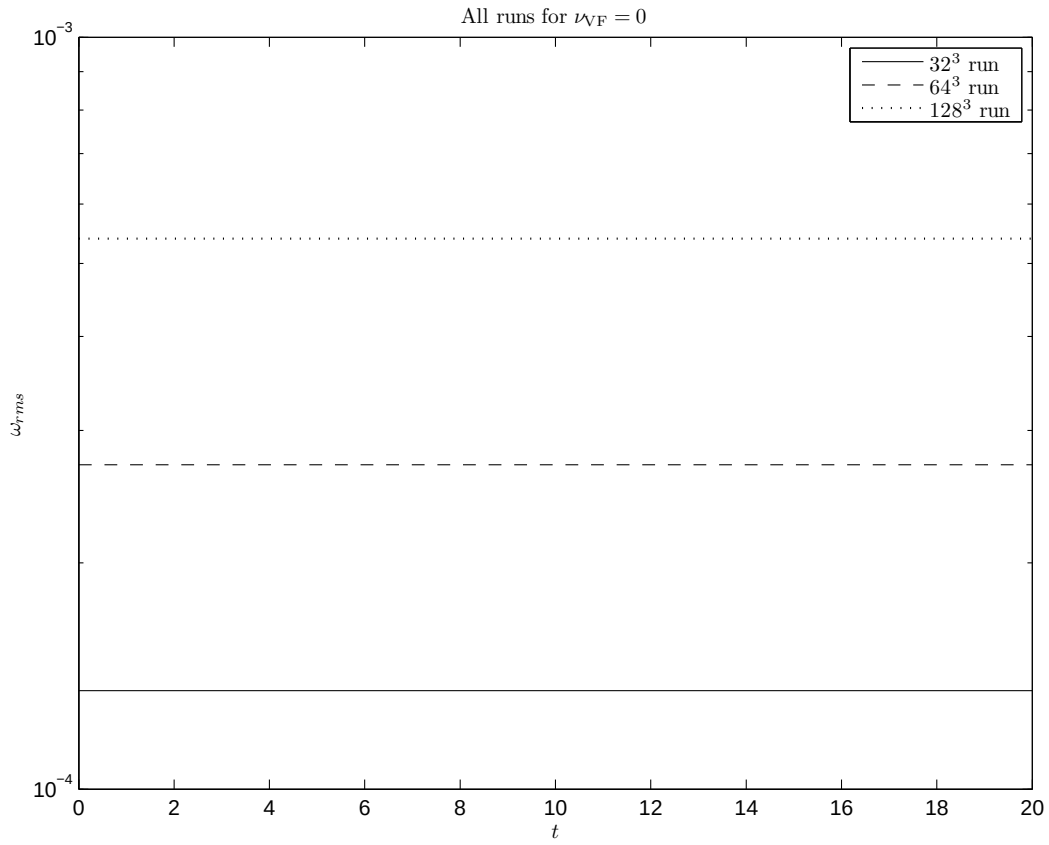

Figure 2.4: *The plots of ω_{rms} versus time for the 32^3, 64^3 and 128^3 boxes. Due to the small growths in ω_{rms} for the duration of the runs, the time evolution of this quantity appears to stay constant. Despite this appearance, however, ω_{rms} is indeed growing very slowly for all the simulation boxes.*

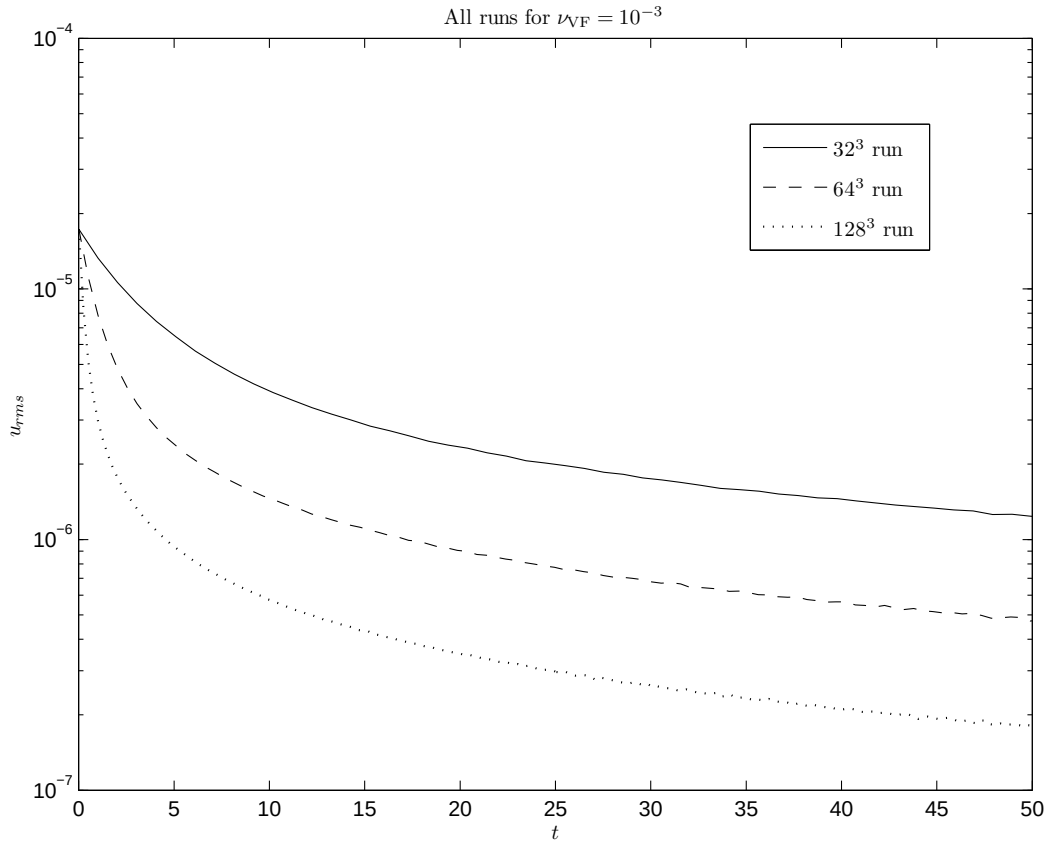

Figure 2.5: *The plots of u_{rms} versus time for the 32^3, 64^3 and 128^3 boxes. A monotonically decaying solution is again observed, with the decay becoming gradually more pronounced for a finer mesh. Here, the value of $\nu_{\rm VF} = 10^{-3}$ was chosen in order to simulate a non-conducting fluid with moderate viscosity in order to observe the resulting behaviour.*

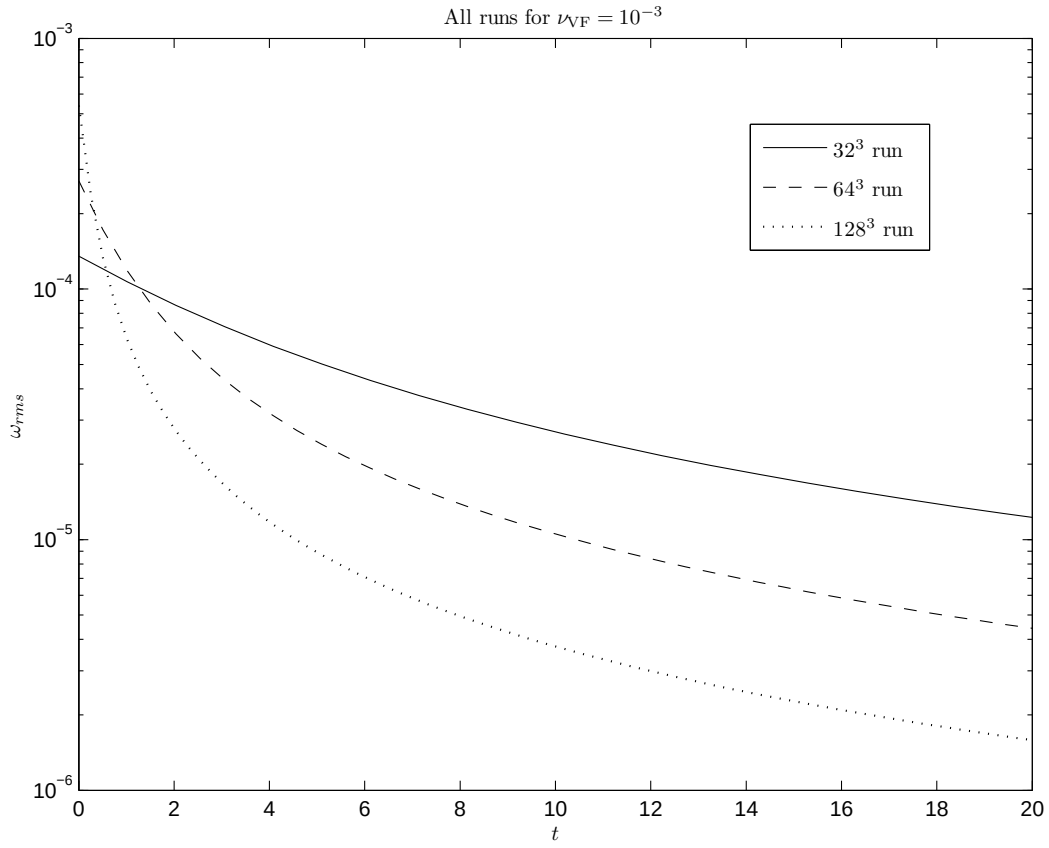

Figure 2.6: *The plots of ω_{rms} versus time for all the 32^3, 64^3 and 128^3 boxes. Monotonic decay in ω_{rms} is now present due to the effects of the diffusive term present in the evolution equations. Once more, the more pronounced decay of the 128^3 solution results in an initially strongerω_{rms} which then decays quickly. Again, the value of $\nu_{\mathrm{VF}} = 10^{-3}$ was chosen in order to simulate a non-conducting fluid with moderate viscosity in order to observe the resulting behaviour.*

but instead remains constant for the duration of the run (see figure 2.4). This is not true, however, due to the growth of ω_{rms} being very small for each of the simulation boxes. As can be seen in figure 2.4, the 128^3 box once more produces the strongest ω_{rms}.

For run 3 we set set $\nu_{\rm VF} = 10^{-3}$, corresponding to a viscous fluid where the corresponding eqn (2.34) has a non-vanishing diffusive term. For these runs, we wished to simulate a non-conducting fluid with a moderate value of viscosity in order to observe the resulting behaviour. We observe more pronounced decay patterns for u_{rms} for all the boxes under consideration, which is expected due to the effect of non-vanishing diffusion. Unlike in the previous case, we also note that ω_{rms} is now also decaying due to the presence of a non-vanishing diffusive term in its evolution equation. For the same reasons given previously, the 128^3 box produces the strongest initial ω_{rms} which then decays sharply, whilst the 32^3 box produces the weakest initial ω_{rms} which then decays slowly when compared to the other two boxes.

Disregarding the differences in strengths of u_{rms} and ω_{rms} produced by the three boxes under consideration, we note that the results obtained are qualitatively identical. Due to fineness of mesh, computation times for the 64^3 and 128^3 boxes are also very much longer than compared to the 32^3 box; the former two stopping at an earlier value of the simulation time t when compared to the 32^3 box. This earlier stopping is due to the time-steps being selected by the PENCIL CODE being markedly smaller due to the finer meshes, as can be deduced from expression (2.54). Overall, the 32^3 box is the most cost-effective choice in terms of time taken to carry out the simulations, as well as the amount of data obtained that is to be stored. Compared to the other boxes, though the time-step is markedly larger, the decay rate it presents in the simulations conducted is slower, thus still allowing us to capture potentially important physics given by the propagation equations, without losing much of the initial information.

For these reasons, we choose to use the 32^3 box as our preferred mesh for simulation. Having selected our preferred mesh resolution, we now turn to comparing the magnetic and viscous fluids in runs with varying values of the diffusivity and viscosity.

2.4.2 Simulating a Hydrodynamical Case: Checking the Analogy for Water at 20°C

Using the known viscosities from table 2.2, we first simulate the charged and non-charged fluids for the case of $\nu = \eta = 10^{-2}$, corresponding to the viscosity of water at 20°C. The results of the behaviours observed between the two fluids are then presented. Afterwards, the values of η and ν are adjusted in each run in such a way that three specific cases of an *effective* magnetic Prandtl number (defined as $\mathrm{Pr}_{\mathrm{M,eff}} = \nu_{\mathrm{VF}}/\eta_{\mathrm{PF}}$) are investigated: $\mathrm{Pr}_{\mathrm{M,eff}} \ll 1$, $\mathrm{Pr}_{\mathrm{M,eff}} = 1$ and $\mathrm{Pr}_{\mathrm{M,eff}} \gg 1$. Here, similar behaviour between the two fluids under consideration is investigated once more.

In these simulations we find it more instructive to define an effective magnetic Prandtl number rather than use the usual magnetic Prandtl number as here we consider the behaviour between two distinct fluids: charged and non-charged. Even though the charged and non-charged fluids themselves need to have equal values of the kinematic viscosity, ν, so that $\nu_{\mathrm{VF}} = \nu_{\mathrm{PF}}$ so that the viscosities of the two fluids remain consistent throughout, we still make the distinction between the two in order to emphasise the difference between the two fluids under consideration.

The usual magnetic Prandtl and Reynolds numbers are important dimensionless parameters in MHD simulations. The magnetic Reynolds number, Re_{M}, which characterises the importance of induction or advection to diffusion in the eqns (2.27b) is useful in determining whether the growth of a magnetic field could possibly be sustained in a given system. Typically, if $\mathrm{Re}_{\mathrm{M}} \ll 1$, the effects of diffusion will be greater than that of advection/induction and no magnetic field will grow due to it being diffused through the fluid quickly. Conversely, if $\mathrm{Re}_{\mathrm{M}} \gg 1$, then the effects of advection/induction will be greater than that of diffusion and allow a magnetic field to grow and be sustained. In stars, for example, the effects of diffusion are generally small and combined with the large length scales, Re_{M} is generally large and allows magnetic fields to grow and be sustained.

Similarly, the magnetic Prandtl number, Pr_{M}, characterises the importance of kinematic viscosity to magnetic diffusion in a given system. Using this quantity, it is possible to determine whether dynamo action may or may not be possible within such a system. Typically, this quantity is studied in the context of small-scale dynamos, where it is generally investigated in the range $\mathrm{Pr}_{\mathrm{M}} \ll 1$ in order to determine whether dynamo action on the small scales may at all be possi-

ble. The relationship between $\mathrm{Pr_M}$ and $\mathrm{Re_M}$ is also often investigated in the context of dynamo action in a given system [24]. In stars like the sun, $\mathrm{Pr_M}$ is typically much less than unity, while in galaxies it is typically much greater than unity ($\mathrm{Pr_M} \sim 10^{11}$) due to the long mean free path [24].

Though we do not formally investigate the onset of dynamo action in the context of our simulations, we calculate $\mathrm{Pr_{M,eff}}$ for each run and group the results of the runs according to this quantity in order to investigate whether similar behaviour between u_{rms} and A_{rms} and ω_{rms} and B_{rms} still exists even in the cases where $\nu_{\mathrm{VF}} \neq \eta$ (i.e. where $\mathrm{Pr_{M,eff}} \neq 1$).

Simulation parameters together with the associated magnetic Reynolds number, $\mathrm{Re_M} \equiv u_{rms}L/\eta$, for that run are summarized in table 2.4.

Run	ν	η	$\mathrm{Pr_{M,eff}}$	$\mathrm{Re_M}$
SP	10^{-2}	10^{-2}	1	N/A
14	10^{-3}	10^{-1}	10^{-2}	6.7317×10^{-5}
15	10^{-3}	10^{-3}	1	0.0031
16	10^{-3}	10^{-5}	10^{2}	0.3063

Table 2.4: Summary of the simulation parameters together with the associated magnetic Reynolds number for that run used to obtain the results presented in this work.

The results of the simulation for the case of $\eta = \nu_{\mathrm{VF}} = 10^{-2}$, corresponding to water at 20°C, are presented in figures 2.7 and 2.8. We note that without the source terms present in systems (2.27) and (2.28), and together with a vanishing Lorentz force, the terms of the equations in the two systems may be compared directly. This allows us to also make a direct comparison between u_{rms} and A_{rms}, and ω_{rms} and B_{rms}, without the need for a comparison taking into account the sign difference of the source terms, as discussed previously. In the presentation of the results here, we make the comparisons of u_{rms} to A_{rms}, and ω_{rms} to B_{rms}.

Provided that $\nu_{\mathrm{VF}} = \eta$, we should expect to see a linear relationship between u_{rms} and A_{rms},

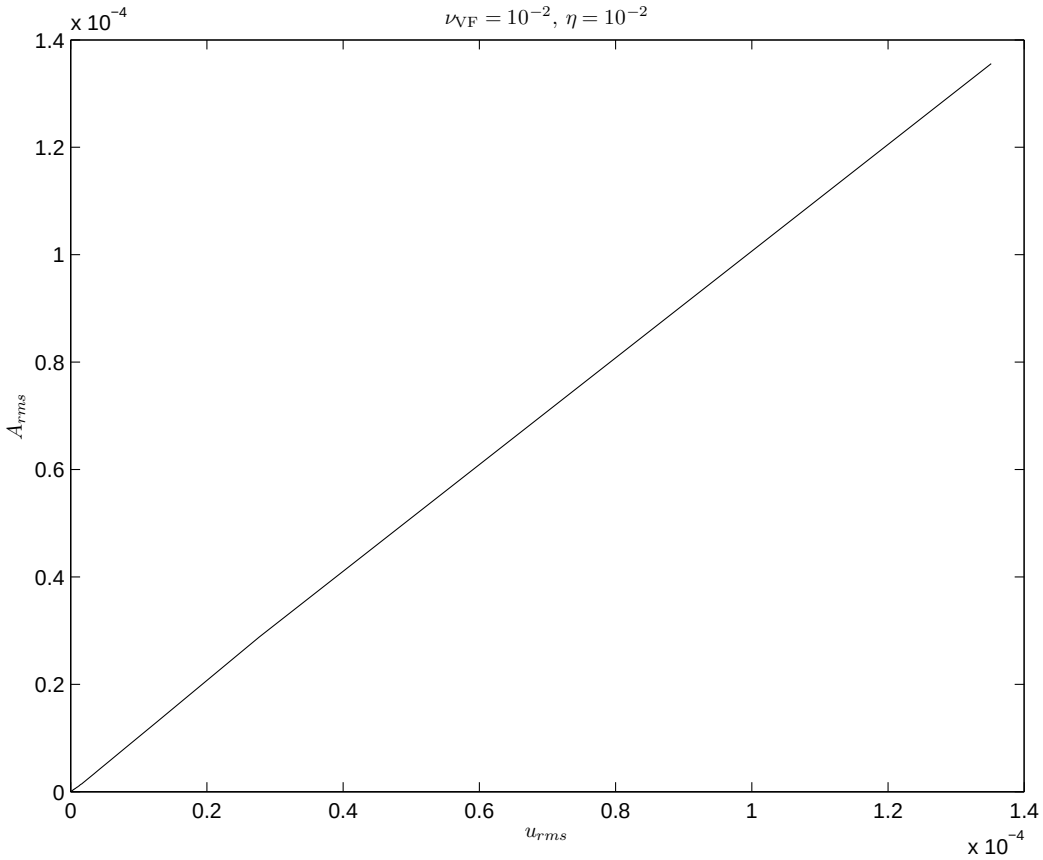

Figure 2.7: *The plot of u_{rms} versus A_{rms} for the special case of $\nu = \eta = 10^{-2}$, corresponding to water. Here, $\mathrm{Pr}_{\mathrm{M,eff}} = 1$. Due to $\nu_{\rm VF} = \eta$, there is indeed a linear relationship between u_{rms} and A_{rms}, showing evidence of an analogy between the magnetic and viscous fluids for these values of the diffusivity and viscosity.*

and ω_{rms} and B_{rms}, which would indicate that the four respective fields are growing at the same rate.

Examining figures 2.7 and 2.8, we see that for the case of $\nu_{\rm VF} = \eta$, both u_{rms} and A_{rms}, as well as ω_{rms} and B_{rms}, exhibit a linear relationship when compared to each other. This suggests that the idea of an analogue in this hydrodynamical case is indeed possible due to the charged and non-charged fluids exhibiting similar behaviour to each other.

From this, we can deduce two possibilities:

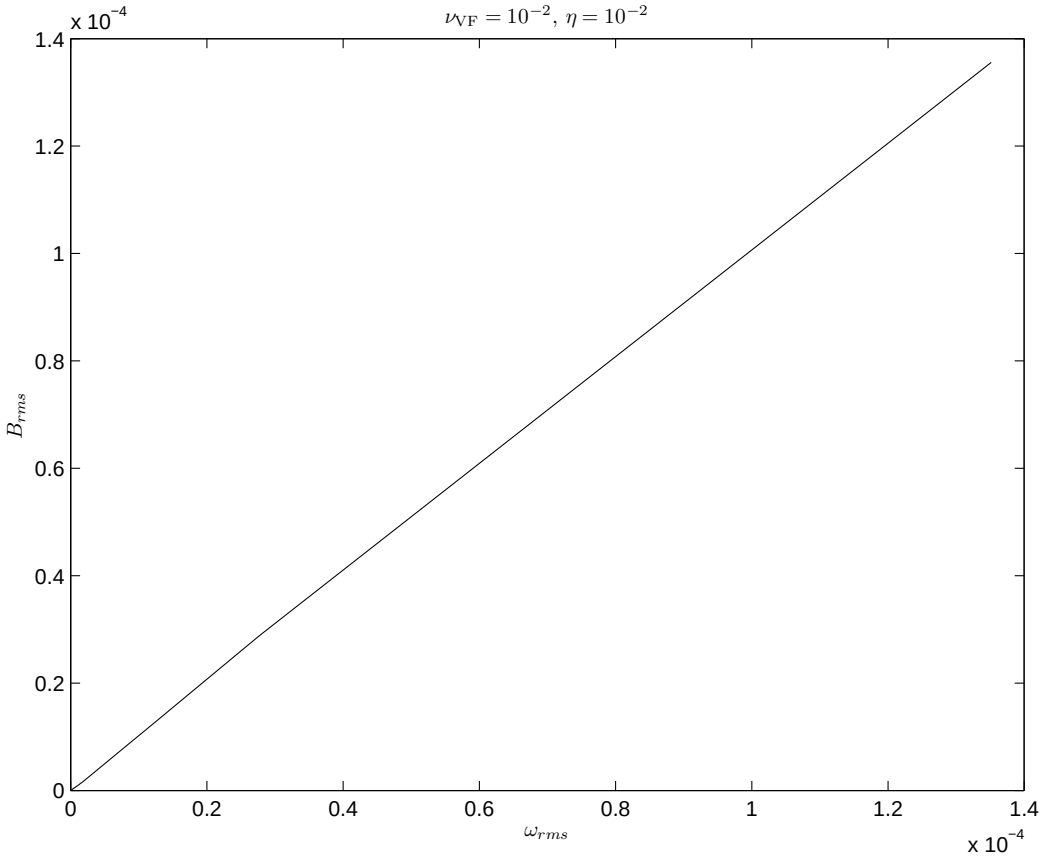

Figure 2.8: *The plot of ω_{rms} versus B_{rms} for the special case of $\nu_{\rm VF} = \eta = 10^{-2}$, corresponding to water. Here, $\mathrm{Pr}_{\rm M,eff} = 1$. Due to $\nu_{\rm VF} = \eta$, there is indeed a linear relationship between ω_{rms} and B_{rms} is observed once more, showing evidence of an analogy between the magnetic and viscous fluids for these values of the diffusivity and viscosity.*

1. For the case of identical initial conditions and equal values of the diffusivity and viscosity, without the presence of any source terms in the evolution equations, it is possible to observe similar behaviour between the charged and non-charged fluids that is indicative of an analogy, or,

2. Initial conditions, as well as the values of the diffusivity and viscosity, may be simulated on a case-by-case basis and fine-tuned in order to recover the linear relationship that is observed between u_{rms} and A_{rms}, and ω_{rms} and B_{rms}, even when the values of the diffusivity and viscosity are *not* equal to each other. From the point-of-view of the equations, this latter case corresponds to the dissipative terms in systems 2.27) and (2.28) having unequal magnitudes.

Using the above points as motivation, we proceed to investigate the cases of charged and non-charged fluids having different values of the magnetic diffusivity and kinematic viscosity, as well as having equal values of these parameters that are different to that of the hydrodynamical case considered here. For ease of reference, the results from these simulations will be interpreted in terms of the effective magnetic Prandtl number defined previously, and we shall discuss all behaviour observed, including that which provides evidence supporting the analogy between the two fluids based on this quantity.

2.4.3 Investigating the Analogy for the Case of $\mathrm{Pr}_{\mathrm{M,eff}} \neq 1$

Having confirmed similar behaviour between the charged and non-conducting fluid for the hydrodynamical case, we now turn to investigating the cases for comparing these fluids when $\mathrm{Pr}_{\mathrm{M,eff}} \neq 1$.

2.4.3.1 Evolution of the Velocity and Vorticity Fields

We first consider the temporal evolution of u_{rms} and ω_{rms} with respect to different values of ν_{VF}. In particular, we are interested in conditions that we would lead to growing field strengths for both quantities. Note once more that due to the assumption of a vanishing Lorentz Force in eqns (2.34), the magnetic field is unable to interact with the fluid. Physically, this corresponds to a

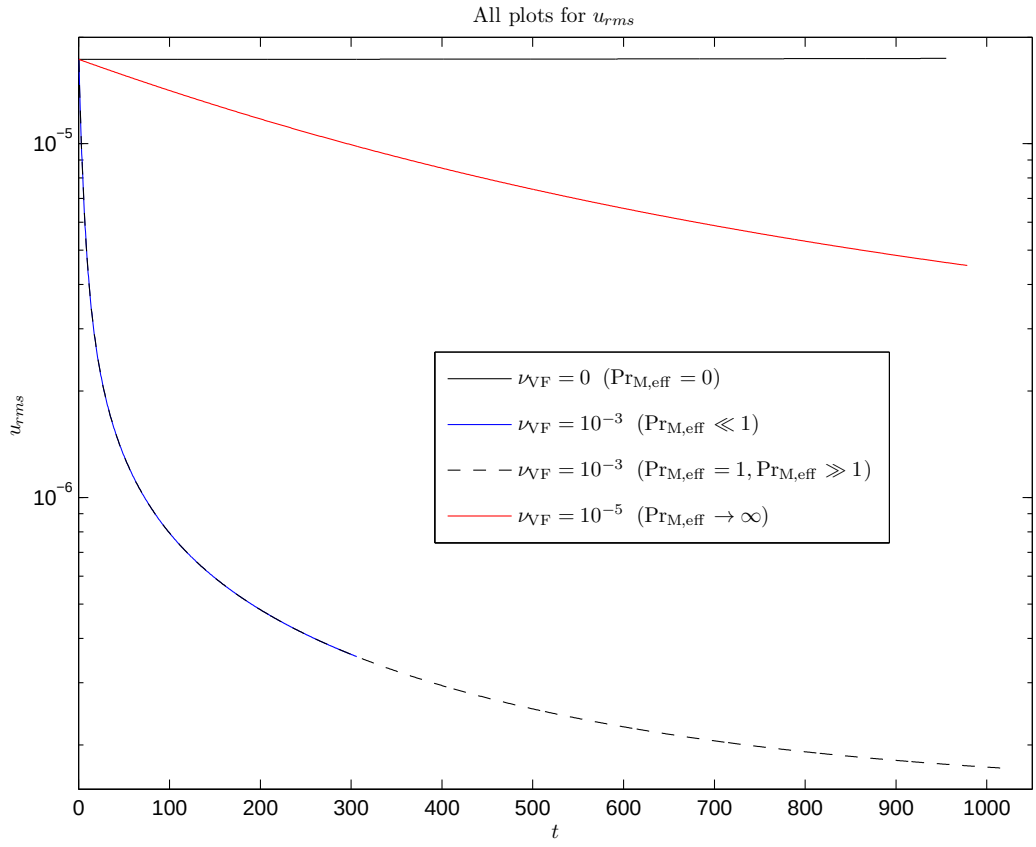

Figure 2.9: *The plots of u_{rms} versus time for all values of $\mathrm{Pr}_{\mathrm{M,eff}}$. It is clear that for strong dissipation, the rms strength decays. Effective magnetic Prandtl numbers are displayed in order to connect the relevant u_{rms} solution to its corresponding A_{rms} counterpart(s).*

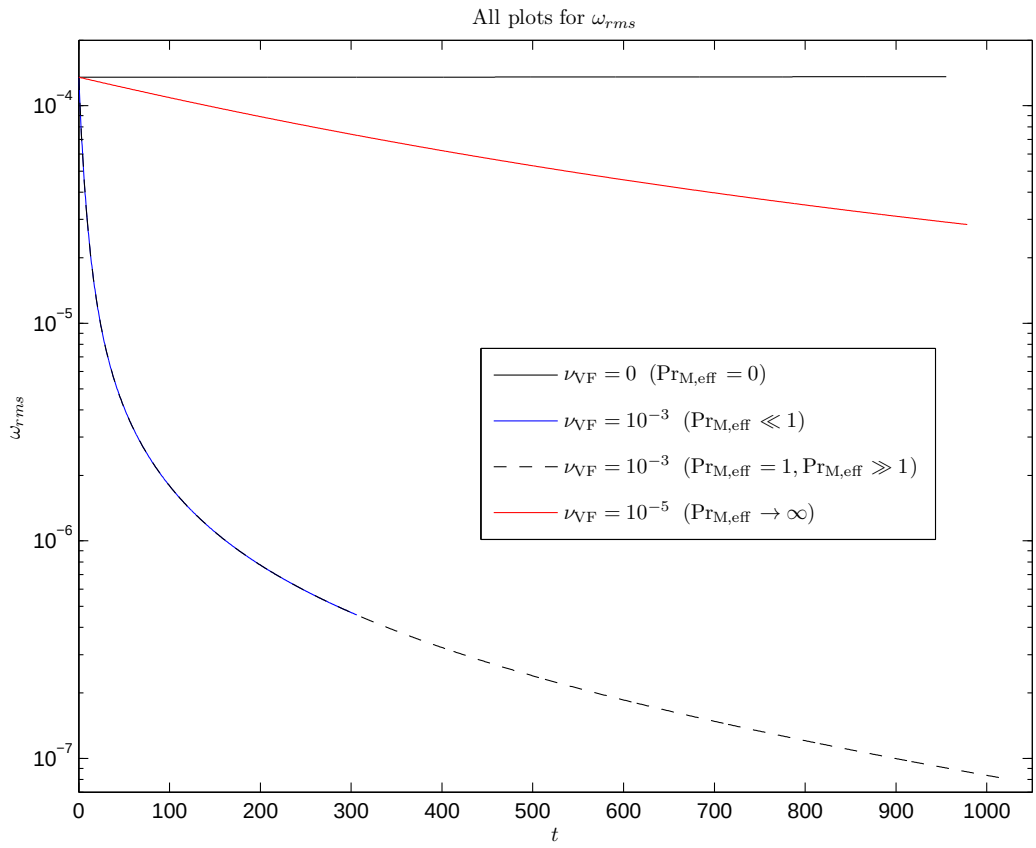

Figure 2.10: *The plots of ω_{rms} versus time for all values of ${\rm Pr}_{\rm M,eff}$. It is clear once more that for strong dissipation, the rms strength decays. As before, effective magnetic Prandtl numbers are displayed in order to connect the relevant ω_{rms} solution to its corresponding $B_{\rm rms}$ counterpart(s).*

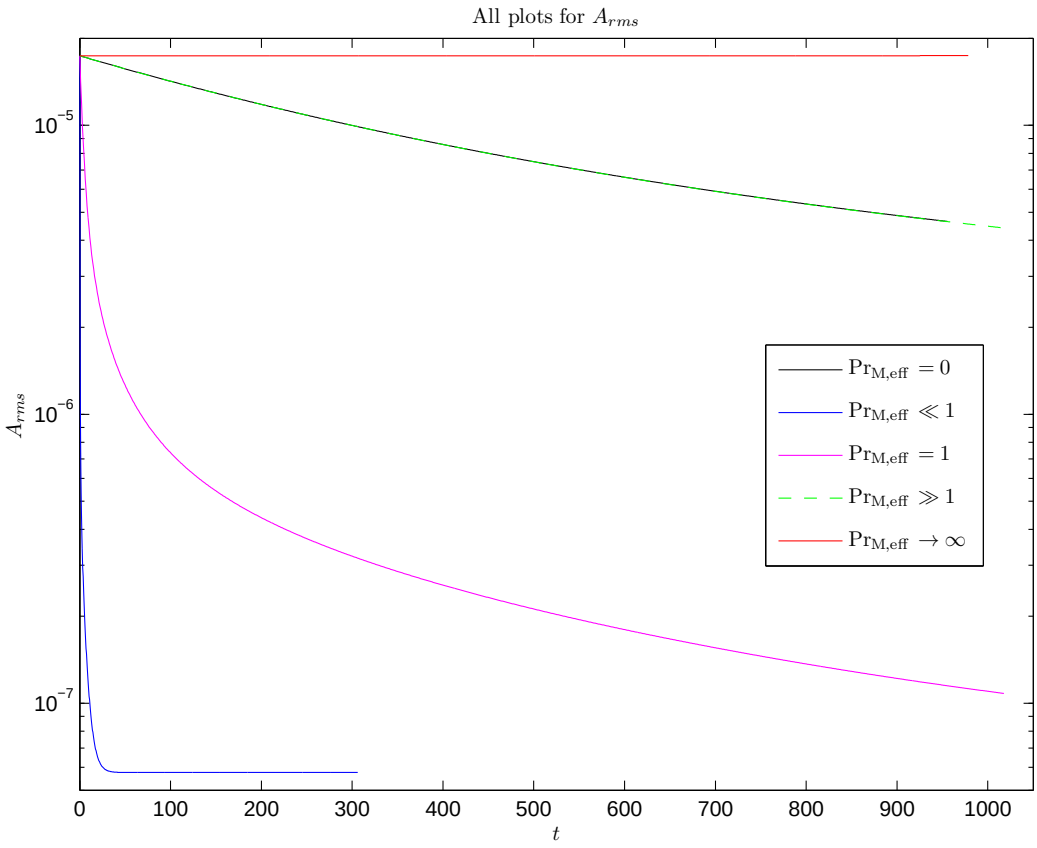

Figure 2.11: *The plots of A_{rms} versus time for all values of $\mathrm{Pr}_{\mathrm{M,eff}}$. It is clear that for strong dissipation, the rms strength decays. Due to the runs for $\mathrm{Pr}_{\mathrm{M,eff}} = 0$ and $\mathrm{Pr}_{\mathrm{M,eff}} \gg 1$ having little difference between them, their lines (the green and black dashed) appear superimposed on each other. This behaviour can more closely be seen in figure 2.12.*

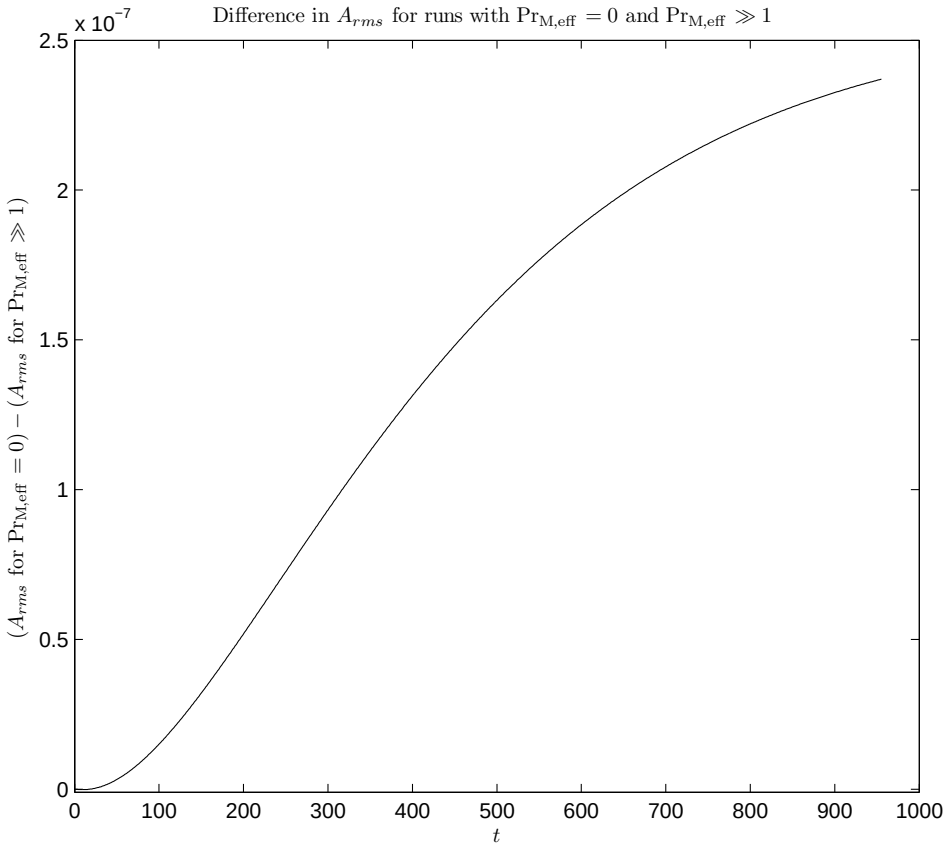

Figure 2.12: *The difference in A_{rms} between the runs where $\mathrm{Pr}_{\mathrm{M,eff}} = 0$ and $\mathrm{Pr}_{\mathrm{M,eff}} \gg 1$ versus time. As described before, there is evidence of A_{rms} for the $\mathrm{Pr}_{\mathrm{M,eff}} = 0$ run becoming stronger than that for the $\mathrm{Pr}_{\mathrm{M,eff}} \gg 1$ run due to the difference in A_{rms} for these two runs gradually becoming larger over time. This phenomenon appears to happen very early in the run, before $t = 100$.*

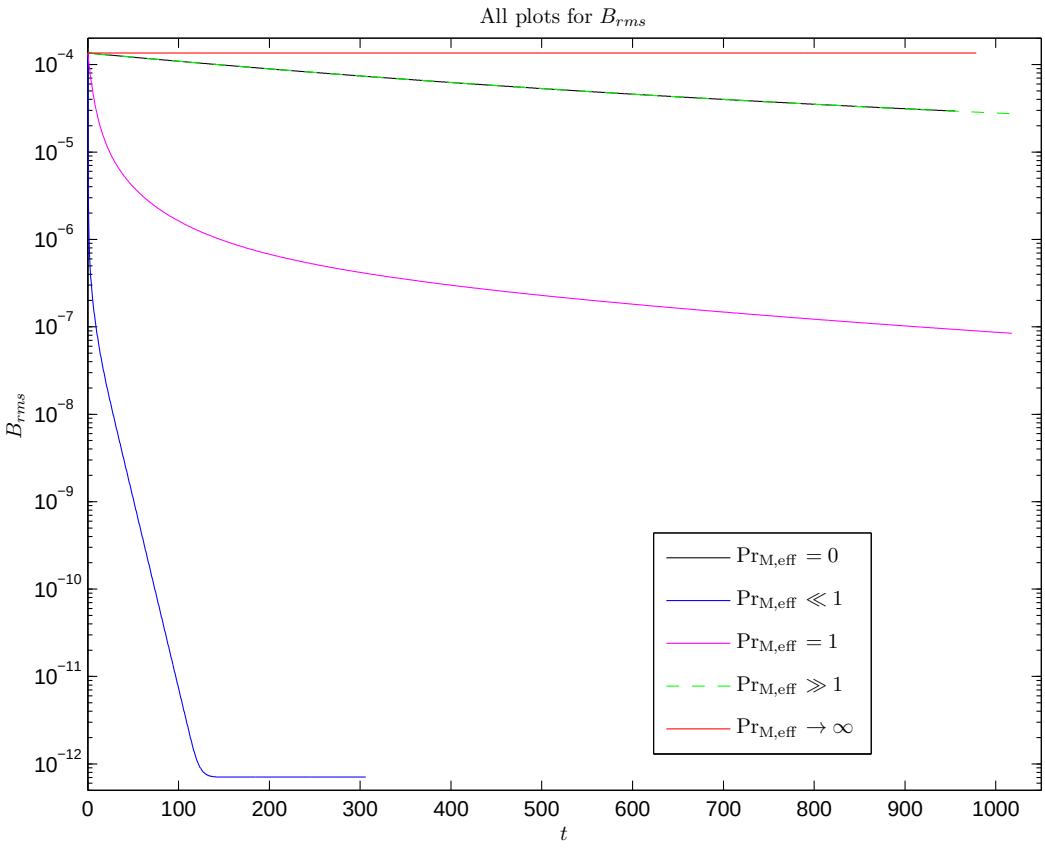

Figure 2.13: *The plots of* $\mathbf{B}_{\mathrm{rms}}$ *versus time for all values of* $\mathrm{Pr}_{\mathrm{M,eff}}$. *It is clear that for strong dissipation, the rms strength decays. Due to the runs for* $\mathrm{Pr}_{\mathrm{M,eff}} = 0$ *and* $\mathrm{Pr}_{\mathrm{M,eff}} \gg 1$ *having little difference between them, their lines (the green and black dashed) appear superimposed on each other. This behaviour can more closely be seen in figure 2.14.*

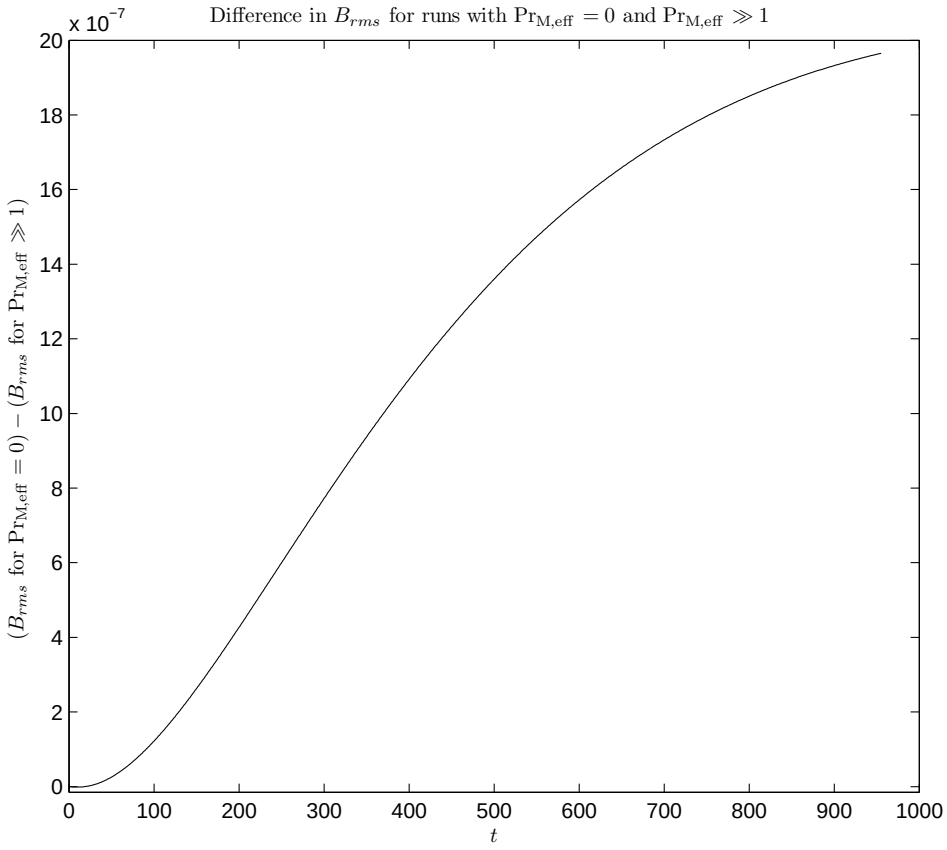

Figure 2.14: *The difference in B_{rms} between the runs where $\mathrm{Pr}_{\mathrm{M,eff}} = 0$ and $\mathrm{Pr}_{\mathrm{M,eff}} \gg 1$ versus time. Again, there is evidence of B_{rms} for the $\mathrm{Pr}_{\mathrm{M,eff}} = 0$ run becoming stronger than that for the $\mathrm{Pr}_{\mathrm{M,eff}} \gg 1$ run due to the difference in B_{rms} for these two runs gradually becoming larger over time. This phenomenon once more appears to happen very early in the run, before $t = 100$.*

system in which the effects of the back-reaction by the magnetic field on the fluid are negligible. In light of this it is more sensible to discuss the temporal evolution of u_{rms} (and hence ω_{rms}) with respect to different values of ν_{VF} rather than with respect to η.

Examining the temporal evolution behaviour displayed by the velocity and vorticity fields in figures 2.9 and 2.10, it is clear that as $\nu_{\mathrm{VF}} \rightarrow 0$, the exponential decay in the rms strengths observed becomes visibly slower until eventually the value of $\nu_{\mathrm{VF}} = 0$ is reached, producing exponentially-growing rms field strengths. From the point-of-view of eqns (2.34), this behaviour is expected, as ν_{VF} essentially amplifies the effect of the diffusive term in a particular way.

As we have chosen to examine the case of systems (2.27) and (2.28) without the presence of their respective source terms, thus dropping the pressure term from eqns (2.34), we also observe no accelerated decay in u_{rms} and ω_{rms} which may be attributed to the presence of these terms.

We now move to consider the evolution of A_{rms} and B_{rms}.

2.4.3.2 Evolution of the magnetic vector potential and magnetic flux density

Results of simulating A_{rms} and B_{rms} for different values of $\mathrm{Pr}_{\mathrm{M,eff}}$ are displayed in figures 2.11 and 2.13. From the temporal evolution behaviour of both A_{rms} and B_{rms}, it appears that as $\mathrm{Pr}_{\mathrm{M,eff}}$ increases, the rate of the exponential decay observed in the rms strengths for both fields becomes progressively slower until a turning point is reached beyond which the fields begin to grow.

The cases for $\mathrm{Pr}_{\mathrm{M,eff}} = 0$ and $\mathrm{Pr}_{\mathrm{M,eff}} \gg 1$ are particularly interesting: initially the rms strengths of A_{rms} and B_{rms} for the case of $\mathrm{Pr}_{\mathrm{M,eff}} \gg 1$ are somewhat greater than the rms strengths of these quantities for the case of $\mathrm{Pr}_{\mathrm{M,eff}} = 0$. However, after a finite amount of time (around 17.4s–17.6s for A_{rms} and 18.2s – 18.4s for B_{rms}, referring to figures 2.12 and 2.14) the strengths of A_{rms} and B_{rms} for the case of $\mathrm{Pr}_{\mathrm{M,eff}} = 0$ end up growing larger than those for the case of $\mathrm{Pr}_{\mathrm{M,eff}} \gg 1$ for the remainder of the run. This may be seen in figures 2.12 and 2.14), where we have plotted the difference between A_{rms} for $\mathrm{Pr}_{\mathrm{M,eff}} = 0$ and $\mathrm{Pr}_{\mathrm{M,eff}} \gg 1$, as well as for B_{rms} in the same manner.

It is evident that both A_{rms} and B_{rms} for $\mathrm{Pr}_{\mathrm{M,eff}} \gg 1$ start out stronger than those for $\mathrm{Pr}_{\mathrm{M,eff}} = 0$ (giving a negative difference), but are soon outgrown in strength as time passes, leaving A_{rms}

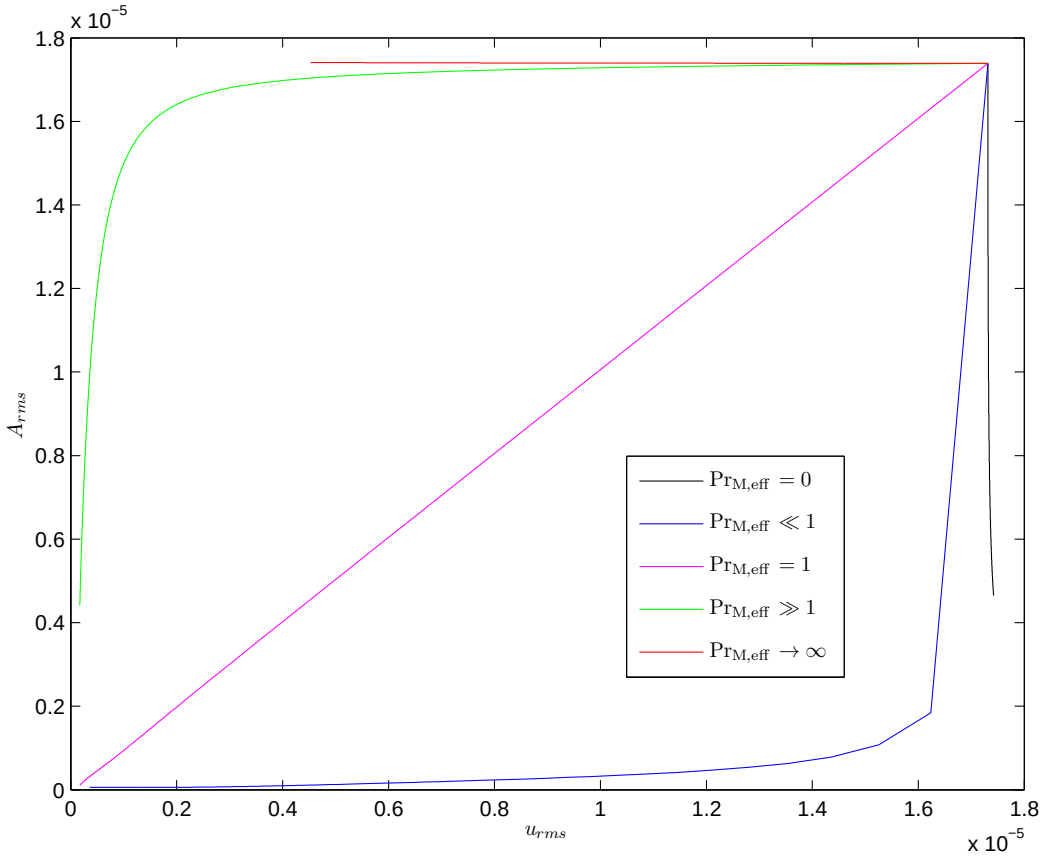

Figure 2.15: u_{rms} *versus* A_{rms} *graphically. The special cases of* $\mathrm{Pr}_{\mathrm{M,eff}} = 0$ *and* $\mathrm{Pr}_{\mathrm{M,eff}} \to \infty$ *appear to form an "envelope" around the cases of* $\mathrm{Pr}_{\mathrm{M,eff}} = 1$ *and* $\mathrm{Pr}_{\mathrm{M,eff}} \neq 1$*; it is apparent that for* $\mathrm{Pr}_{\mathrm{M,eff}} = 1$*, the analogy holds exactly.*

and B_{rms} for $\mathrm{Pr}_{\mathrm{M,eff}} = 0$ dominant for the remainder of the run (and thus a growing, positive difference). This is not easily seen in figures 2.11 and 2.13 due to the difference between the strengths of A_{rms} and B_{rms} for these fields being very small; the lines describing their temporal evolution appear to be superimposed onto each other as a result thereof. The final difference in strength can explain the apparent contradiction by recalling that we had observed exponentially-growing field strengths for u_{rms} and ω_{rms} for the case of $\nu = 0$ (and hence $\mathrm{Pr}_{\mathrm{M,eff}} = 0$). As the velocity field interacts with the magnetic field, we would expect to see a slightly stronger magnetic field rms strength for the case of $\mathrm{Pr}_{\mathrm{M,eff}} = 0$ after some time, as the velocity field rms strength is growing exponentially, despite the exponential decay in rms strength of the former field.

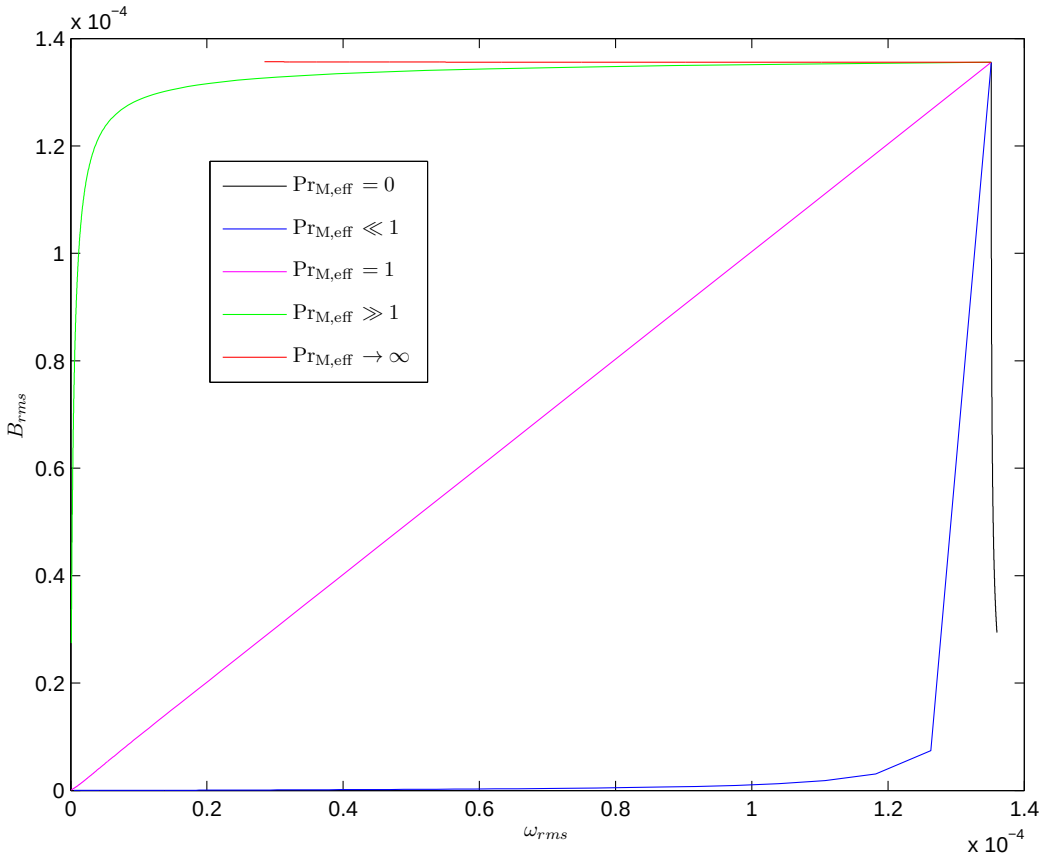

Figure 2.16: ω_{rms} *versus* B_{rms} *graphically. The special cases of* $\mathrm{Pr}_{\mathrm{M,eff}} = 0$ *and* $\mathrm{Pr}_{\mathrm{M,eff}} \to \infty$ *again appear to form an "envelope" around the cases of* $\mathrm{Pr}_{\mathrm{M,eff}} = 1$ *and* $\mathrm{Pr}_{\mathrm{M,eff}} \neq 1$. *Once more it is apparent that the analogy holds exactly for* $\mathrm{Pr}_{\mathrm{M,eff}} = 1$.

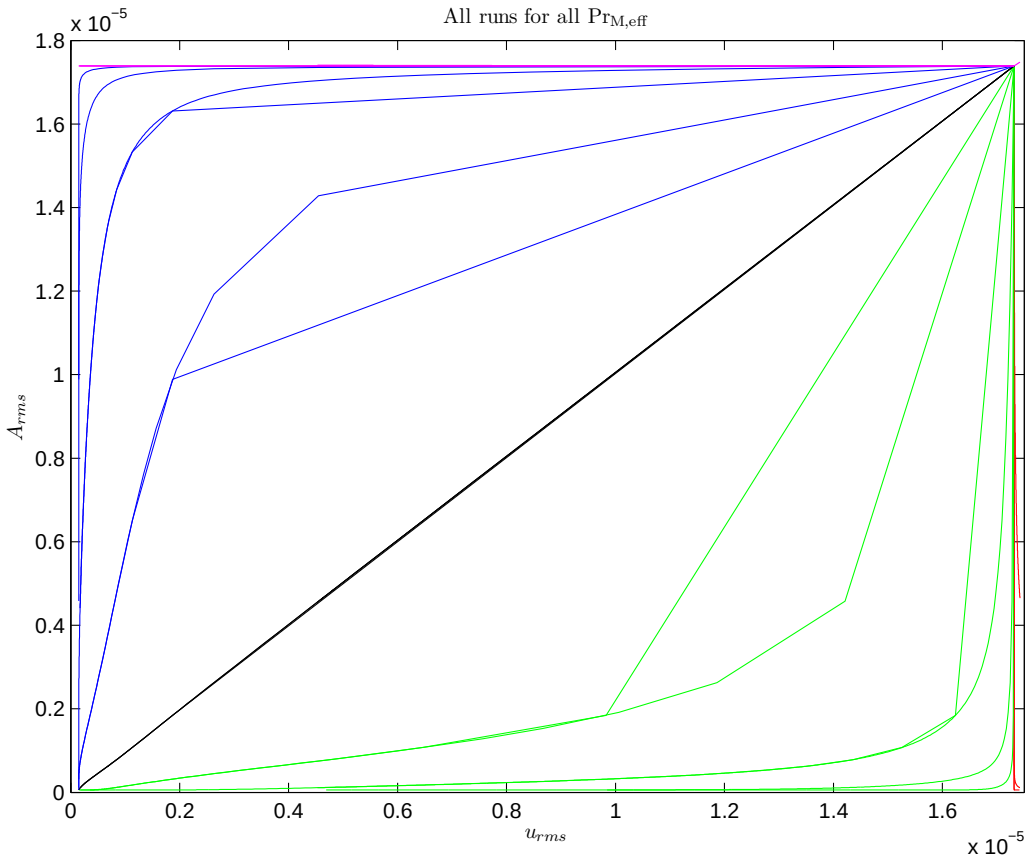

Figure 2.17: *u_{rms} versus A_{rms} graphically for all runs considered. It is clear that the analogous relationship between u_{rms} versus A_{rms} holds exactly for the cases of* $\mathrm{Pr_{M,eff}} = 1$.

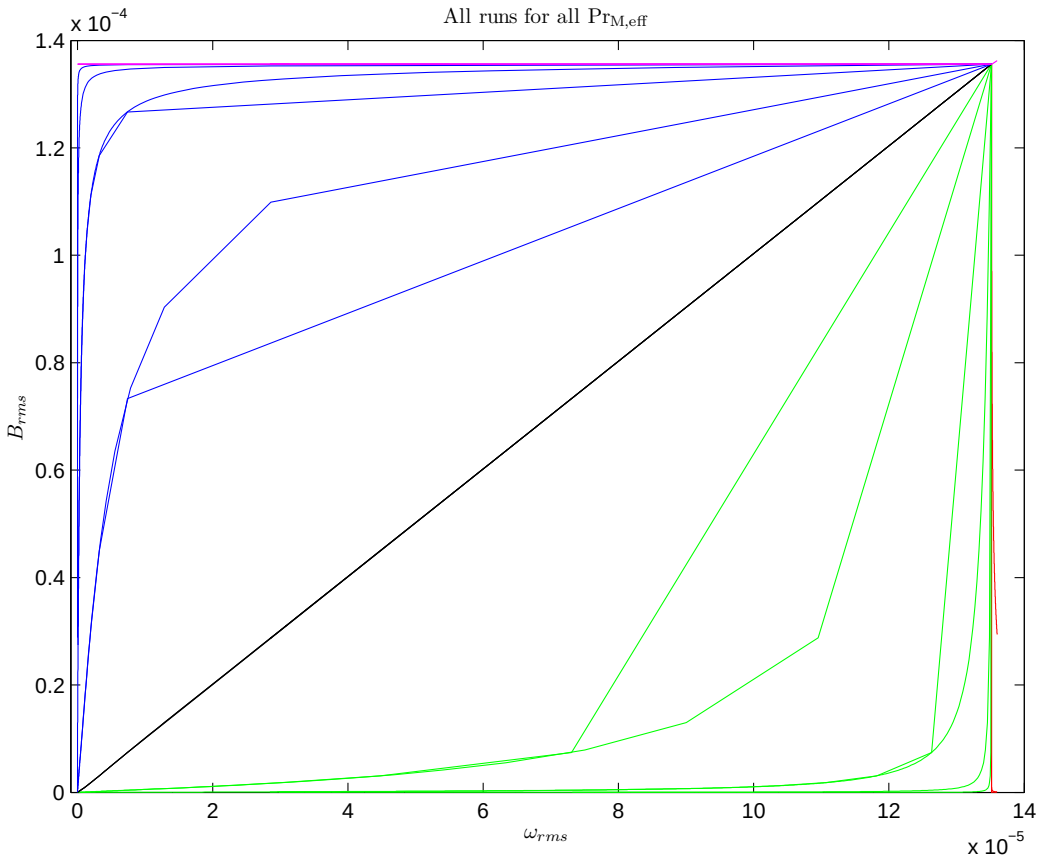

Figure 2.18: *ω_{rms} versus B_{rms} graphically. Again, it is clear that the analogous relationship between ω_{rms} versus B_{rms} holds exactly for the cases of* $\mathrm{Pr_{M,eff}} = 1$.

2.4.3.3 The analogy between the vorticity and magnetic fields

We now discuss the analogy between the equations of system (2.27), as well as their counterparts in system (2.28). The simulation results discussed in this section are presented in figures 2.15 and 2.16.

As was noted for the hydrodynamical case, the analogy between the vorticity and magnetic fields (as well as the velocity and magnetic vector potential fields by extension) appears to hold true when $\mathrm{Pr}_{\mathrm{M,eff}} = 1$ due to similar behaviour being observed between the charged and non-charged fluids. It can also be seen that as $\omega_{rms} \to 0$, $-B_{\mathrm{rms}} \to 0$, indicating a correlation between the growth or decay of the rms strength of the vorticity field and the rms strength of the magnetic field. Although the linear relationship breaks down for the cases where $\mathrm{Pr}_{\mathrm{M,eff}} \neq 1$, the aforementioned correlation still holds, with the straight line now being replaced by curved lines instead. This curved-line relationship may be explained simply by noting that due to having $\nu_{\mathrm{VF}} \neq \eta$, there is the opportunity that one quantity would grow or decay faster than the other.

Presented in figures 2.17 and 2.18 are the cases of u_{rms} versus A_{rms} and ω_{rms} versus B_{rms} for all of the simulations that were conducted. Again, it can be seen that as $\mathrm{Pr}_{\mathrm{M,eff}} \to 0$ and $\mathrm{Pr}_{\mathrm{M,eff}} \to \infty$, the linear relationships seen for the case of $\mathrm{Pr}_{\mathrm{M,eff}} = 1$ vanish. It clear that as $\mathrm{Pr}_{\mathrm{M,eff}}$ approaches the bounds at zero and infinity, these non-linear curves appear to form an "envelope" around the cases for the various $\mathrm{Pr}_{\mathrm{M,eff}}$.

2.4.4 Simulations Including the Source Terms

We now finally include the source terms from systems (2.27) and (2.28) into our simulations and explore the possibility of an analogue of a thermally-generated magnetic field. As before, a summary of the simulation parameters for these runs is presented in table 2.5. Simulations were conducted using a seed field of low-moderate strength (10^{-5}), along with a plasma ionization factor of $\chi = 0$. Due to the presence of a seed field for the battery term to operate on, no numerical forcing was introduced via eqns (2.34). Once more, we considered a 32^3 simulation box with periodic boundaries.

Run	ν	η	$\mathrm{Pr}_{\mathrm{M,eff}}$
B1	10^{-3}	10^{-3}	1
B2	10^{-5}	10^{-3}	10^{-2}
B8	10^{-5}	10^{-5}	1
B15	10^{-6}	10^{-6}	1
B21	10^{-6}	10^{-7}	10
B22	10^{-7}	10^{-7}	1
B23	10^{-8}	10^{-7}	10^{-1}
B29	10^{-8}	10^{-8}	1
B35	10^{-8}	10^{-10}	10^{2}
B36	10^{-10}	10^{-10}	1

Table 2.5: Summary of the simulation parameters for the case of the systems (2.27) and (2.28) with their respective source terms, together with the associated magnetic Reynolds, Prandtl and battery numbers for the runs used to obtain the results presented in this section.

The results of the simulations are presented in figures 2.19 – 2.24. Here, we consider the behaviour of B_{rms} and ω_{rms} based on system (2.27). For ease of reference, this system is repeated once more below:

$$\frac{\partial \boldsymbol{\omega}_{\mathrm{VF}}}{\partial t} = \nabla \times (\mathbf{u}_{\mathrm{VF}} \times \boldsymbol{\omega}_{\mathrm{VF}}) + \nu \nabla^2 \boldsymbol{\omega}_{\mathrm{VF}} - \frac{\nabla p_{\mathrm{VF}} \times \nabla \rho_{\mathrm{VF}}}{{\rho_{\mathrm{VF}}}^2}$$

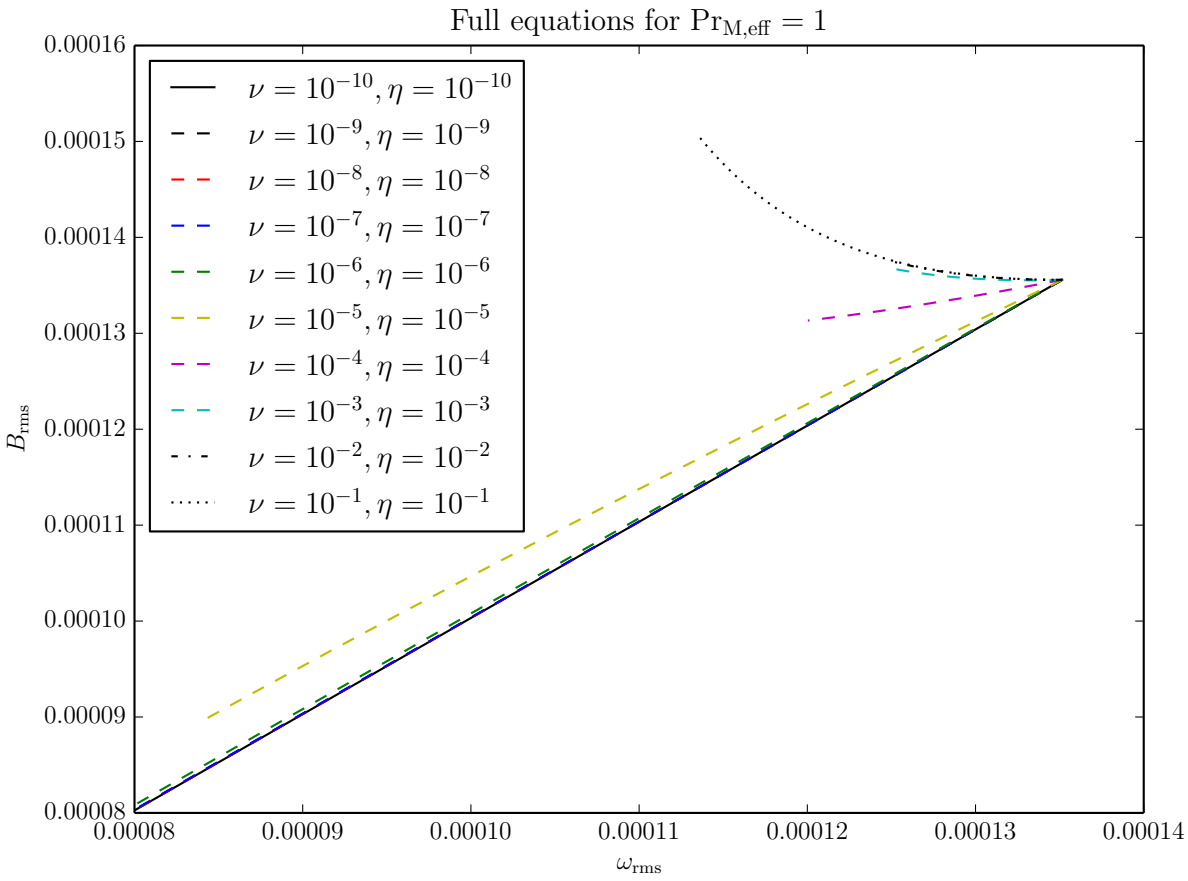

Figure 2.19: We have plotted B_{123} against ω_{123} for different values of ν_{VF} and η while keeping $\mathrm{Pr_{M,eff}} = 1$. It is apparent that as dissipation becomes stronger the graph tends toward a straight line. Here, the notation of $\nu \equiv \nu_{\mathrm{VF}}$ applies.

$$\frac{\partial \mathbf{B}}{\partial t} = \nabla \times (\mathbf{u}_{\mathrm{PF}} \times \mathbf{B}) + \eta \nabla^2 \mathbf{B} + \frac{m_{\mathrm{p}}}{e(1+\chi)} \frac{\nabla p_{\mathrm{PF}} \times \nabla \rho_{\mathrm{PF}}}{{\rho_{\mathrm{PF}}}^2},$$

One of our objectives for the case of including source terms in the equations is to assess their contribution to the growth of the seed field. In order to do this, we consider the equations in system (2.27) both with the source term, notating them as B_{123} and ω_{123} in order to refer to the equations *with* the source terms, and B_{12} and ω_{12} in order to refer to the equations *without* the source terms. We also focus on the case for very small diffusion and viscosity ($\nu_{\mathrm{VF}} = \eta = 10^{-10}$) in the discussions which follow.

In figures 2.19 and 2.20 we present the results of B_{rms} versus ω_{rms} for the cases of $\mathrm{Pr_{M,eff}} = 1$

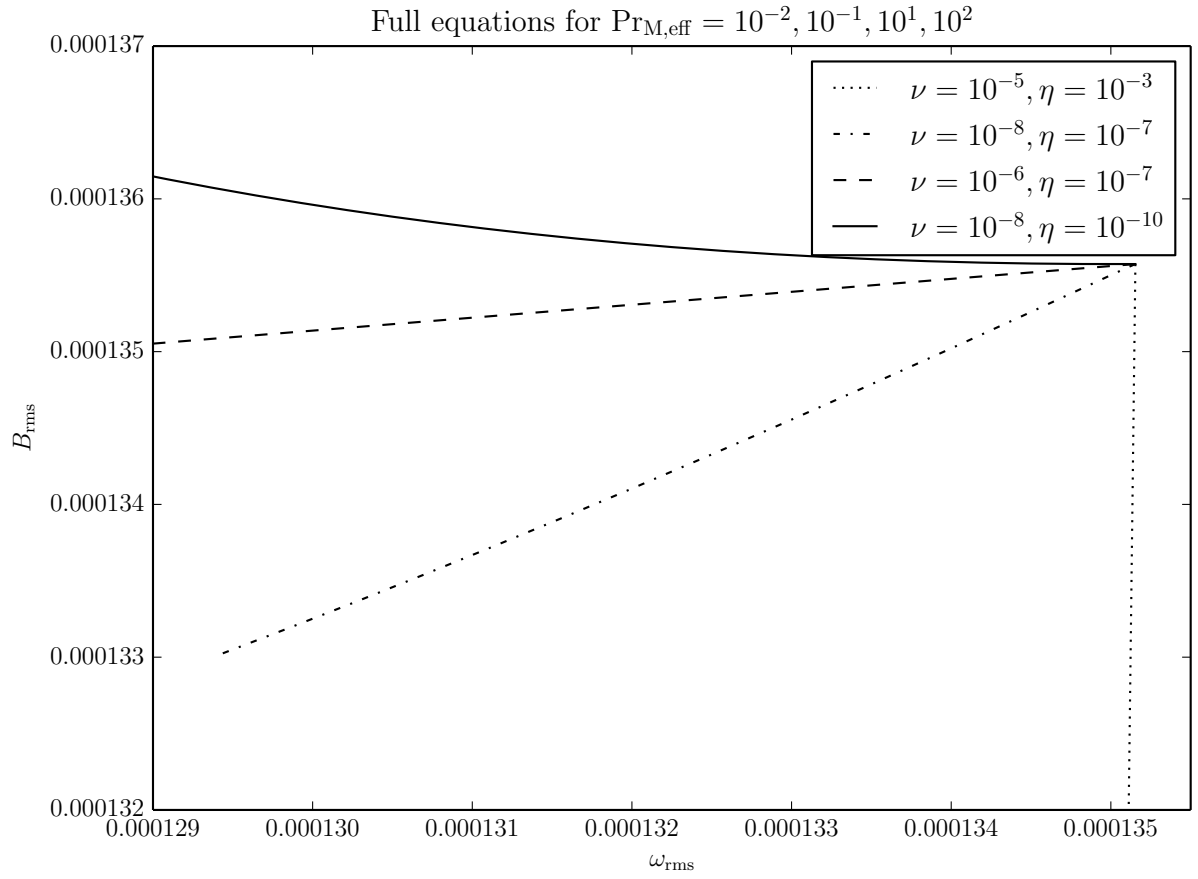

Figure 2.20: We have plotted B_{123} against ω_{123} for different values of ν_{VF} and η while keeping $\mathrm{Pr}_{\mathrm{M,eff}} \neq 1$. Here too it is clear that stronger dissipation straightens the curve. Once more, the notation $\nu \equiv \nu_{\mathrm{VF}}$ applies.

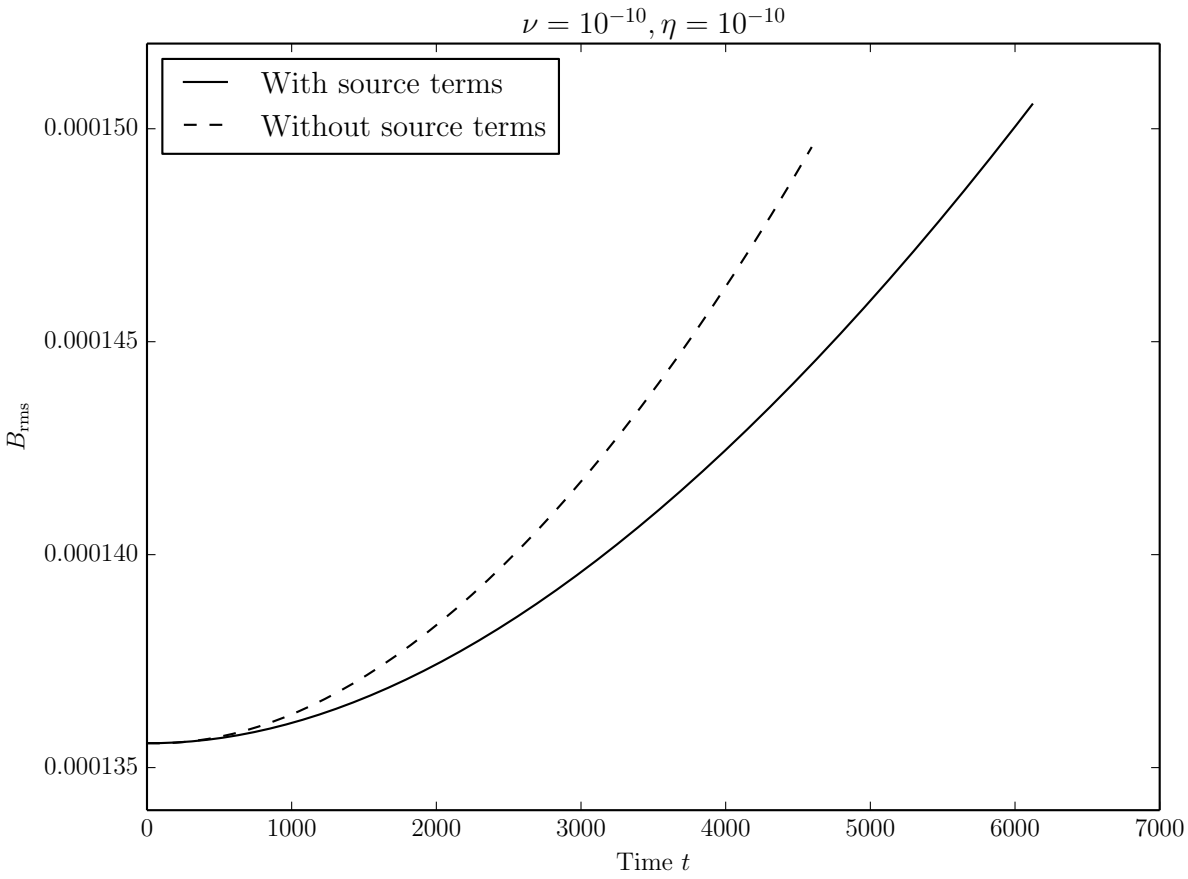

Figure 2.21: The dashed line represents B_{12} (without battery term) while the solid line represents B_{123} (with battery term). The notation $\nu \equiv \nu_{\rm VF}$ applies.

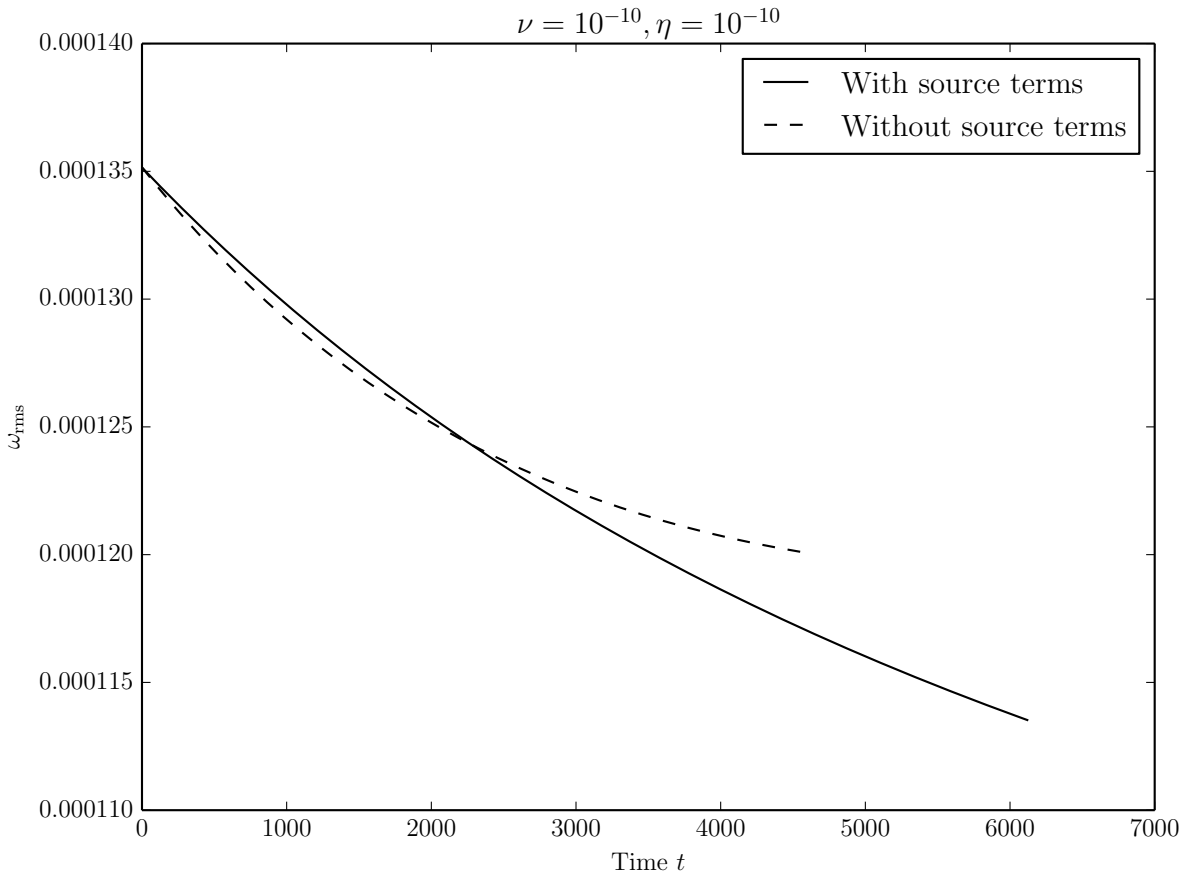

Figure 2.22: The dashed line represents ω_{12} (without source term), while the solid line represents ω_{123} (with source term). The notation $\nu \equiv \nu_{\rm VF}$ applies.

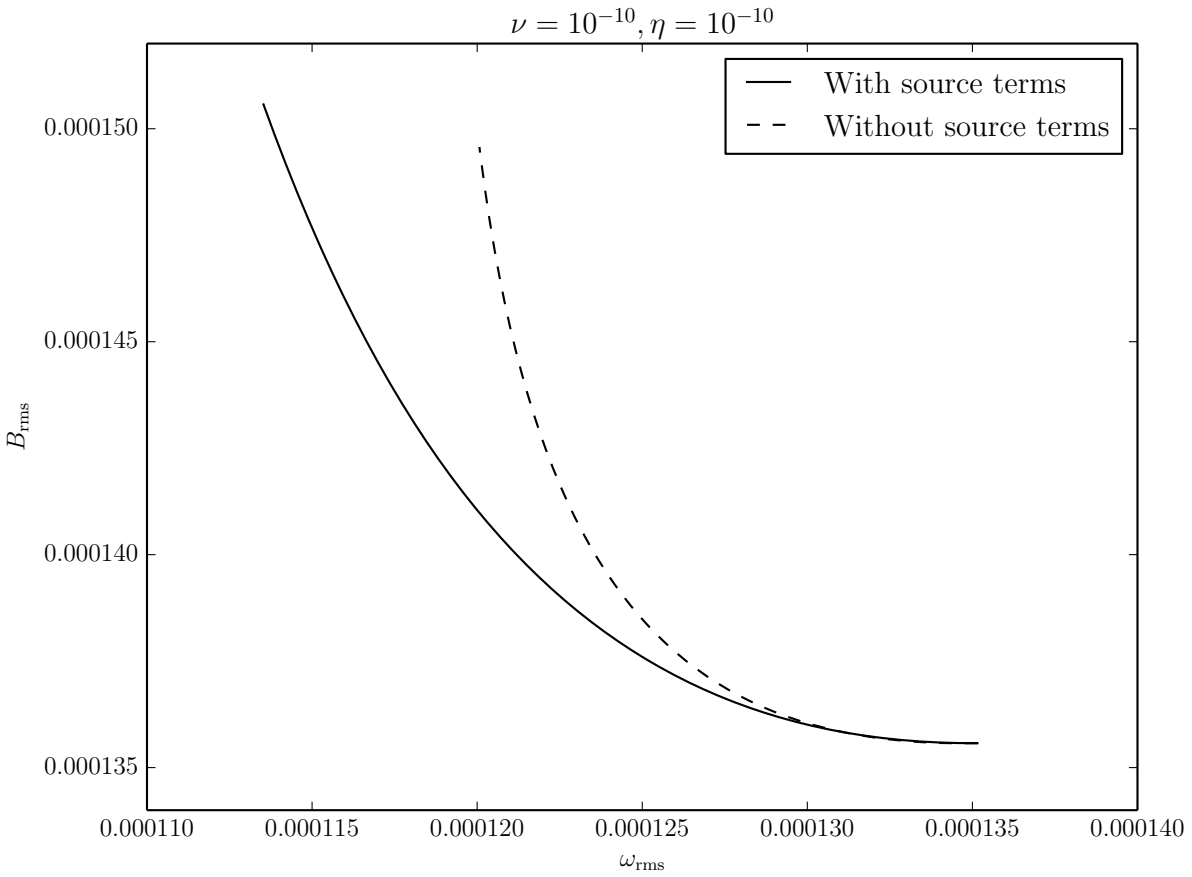

Figure 2.23: Again, the dashed line represents B_{12} (without battery term), while the solid line represents B_{123} (with battery term). The notation $\nu \equiv \nu_{\rm VF}$ applies.

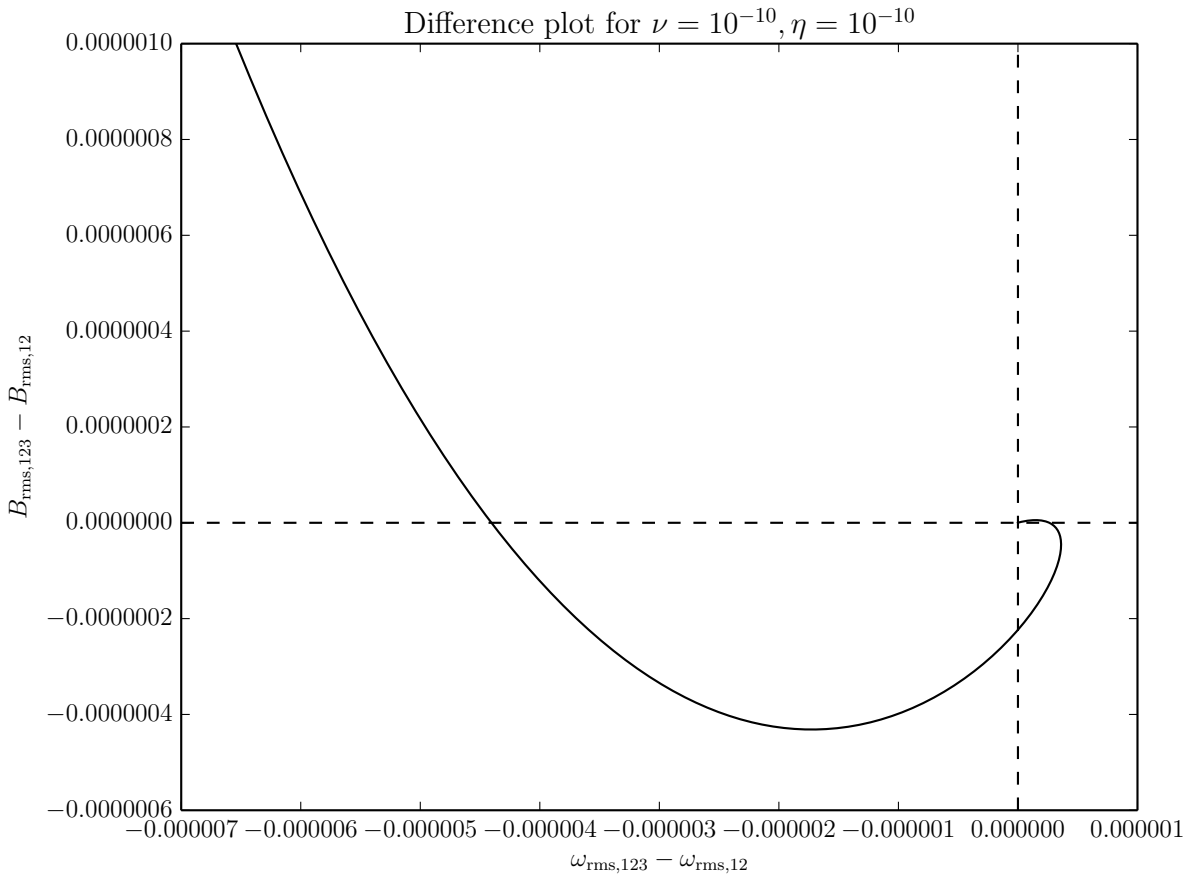

Figure 2.24: The graph represents the plot of the time varying difference $B_{123} - B_{12}$ against the time varying difference $\omega_{123} - \omega_{12}$. Here, a set of axes has been superimposed over the curve's starting point, with the curve evolving in a clockwise direction. The notation $\nu \equiv \nu_{\mathrm{VF}}$ applies.

and $\mathrm{Pr_{M,eff}} \neq 1$ for different values of ν_{VF} and η. For the case of $\mathrm{Pr_{M,eff}} = 1$, it is apparent that the similar behaviour observed in the case without the source term still holds, but this time only for strong dissipation (corresponding to $\nu_{\mathrm{VF}} = \eta_{\mathrm{PF}} = 10^{-6}$ and larger values). For $\nu_{\mathrm{VF}} = \eta < 10^{-6}$, however, similar behaviour is no longer observed, producing a curved line when comparing B_{rms} and ω_{rms}. Recall that observing the straight line when comparing B_{rms} to ω_{rms} is indicative of similar behaviour between the conducting fluid and non-conducting fluid, and evidence for an analogy between the two. For small values of dissipation, this does not appear to hold. Examining figure 2.20, it is once more apparent that there is no similar behaviour between B_{rms} and ω_{rms} for the case of $\nu_{\mathrm{VF}} \neq \eta$.

We now turn our attention to figures 2.21, 2.22 and 2.23. Here, we have chosen to focus on the comparison for the behaviour between B_{rms} and ω_{rms} both against time and against each other for the case of $\nu_{\mathrm{VF}} = \eta_{\mathrm{PF}} = 10^{-10}$, representing a very small value for dissipation. As can already be noted in figure 2.19, the similar behaviour seen when comparing B_{rms} to ω_{rms} which is represented by a straight line no longer exists for small values of dissipation, being replaced instead by a curve. This relationship also appears to hold for the case of the equations where no source term is present and can be seen in figure 2.23. Before we discuss this behaviour, however, we first turn our attention to figures 2.21 and 2.22.

The temporal evolution of B_{rms} is displayed in figure 2.21. Here, one can see two distinct points of intersection between the curves representing the temporal evolution with (field $B_{rms,123}$) and without (field $B_{rms,12}$) the presence of a battery term. The first of these occurs at the beginning of the simulation, when only the seed field is present, while the second occurs some time after. Between these two points of intersection, the seed field is amplified due to the effects of the inductive term and dissipated due to the effects of the diffusion term present in the Induction Equations in system (2.27), with the resulting magnetic field will also being dependent on whether the battery term is present or not. Before the second point of intersection, it can be seen that field $B_{rms,123}$ is clearly stronger than field $B_{rms,12}$, the former having also been subjected to the presence of the battery term. The growth of field $B_{rms,12}$ eventually catches up to that of $B_{rms,123}$ and the two become equal in strength, producing the second point of intersection. Beyond this, field $B_{rms,12}$ appears to grow at a faster rate than $B_{rms,123}$, producing a stronger overall field at the end of the simulation.

Turning to the source number, $\mathrm{S_M}$, defined in section 2.2.3.2 and defining magnetic Reynolds

numbers for the induction equations with and without the battery terms, $\mathrm{Re_M}^{(123)}$ and $\mathrm{Re_M}^{(12)}$ respectively, we provide a complementary discussion regarding the growth of fields B_{123} and B_{12}.

Since the magnetic Reynolds number characterises the importance of induction to diffusion in the Induction Equations, we know that for $\mathrm{Re_M} > 1$ we should expect growing magnetic fields due to dynamo action, and for $\mathrm{Re_M} < 1$ would be decaying magnetic fields due to the effects of diffusion being far greater than the dynamo action. This would be the expected case for the Induction Equations with no battery term, and can thus describe the evolution of field B_{12} corresponding to magnetic Reynolds number $\mathrm{Re_M}^{(12)}$. In the presence of the battery term, it is possible that growing magnetic fields can still be observed for $\mathrm{Re_M}^{(123)} < 1$ provided that $\mathrm{Re_M}^{(123)} + \mathrm{S_M} > 1$. Here, the presence of the battery term results in a battery-aided dynamo, allowing a magnetic field to grow.

Applying the above to the evolution of $B_{rms,123}$ and $B_{rms,12}$ in figure 2.21, the initially-stronger field $B_{rms,123}$ could be the result of the battery-aided dynamo arising due to the presence of the battery term in its evolution equation. From the Navier-Stokes equations in system (2.28) however, it can be seen that the pressure term $\nabla p_{\mathrm{PF}}/\rho_{\mathrm{PF}}$ is able to reduce the dynamo's effect on the magnetic field through its interaction with the velocity field. Despite this, however, the presence of the battery term in the Induction Equations is able to compensate for any losses, thereby leading to the stronger field $B_{rms,123}$ when compared to field $B_{rms,12}$ whose Induction Equations do not have the battery term present. Eventually, the changing velocity field causes both magnetic fields to continue growing through the dynamo effect, but in the case of field $B_{rms,123}$, the reduced battery-aided dynamo keeps on operating but cannot allow the field to grow stronger than when its strength is compared to that of $B_{rms,12}$ as the contribution from the battery term remains constant in time and is less than that of the losses incurred due to the pressure term in the Navier-Stokes equations from the velocity field. Due to this, the field strength $B_{rms,12}$ increases and grows at a faster rate than that of $B_{rms,123}$, resulting in a stronger field strength. This faster growth rate of $B_{rms,12}$ results in the second intersection point and its continued faster growth rate for the remainder of the run.

The temporal growth of $\omega_{rms,123}$ and $\omega_{rms,12}$ is displayed in figure 2.22. We can define two fluid Reynolds numbers, $\mathrm{Re}^{(123)}$ and $\mathrm{Re}^{(12)}$, which would refer to the vorticity equations with and without the source term respectively, as well as a source number, $\mathrm{S_V}$, that is determined in a

similar to $\mathrm{S_M}$, in order to describe the behaviour observed in the decay of these two fields. For growth in vorticity to result in the presence of the source term, we require that $\mathrm{Re}^{(123)} - \mathrm{S_V} > 1$. At the first intersection point in figure 2.22, $\omega_{rms,123}$ and $\omega_{rms,12}$ are equal due to the seed field only being present, whilst at the second point of intersection, the strength of $\omega_{rms,12}$ becomes equal to that of $\omega_{rms,123}$ due to the contributions from all of the terms in the evolution equations for ω_{123} and ω_{12} becoming equal. Beyond the second point of intersection, both fields continue to decay, with $\omega_{rms,123}$ being weaker than $\omega_{rms,12}$ due to the presence of both the pressure term in the Navier-Stokes equations (leading to a decreased velocity field), as well as the presence of the source term in the evolution equations for the vorticity itself.

Now that we have discussed the observed temporal evolution relationships of B_{rms} and ω_{rms}, we finally compare the two quantities to each other for the case of $\nu = \eta = 10^{-10}$, which produced a curved relationship, as noted before. Note that the straight line relationship between B_{rms} and ω_{rms} is indicative of similar behaviour between the charged and non-charged fluids, supporting the case for an analogy between them; a relationship described by a curve, however, is not. In order to determine whether the observed breakdown in the relationship between B_{rms} and ω_{rms} for small values of dissipation, with $\nu_{\mathrm{VF}} = \eta_{\mathrm{PF}}$, may be due to systemic effects within the code itself, we opt to analyse the difference between the values of B_{rms} and ω_{rms} produced by simulating the equations B_{123} and ω_{123} and B_{12} and ω_{12}; that is, we graphically compare $B_{123} - B_{12}$ (the magnetic difference) to $\omega_{123} - \omega_{12}$ (the vorticity difference) with the idea that any systemic effects that may be introduced in the simulation of both equations would be eliminated when the difference between the full equations and the equations without the source terms is taken. We display this plot in figure 2.24.

Superimposing a set of axes centered at the origin in figure 2.24, it would be clear that the difference curve spends most of its time in both the second and third quadrants[6]. Initially, the curve begins at the origin, where the magnetic and vorticity are equal, and then enters the first quadrant. In this quadrant, the magnetic and vorticity differences are both positive, with the vorticity difference growing faster than its decaying magnetic counterpart, due to the presence of the source term. This growth continues until the curve reaches the horizontal axis where the magnetic difference is zero due to the source term modifying the equations B_{123} in such a way that there appears to be no difference when compared to the equations B_{12}. Beyond

[6]Here, the quadrants are numbered in the standard way: the first quadrant occurs where all values are positive, and the remaining quadrants are numbered in an anti-clockwise fashion.

the horizontal axis, the curve then enters the fourth quadrant, where the magnetic difference is negative and the vorticity differences is positive. The growth of the magnetic difference in this quadrant is faster than that of the vorticity difference, causing the curve to turn towards the horizontal axis, during which the magnetic difference continues to grow whilst the vorticity difference decreases after reaching its maximum positive value here. After turning, the curve then reaches the horizontal axis, where the vorticity difference is now zero once more due to the source term modifying equations ω_{123} in such a way that there appears to be no difference when compared to equations ω_{12}. Now in the third quadrant, both the vorticity and magnetic differences are negative. In this quadrant, the magnetic difference reaches its largest negative value and begins to increase towards zero, while the vorticity difference continues to decrease, becoming more negative. The curve once more crosses the horizontal axis and enters the second quadrant, where both the vorticity difference is negative and magnetic difference is positive. Here, the vorticity difference continues to increase, becoming more negative, whilst the magnetic difference continues to increase, becoming more positive. The respective decrease and increase appear to happen at an almost-identical rate.

Should similar behaviour have been observed between B_{rms} and ω_{rms} for the case of small dissipation, the graph of the difference between $B_{123} - B_{12}$ to $\omega_{123} - \omega_{12}$ would be expected to spend its entire life in the second quadrant. This, however, is not true for the case above.

2.5 Conclusion

In this chapter we studied the problem of Analogue Magnetism in the context of comparing the vorticity $\boldsymbol{\omega}$, of a non-conducting fluid to the magnetic field $\mathbf{B}$ present within a conducting fluid through the use of MHD simulations using the PENCIL CODE in order to simulate the relevant evolution equations.

Some time was first spent discussing the MHD fluid approximation and how it applies to magnetic fluids. Using the relevant length- and time scales discussed, we formulated and presented the analogous systems that were to be studied: the first containing the Induction and vorticity evolution equations, and the second containing the Navier-Stokes and magnetic vector potential evolution equations. It was pointed out that the latter system is simply the uncurled version of the

former system that was to be studied. In particular, we noted that the velocity fields present in the evolution equations were different, representing two different fluids; the Induction and magnetic vector potential evolution equations took into account the velocity field of the conducting fluid (notated as $\mathbf{v}_{\mathrm{PF}}$ for *plasma fluid*) and the Navier-Stokes and vorticity evolution equations took into account the velocity field of the non-conducting fluid (notated as $\mathbf{u}_{\mathrm{VF}}$ and $\boldsymbol{\omega}_{\mathrm{VF}}$ in order to denote the relevant velocity *and* vorticity fields for the *viscous fluid*). We also noted that the conducting fluid's velocity and vorticity fields would evolve according to their own propagation equations, but that it was not considered here – we sought only to compare the non-conducting fluid to the conducting fluid.

It was shown from both of the systems established that the evolution equations for the velocity field $\mathbf{u}$ (i.e. the Navier-Stokes equations) and for $\mathbf{A}$ (i.e. the magnetic vector potential evolution equations), as well as those for $\boldsymbol{\omega}$ and $\mathbf{B}$ were structurally similar to each other when no source terms were present. Provided that the values of the kinematic viscosity ν and magnetic diffusivity η were equal to each other, similar behaviour between $\mathbf{u}$ and $\mathbf{A}$, and $\boldsymbol{\omega}$ and $\mathbf{B}$, should expected to be observed when these fields are compared to each other. With the inclusion of the source terms in the systems, the structural similarity still persisted, however, the source terms now had alternating signs between the evolution equations for $\mathbf{u}$ and $\mathbf{A}$, and $\boldsymbol{\omega}$ and $\mathbf{B}$ respectively. Structural similarity between the equations in both systems was regained completely by defining $\tilde{\mathbf{u}}_{\mathrm{VF}} \equiv -\mathbf{u}_{\mathrm{VF}}$ in the uncurled system, and $\tilde{\boldsymbol{\omega}} \equiv -\boldsymbol{\omega}$. This lead to the proposal to compare $\mathbf{u}_{\mathrm{VF}}$ to $-\mathbf{A}$, and $\boldsymbol{\omega}_{\mathrm{VF}}$ to $-\mathbf{B}$ in the simulations that were to be run.

Some general details regarding the numerical implementation of the high-order finite differences method used by the PENCIL CODE were then discussed, with particular attention being paid to the effect of the mesh size on the size of the time-steps selected by the code automatically at each iteration in the simulation.

The systems (2.28) and (2.27) were simulated using the PENCIL CODE. The effect of the mesh size on the resulting solution obtained from simulating a non-conducting fluid was first investigated. Here, simulation boxes of sizes 32^3, 64^3 and 128^3 were considered together with the kinematic viscosity ν_{VF} set to 0 and 10^{-3} in order to investigate the solutions obtained for the case of an inviscid non-conducting fluid, as well as for a non-conducting fluid having moderate viscosity. It was found that the 32^3 was the most cost-effective simulation box to use in terms of actual computation time required, as well as quality of the solution obtained, and was the

preferred mesh size to be used for the rest of the simulations that were conducted.

A hydrodynamical case for $\nu_{\rm VF} = \eta = 10^{-2}$, corresponding to the viscosity of water at 20°C was then considered in order to determine whether any similar behaviour between the two fluids could be observed. Here, the evolution equations in system (2.27) were considered without their respective source terms. Plotting B_{rms} against ω_{rms}, we noted that a straight line relationship was displayed. This was to be expected due to the evolution equations being noted to be structurally-similar, together with the fact that we had $\nu_{\rm VF} = \eta$. The same relationship was also displayed for u_{rms} versus A_{rms}.

Continuing to leave any source terms turned off in the evolutions, we then considered other values of $\nu_{\rm VF} = \eta$, as well as pairs of values where $\nu_{\rm VF} \neq \eta$. Simulation results obtained here were classified according to an *effective* magnetic Prandtl number, $\mathrm{Pr}_{\rm M,eff}$, which was defined as the ratio between the viscosity of the non-conducting fluid, to the magnetic diffusivity of the conducting fluid. This was chosen in order to differentiate from the usual magnetic Prandtl number, $\mathrm{Pr}_{\rm M}$, which only takes into account the viscosity and magnetic diffusivity of the conducting fluid itself. Thus, the cases of $\mathrm{Pr}_{\rm M,eff} = 1$ and $\mathrm{Pr}_{\rm M,eff} \neq 1$ were investigated for other cases of $\nu_{\rm VF} = \eta$ and $\nu_{\rm VF} \neq \eta$ respectively.

Results for these simulations showed that both the charged and non-charged fluids maintained similar behaviour for the cases of $\nu_{\rm VF} = \eta$, with both ω_{rms} versus B_{rms} and u_{rms} versus A_{rms} displaying a straight-line relationship when plotted against each other. This straight line relationship appeared to break down once pairs of $\nu_{\rm VF} \neq \eta$ for $\mathrm{Pr}_{\rm M,eff} \neq 1$ were simulated, becoming curves instead of straight lines. In particular, for the cases where $\nu_{\rm VF} > \eta$, dissipation due to kinematic viscosity appeared to dominate, causing all of the curves describing the comparison between ω_{rms} versus B_{rms} and u_{rms} versus A_{rms} to lie above the straight line indicating the case of $\nu_{\rm VF} = \eta$, whilst for the case of $\nu_{\rm VF} < \eta$, all these curves lay below the straight line instead. This deviation from the straight-line relationship for the cases of $\nu_{\rm VF} \neq \eta$ was to be expected, as the dissipative terms in the evolution equations for the magnetic and vorticity fields would be operating at different rates, causing dissimilar behaviour between the two fluids, and thus a breakdown in the analogy. However, the parameter space for $\nu_{\rm VF} \neq \eta$ could still be scanned for pairs of $\nu_{\rm VF}$ and η that could cause the two fluids to display approximately similar behaviour and thus an almost-straight line when looking at ω_{rms} versus B_{rms} and u_{rms} versus A_{rms}. In this way, a threshold for where the analogy could still hold can be determined for the case of $\mathrm{Pr}_{\rm M,eff} \neq 1$.

The source terms were finally included in the evolution equations in system (2.27), and once more the cases of $\mathrm{Pr}_{\mathrm{M,eff}} = 1$ and $\mathrm{Pr}_{\mathrm{M,eff}} \neq 1$ were investigated for similar behaviour between the non-charged and charged fluids. The magnetic and vorticity fields in these runs were not generated from zero initial conditions, having a small seed field being provided for the source terms to operate on instead. Again it was clear that for $\mathrm{Pr}_{\mathrm{M,eff}} \neq 1$, no similar behaviour between the two fluids existed, leading to a breakdown in the analogy. However, the parameter space for $\nu_{\mathrm{VF}} \neq \eta$ could still be scanned in this case to check for values of ν_{VF} and η_{PF} that may admit approximately-similar behaviour between the two fluids, thus giving some supporting evidence for the existence of an approximate analogy in the case where source terms are present and $\mathrm{Pr}_{\mathrm{M,eff}} \neq 1$.

For the case of $\mathrm{Pr}_{\mathrm{M,eff}} = 1$, however, similar behaviour between the two fluids was observed for cases of strong dissipation. In particular, we observed that for values of $\nu_{\mathrm{VF}} = \eta \geq 10^{-6}$ a straight line relationship between ω_{rms} and B_{rms} was observed, thus giving support for the existence of an analogy in the presence of source terms in the evolution equations. For values of $\nu_{\mathrm{VF}} = \eta \leq 10^{-7}$, however, the curved relationship between ω_{rms} and B_{rms} returned once more, indicating a breakdown in the analogy at these values due to no similar behaviour being observed between the two fluids. Examining the case of $\nu_{\mathrm{VF}} = \eta = 10^{-10}$, the case for the weakest dissipation, we investigated whether the breakdown in the straight-line relationship could be due to systemic effects within the code itself. To this end, we chose to compare ω_{rms} and B_{rms} for the difference between the full evolution equations (notated as B_{123} and ω_{123}) and the evolution equations without the source terms (notated as B_{12} and ω_{12}) respectively. It was reasoned that since both evolution equations would be subject to the same systemic effects within the code itself, and such numerical artifacts would vanish once the difference between these two equations was taken. The evolution of $B_{rms,123}$ and $B_{rms,12}$, as well as that of $\omega_{rms,123}$ and $\omega_{rms,12}$ were also plotted against time and compared to each other. In particular, it was found that two intersection points were observed in the curves of $B_{rms,123}$ and $B_{rms,12}$ versus time; the first point of intersection was observed to occur at the start of the run, when both fields had magnitudes equal to that of the initial seed field. As the run proceeded, $B_{rms,123}$ was observed to be the stronger field, indicating the presence of a possible battery-aided dynamo, which is an amendment to the standard dynamo theory. As the run proceeded, the growth rate of $B_{rms,12}$ slowly increased, eventually causing $B_{rms,12}$ to grow stronger than $B_{rms,123}$, resulting in the second intersection point. In this case, $B_{rms,12}$ remained the strongest field for the remainder of the run. This dif-

ference in strength of $B_{rms,123}$ and $B_{rms,12}$ after the second point of intersection was reasoned to be due to the fact that the battery term could only provide a constant contribution to the growth of $B_{rms,123}$ which was not enough to overcome the effects of the pressure term in the Navier-Stokes equations that came into the Induction equations via the changing velocity field. Thus, even though both fields grew in strength due to the dynamo effect brought on by the changing velocity field, the field $B_{rms,12}$ grew stronger than $B_{rms,123}$ due to the battery term's inability to further aid the dynamo. A similar case was seen for plotting $\omega_{rms,123}$ and $\omega_{rms,12}$ against time, with the behaviour observed there also being explained with similar reasoning to the magnetic fields case.

By defining the source numbers, $\mathrm{S_M}$ and $\mathrm{S_V}$ for the magnetic and vorticity evolution equations respectively, we determined that for growth in the magnetic field to occur in the equations with the source terms present, we would require that $\mathrm{Re_M^{(123)}} + \mathrm{S_M} > 1$ and $\mathrm{Re^{(123)}} - \mathrm{S_V} > 1$ for the magnetic and vorticity evolution equations respectively. Here, $\mathrm{Re_M^{(123)}}$ and $\mathrm{Re^{(123)}}$ are the magnetic and fluid Reynolds numbers for the respective fluids together with the source terms in their respective evolution equations. It was noted here that magnetic field growth could occur with $\mathrm{Re_M^{(123)}} + \mathrm{S_M} > 1$, even if $\mathrm{Re_M^{(123)}} < 1$, as long as the former condition was fulfilled. This lead to the idea of a battery-aided dynamo, and was observed when B_{rms} for the evolution equations with and without the source term were plotted against time. Similar behaviour was also seen in the case of the vorticity. Using what we had learned here, we were able to interpret the difference curve obtained in terms of these results, thus finding no evidence for the breakdown in the analogy for small dissipation due to any systemic effects present in the code itself. This meant that further investigation into possible reasons for this breakdown in the low-dissipation regime for $\nu_{\mathrm{VF}} = \eta$, and thus $\mathrm{Pr_{M,eff}} = 1$, would be required.

Through the MHD simulations conducted in this chapter, we found that we could indeed find a non-conducting fluid that exhibited the behavioural properties of a conducting fluid. This was seen in the hydrodynamical simulations for the case of $\nu_{\mathrm{VF}} = \eta = 10^{-2}$, corresponding to the viscosity of water at 20°C, as well as for the other runs that scanned the $\nu_{\mathrm{VF}} = \eta$ parameter space with (for the case of strong dissipation) and without the presence of source terms in the analogous system that was studied. Furthermore, it was found for these cases that due to the similar behaviour observed between the two fluids, we could conclude that the non-conducting fluid did indeed approximate the behaviour of the conducting fluid very well. Thus, our first and second guiding questions could be answered.

For the the parameter space of $\nu_{\mathrm{VF}} \neq \eta$, no such non-conducting fluid could be found, but the parameter space of $\nu_{\mathrm{VF}} \approx \eta$ could still be studied in order to determine an empirical range over which a non-conducting fluid could approximate the behaviour of a conducting fluid. Even in this case, it may still be possible to answer our first two guiding questions.

We note that in order to answer our final guiding question, further simulation of charged and non-charged fluids in extreme environments would be required. However, the results from the simulations conducted in this chapter do suggest that the behaviour of magnetic fields in extreme environments could be studied using analogue magnetism, as it was possible to find non-charged fluids that could approximate the behaviour of charged fluids very well.

One of the key conditions needing to be met in order to begin an investigation into an analogy is that of structural similarity between the governing equations of the system(s) under consideration. The idea of this structural similarity can also be expanded to, for example, mean-field theory when studying large- and small-scale magnetic fields. In the final chapter of this work, we now move to briefly discuss some known analogues arising in the study of mean-field theory, and present some additional results obtained from the expansion of the mean EMF.

Chapter 3

Considerations in the Generalised Mean Electromotive Force

Now that we have completed our study of Analogue Magnetism through the use of MHD simulations, we turn to briefly consider another case where the theory of analogues could be applied: the study of phenomena in MFMHD.

In this chapter we discuss some of the key assumptions that go into formulating the equations of mean-field MHD, paying special attention to the mean EMF, which arises in the governing equations as a natural consequence of the assumptions that are made. The mean EMF itself is then considered and the problem of determining a functional form for it, given some random, turbulent fluctuating small-scale velocity field, is discussed in detail. We show how the well-known α- and β-effects arise from the Taylor expansion of the mean EMF, and consider two new higher-order terms in the expansion, γ and ζ.

Higher-order terms in the expansion of the mean EMF need to be considered in two primary cases: 1) in order to improve the characterisation of the kernel of the mean EMF when the mean magnetic field cannot be characterised as being constant in space and time (this is considered in works such as [19,20,28,40,80,81]), and 2) when the characterisation of the coefficients such as α and β that arise in the mean EMF expansion must be improved, which can happen in cases where the leading coefficients α and β, whose effects are well-known, could show a linear increase with

increasing $\mathrm{Re_M}$, but in reality either saturate or exhibit complicated behaviour (such as the cases studied in works such as [22, 76, 77]). Detailed calculations of higher-order coefficients in the mean EMF expansion are also discussed in paper X of [83] for the most general case.

The mean-field Induction equations and Ohm's law incorporating the effects of these new terms are derived, and the contributions that the new terms make to the evolution of the large- and small-scale magnetic fields are discussed. The new terms are also analysed through scale analysis, and their relative effects are then compared to other terms in the Induction Equations in order to determine on which scales the effects of these terms may become relevant.

In closing, we briefly discuss the known analogy between the mean EMF and Reynolds stress tensor from Fluid Dynamics, which is known to be the fluid analogue of the mean EMF, by considering work that has been done in studying the so-called anisotropic kinetic alpha effect, which is the known fluid analogue of the MHD α-effect.

Note that some of the notation presented in this chapter differs from the usual notation used in previous chapters of this work; where this is the case, clarification will be made to the reader.

3.1 The Equations of Mean-Field Dynamo Theory

The key assumption of mean-field MHD regards the magnetic and velocity fields as superpositions of at least two distinct components: the mean or large-scale field, as well as the fluctuating or small-scale field. Using this assumption, we write the *total* magnetic flux density, $\mathbf{B}(\mathbf{x}, t)$, and the *total* velocity field, $\mathbf{U}(\mathbf{x}, t)$, as:

$$\mathbf{B}(\mathbf{x}, t) = \overline{\mathbf{B}}(\mathbf{x}, t) + \mathbf{b}(\mathbf{x}, t) \tag{3.1a}$$

$$\mathbf{U}(\mathbf{x}, t) = \overline{\mathbf{U}}(\mathbf{x}, t) + \mathbf{u}(\mathbf{x}, t), \tag{3.1b}$$

where the overline denotes the mean field, and the lower-case letter denotes the fluctuating field[1]. The mean fields $\overline{\mathbf{B}}(\mathbf{x}, t)$ and $\overline{\mathbf{U}}(\mathbf{x}, t)$ are defined as averages by means of proper averaging

[1]Note that this differs from our usual notation of using $\mathbf{u}(\mathbf{x}, t)$ to denote the total velocity field, as was done in the previous chapter.

procedures done over both space and time. Using the notation of [74] we define a generalised spatial average for a general scalar quantity, $Q(\mathbf{x}, t)$, as:

$$\overline{Q}(\mathbf{x}, t) = \int_{\infty} Q(\mathbf{x} + \boldsymbol{\xi}, t) f(\boldsymbol{\xi}) \mathrm{d}^3\xi, \tag{3.2a}$$

$$\int_{\infty} f(\boldsymbol{\xi}) \mathrm{d}^3\xi = 1, \tag{3.2b}$$

and a generalised time average for the same quantity as:

$$\overline{Q}(\mathbf{x}, t) = \int_{\infty} Q(\mathbf{x}, t + \tau) f(\tau) \mathrm{d}\tau, \tag{3.3a}$$

$$\int_{\infty} f(\tau) \mathrm{d}\tau = 1, \tag{3.3b}$$

where the functions $f(\boldsymbol{\xi})$ and $f(\tau)$ are weight functions over which the integrals (done either in $\boldsymbol{\xi}$- or τ-space) are non-zero only in some small region around either $\boldsymbol{\xi} = \mathbf{0}$ or $\tau = 0$. Here, $\boldsymbol{\xi}$ and τ are typical length and time scales whose restrictions will be defined later in this section. In this way, the averages defined by (3.2a) and (3.3a) may be identified as ensemble averages which obey the Reynolds averaging rules.

For a constant c and two general quantities X and Y which are functions of space and time, and consist of both a mean and fluctuating part, thus admitting the decompositions $Y = \overline{Y} + y$ and $Z = \overline{Z} + z$, whose mean parts have been defined via the averaging rules given in expressions (3.2a) and (3.3a), the Reynolds averaging rules are given as follows:

$$\overline{Y + Z} = \overline{Y} + \overline{Z} \tag{3.4a}$$

$$\overline{cY} = c\overline{Y} \tag{3.4b}$$

$$\overline{\overline{Y}} = \overline{Y} \tag{3.4c}$$

$$\overline{y} = 0 \tag{3.4d}$$

$$\overline{YZ} = \overline{Y}\ \overline{Z} + \overline{yz} \tag{3.4e}$$

$$\overline{\overline{Y}Z} = \overline{Y}\,\overline{Z} \tag{3.4f}$$

$$\overline{\frac{\partial Y}{\partial x}} = \frac{\partial \overline{Y}}{\partial x} \tag{3.4g}$$

$$\overline{\frac{\partial Y}{\partial t}} = \frac{\partial \overline{Y}}{\partial t}. \tag{3.4h}$$

The results given by rules (3.4c), (3.4d), (3.4e), (3.4g), and (3.4h) are of great importance in deriving the governing equations of mean-field Electrodynamics (MFEM) that are discussed later in this chapter. Rule (3.4c) assures us that once a quantity has been averaged, it remains averaged, whilst rule (3.4d) assures us that the average of a fluctuating quantity is zero. Similarly, rules (3.4g) and (3.4h) assure us of the commutativity of the averaging and differentiation operators: the average of the derivative of the quantity Y or Z is equal to the derivative of the average of these quantities. Note that the commutativity of the averaging and derivative operators depends on the definition of the average itself. Using the definitions given by (3.2a) and (3.3a), it can be shown that commutativity between these two operators is indeed possible.

Lastly, we point out rule (3.4e), which states that the average of the product of the two quantities Y and Z is not only equal to the product of the individual averages of these quantities, but also includes an additional term. Recalling that $\overline{YZ} = \overline{(\overline{Y} + y)(\overline{Z} + z)}$, the result of (3.4e) is obtained after some algebra.

Recall that in their *total* form, the Induction Equations are given by:

$$\frac{\partial \mathbf{B}}{\partial t} = \nabla \times (\mathbf{U} \times \mathbf{B}) + \eta \nabla^2 \mathbf{B}. \tag{3.5}$$

Applying the averaging operator to eqns (3.5) then yields the *mean-field* Induction Equations, given by:

$$\frac{\partial \overline{\mathbf{B}}}{\partial t} = \nabla \times \overline{(\mathbf{U} \times \mathbf{B})} + \eta \nabla^2 \overline{\mathbf{B}}. \tag{3.6}$$

It can be seen that eqns (3.5) and (3.6) are structurally-similar to each other, save for the fact that one describes the temporal evolution of the total magnetic field, whilst the other describes only the evolution of the mean magnetic field. Using rule (3.4e), we expand the term $\overline{\mathbf{U} \times \mathbf{B}}$:

$$\overline{\mathbf{U} \times \mathbf{B}} = \overline{\mathbf{U}} \times \overline{\mathbf{B}} + \overline{\mathbf{u} \times \mathbf{b}},$$

which leaves eqns (3.6) as:

$$\frac{\partial \overline{\mathbf{B}}}{\partial t} = \nabla \times \left(\overline{\mathbf{U}} \times \overline{\mathbf{B}} \right) + \nabla \times \mathcal{E} + \eta \nabla^2 \overline{\mathbf{B}}. \tag{3.7}$$

The term $\mathcal{E} = \overline{\mathbf{u} \times \mathbf{b}}$ is called the turbulent or mean electromotive force (EMF), and is of great significance in the study of MFEM and mean-field MHD. A consequence of this term is that even if there is no initial mean field present (i.e. $\overline{\mathbf{B}} = \mathbf{0}$), one will develop if non-zero fluctuating velocity and magnetic fields are present within the system.

Recalling the decomposition (3.1a), it is possible to determine an evolution equation for the fluctuating magnetic field, $\mathbf{b}$, by taking the difference between eqns (3.5) and (3.7). After some algebra, we are left with the Induction equations for the small-scale or fluctuating magnetic field:

$$\frac{\partial \mathbf{b}}{\partial t} = \nabla \times (\overline{\mathbf{U}} \times \mathbf{b} + \mathbf{u} \times \overline{\mathbf{B}}) + \nabla \times \mathcal{G} + \eta \nabla^2 \mathbf{b}, \tag{3.8}$$

where the term $\mathcal{G} = \mathbf{u} \times \mathbf{b} - \mathcal{E}$, which is the difference between the cross-product of the small-scale fields and the mean EMF. The mean EMF thus also makes an important appearance in these evolution equations.

Collecting eqns (3.7) and (3.8) into a set, they are given as:

$$\frac{\partial \overline{\mathbf{B}}}{\partial t} = \nabla \times (\overline{\mathbf{U}} \times \overline{\mathbf{B}}) + \nabla \times \mathcal{E} + \eta \nabla^2 \overline{\mathbf{B}} \tag{3.9a}$$

$$\frac{\partial \mathbf{b}}{\partial t} = \nabla \times (\overline{\mathbf{U}} \times \mathbf{b} + \mathbf{u} \times \overline{\mathbf{B}}) + \nabla \times \mathcal{G} + \eta \nabla^2 \mathbf{b}, \tag{3.9b}$$

where the reader is reminded that $\mathcal{E} = \overline{\mathbf{u} \times \mathbf{b}}$ and $\mathcal{G} = \mathbf{u} \times \mathbf{b} - \mathcal{E}$. As with the total magnetic field, $\mathbf{B}$, we also have that $\nabla \cdot \overline{\mathbf{B}} = 0$ and $\nabla \cdot \mathbf{b} = 0$.

Eqns (3.9b) tell us that $\mathbf{b}$ is functionally-dependent on $\mathbf{u}$, $\overline{\mathbf{U}}$ and $\overline{\mathbf{B}}$, while also being linear (but not necessarily homogeneous [75]) in $\overline{\mathbf{B}}$. Furthermore, if we suppose that $\mathbf{b} = \mathbf{0}$ initially,

it can be seen that eqns (3.9a) and (3.9b) are linearly-related to each other, implying a linear relationship between $\mathbf{b}$ and $\overline{\mathbf{B}}$ by virtue of eqn (3.9b)'s linearity in $\overline{\mathbf{B}}$. The term $\nabla \times (\mathbf{u} \times \overline{\mathbf{B}})$, in the presence of an initially-zero $\mathbf{b}$ can be seen as a source term that generates $\mathbf{b}$ through the interaction of $\mathbf{u}$ with $\overline{\mathbf{B}}$.

The averaging procedure can also be applied to the governing equations for $\mathbf{U}$ in order to produce a set of coupled evolution equations for $\overline{\mathbf{U}}$ and $\mathbf{u}$, but for the purposes of the work presented here we shall regard both $\overline{\mathbf{U}}$ and $\mathbf{u}$ as given. Averaging the evolution equations for $\mathbf{U}$ gives rise to the Reynolds stress tensor, $\rho\overline{u_i u_j}$[2], which is also known as the quadratic mean [24, 67]. This tensor is often thought of as the fluid analogue to the mean EMF, $\mathcal{E}$ [24, 67], and is discussed further in section 3.3.

As a consequence of $\mathbf{b}$'s functional dependence on $\mathbf{u}$, $\overline{\mathbf{U}}$ and $\overline{\mathbf{B}}$, it follows that $\mathcal{E} = \overline{\mathbf{u} \times \mathbf{b}}$ too is functionally-dependent on these quantities, admitting the decomposition [75]:

$$\mathcal{E} = \mathcal{E}^{(0)} + \mathcal{E}^{(\overline{\mathbf{B}})}, \tag{3.10}$$

where the part $\mathcal{E}^{(0)}$ is *not* functionally-dependent on $\overline{\mathbf{B}}$, but the part $\mathcal{E}^{(\overline{\mathbf{B}})}$ is. If we assume that $\mathbf{b}$ decays to zero once $\overline{\mathbf{B}}$ vanishes, then it is possible to disregard $\mathcal{E}^{(0)}$ and set $\mathcal{E} = \mathcal{E}^{(\overline{\mathbf{B}})}$, allowing us to express $\mathcal{E}$ in an integral form as:

$$\mathcal{E}_i(\mathbf{x}, t) = \int_0^\infty \int_\infty K_{ij}(\mathbf{x}, t; \boldsymbol{\xi}, \tau) \overline{B}_j(\mathbf{x} - \boldsymbol{\xi}, t - \tau) \mathrm{d}^3\xi \mathrm{d}\tau \tag{3.11}$$

where K_{ij} is a kernel that is functionally-dependent on $\mathbf{u}$ and $\overline{\mathbf{U}}$ [75]. Here, we have chosen to revert to indicial notation of vector and tensor quantities for the sake of convenience, and choose to work in Cartesian co-ordinates. The indices i and j refer to the spatial components of the quantities to which they're attached. It is assumed that $l_0 \ll \xi \ll L$ and $t_0 \ll \tau \ll T$, where l_0 and t_0 are the length and time scales associated with the energy-containing eddies and fluctuating part of the total velocity field respectively, and L and T are the length and time scales associated with the mean magnetic flux density and velocity fields respectively [67]. Here, it is understood that $|\boldsymbol{\xi}| = \xi$. These assumptions have two important implications [74]:

[2]Here i and j are indices referring to $\mathbf{u}$'s spatial components.

1. The kernel, K_{ij}, will only be non-zero if and only if ξ and τ stay within their defined time and length scales, as per the definition of the averages defined in (3.2a) and (3.3a), and,

2. $\overline{B}_j$ may be replaced by a rapidly-converging Taylor expansion about $\boldsymbol{\xi}$ and τ under the integral.

For the remainder of the derivation, we make use of index notation and follow the summation convention. Using this, the Taylor expansion for $\overline{B}_j$ about $\boldsymbol{\xi}$ and τ is given by:

$$\begin{aligned}\overline{B}_j(\mathbf{x}-\boldsymbol{\xi},t-\tau) = \overline{B}_j(\mathbf{x},t) - \frac{\partial \overline{B}_j(\mathbf{x},t)}{\partial x_k}\xi_k - \frac{\partial \overline{B}_j(\mathbf{x},t)}{\partial t}\tau + \frac{\partial^2 \overline{B}_j(\mathbf{x},t)}{\partial x_k \partial x_l}\xi_k\xi_l + \\ \frac{1}{2!}\frac{\partial^2 \overline{B}_j(\mathbf{x},t)}{\partial {x_k}^2}{\xi_k}^2 + \frac{1}{2!}\frac{\partial^2 \overline{B}_j(\mathbf{x},t)}{\partial {x_l}^2}{\xi_l}^2 + \frac{1}{2!}\frac{\partial^2 \overline{B}_j(\mathbf{x},t)}{\partial t^2}\tau^2 \\ - \frac{1}{3!}\frac{\partial^3 \overline{B}_j(\mathbf{x},t)}{\partial x_k \partial x_l \partial x_m}\xi_k\xi_l\xi_m - \frac{1}{3!}\frac{\partial^3 \overline{B}_j(\mathbf{x},t)}{\partial {x_k}^3}{\xi_k}^3 - \frac{1}{3!}\frac{\partial^3 \overline{B}_j(\mathbf{x},t)}{\partial {x_l}^3}{\xi_l}^3 - \\ \frac{1}{3!}\frac{\partial^3 \overline{B}_j(\mathbf{x},t)}{\partial {x_m}^3}{\xi_m}^3 - \frac{1}{3!}\frac{\partial^3 \overline{B}_j(\mathbf{x},t)}{\partial t^3}\tau^3 + \dots .\end{aligned} \tag{3.12}$$

Terms involving mixed spatio-temporal derivatives also appear in this expansion, but are dropped in further calculations and thus are not shown above. For simplicity, we also drop all the terms involving temporal derivatives, noting that by using eqns (3.9a), they may be replaced by their spatial counterparts. Terms containing non-mixed spatial partial derivatives are also dropped from the expansion for simplicity. The Taylor expansion (3.12) is then truncated at the third-order derivatives, and the result substituted back into expression (3.11), leaving us with:

$$\mathcal{E}_i = \int_0^\infty \int_\infty K_{ij}\left[\overline{B}_j - \frac{\partial \overline{B}_j}{\partial x_k}\xi_k + \frac{\partial^2 \overline{B}_j}{\partial x_k \partial x_l}\xi_k\xi_l - \frac{\partial^3 \overline{B}_j}{\partial x_k \partial x_l \partial x_m}\xi_k\xi_l\xi_m\right] \mathrm{d}^3\xi \mathrm{d}\tau, \tag{3.13}$$

where the functional dependencies have now been dropped for ease of notation. Using expression (3.13), it is possible after some algebra to write $\mathcal{E}_i$ in a form similar to a truncated Taylor expansion as [67, 74]:

$$\mathcal{E}_i = \alpha_{ij}\overline{B}_j + \beta_{ijk}\frac{\partial \overline{B}_j}{\partial x_k} + \gamma_{ijkl}\frac{\partial^2 \overline{B}_j}{\partial x_k \partial x_l} + \zeta_{ijklm}\frac{\partial^3 \overline{B}_j}{\partial x_k \partial x_l \partial x_m}, \tag{3.14}$$

where we identify that

$$\alpha_{ij} = \int_0^\infty \int_\infty K_{ij} \mathrm{d}^3\xi \mathrm{d}\tau \tag{3.15a}$$

$$\beta_{ijk} = -\int_0^\infty \int_\infty K_{ij}\xi_k \mathrm{d}^3\xi \mathrm{d}\tau \tag{3.15b}$$

$$\gamma_{ijkl} = \int_0^\infty \int_\infty K_{ij}\xi_k\xi_l \mathrm{d}^3\xi \mathrm{d}\tau \tag{3.15c}$$

$$\zeta_{ijklm} = -\int_0^\infty \int_\infty K_{ij}\xi_k\xi_l\xi_m \mathrm{d}^3\xi \mathrm{d}\tau. \tag{3.15d}$$

Here, the quantities α_{ij}, β_{ijk}, γ_{ijkl} and ζ_{ijklm} are tensors that are dependent on, and totally determined by, $\mathbf{u}$ and $\overline{\mathbf{U}}$, as well as the value of the magnetic diffusivity, η [67].

The tensors α_{ij} and β_{ijk} defined in expressions (3.15a) and (3.15b) respectively are well-known in MFEM and mean-field MHD, and their effects have been extensively studied. For the purposes of this work, we focus our attention on the two higher-order tensors γ_{ijkl} and ζ_{ijklm}, whose forms are given in (3.15c) and (3.15d).

3.2 The Tensors γ_{ijkl} and ζ_{ijklm}

In order to quantify the tensors introduced in the previous section, we begin by considering the simple case where the field $\mathbf{u}$ corresponds to a turbulent small-scale velocity field that is both homogeneous and isotropic. As we had pointed out that the tensors α_{ij}, β_{ijk}, γ_{ijkl} and ζ_{ijklm} are all totally determined in part by $\mathbf{u}$, it stands to reason that the components of γ_{ijlk} and ζ_{ijlkm}, just as their counterparts $\alpha_i j$ and β_{ijk}, have to be invariant under any arbitrary translations of the field $\mathbf{u}$, as well as any rotations about some arbitrary axis in the co-ordinate system [67]. The assumption of the homogeneity and isotropy of $\mathbf{u}$ again allows us to conclude that the tensors γ_{ijlk} and ζ_{ijlkm} are also both homogeneous and isotropic.

The assumption of the isotropy of γ_{ijkl} and ζ_{ijklm} allows us to express them in the simple forms given by:

$$\gamma_{ijkl} = \gamma \varepsilon_{ijkl} \tag{3.16a}$$

$$\zeta_{ijklm} = \zeta \varepsilon_{ijklm}, \tag{3.16b}$$

where the quantities γ and ζ are scalars that are determined by $\mathbf{u}$ only, and ε_{ijkl} and ε_{ijklm} are the fourth- and fifth-order permutation tensors defined as

$$\varepsilon_{ijkl} = \begin{cases} +1 & \text{if } (i,j,k,l) \text{ is an even permutation of } (1,2,3,4) \\ -1 & \text{if } (i,j,k,l) \text{ is an odd permutation of } (1,2,3,4) \\ 0 & \text{otherwise} \end{cases},$$

and

$$\varepsilon_{ijklm} = \begin{cases} +1 & \text{if } (i,j,k,l,m) \text{ is an even permutation of } (1,2,3,4,5) \\ -1 & \text{if } (i,j,k,l,m) \text{ is an odd permutation of } (1,2,3,4,5) \\ 0 & \text{otherwise} \end{cases}$$

respectively. Note that in the general case, γ_{ijkl} and ζ_{ijklm} may be expressed as:

$$\gamma_{ijkl} = \gamma_1 \delta_{ij}\delta_{kl} + \gamma_2 \delta_{ik}\delta_{kl} + \gamma_3 \delta_{il}\delta_{jk} \tag{3.17a}$$

$$\zeta_{ijklm} = \zeta_1 \delta_{ij}\varepsilon_{klm} + \zeta_2 \delta_{ik}\varepsilon_{jlm} + \zeta_3 \delta_{il}\varepsilon_{jkm} + \zeta_4 \delta_{im}\varepsilon_{jkl}, \tag{3.17b}$$

using the most general forms for isotropic fourth- and fifth-order tensors.

Now that we have determined simple forms for γ_{ijkl} and ζ_{ijklm}, we re-derive Ohm's law and the Induction Equations in order to determine the effects that these tensors may have on the evolution of the fields $\overline{\mathbf{B}}$ and $\mathbf{b}$.

3.2.1 The Induction Equations Reformulated

Substituting (3.16a) and (3.16b) into (3.14), the mean EMF may be expressed as:

$$\mathcal{E} = \alpha\overline{\mathbf{B}} - \beta\nabla\times\overline{\mathbf{B}} + \gamma\nabla\times\nabla\times\overline{\mathbf{B}} - \zeta\nabla\times\nabla\times\nabla\times\overline{\mathbf{B}}, \tag{3.18}$$

from where we may obtain a corresponding expression for Ohm's Law:

$$\overline{\mathbf{J}} = \sigma\left(\overline{\mathbf{E}} + \overline{\mathbf{U}}\times\overline{\mathbf{B}} + \alpha\overline{\mathbf{B}} - \beta\nabla\times\overline{\mathbf{B}} + \gamma\nabla\times\nabla\times\overline{\mathbf{B}} - \zeta\nabla\times\nabla\times\nabla\times\overline{\mathbf{B}}\right). \tag{3.19}$$

Here, σ is the electric conductivity and α and β are scalars that are also determined by $\mathbf{u}$. The Induction Equations may be re-derived taking into account the new higher-order terms in the mean EMF. Substituting expression (3.18) into eqns (3.9a) and (3.9b), we arrive at the following evolution equations for $\overline{\mathbf{B}}$ and $\mathbf{b}$ after some algebra:

$$\frac{\partial\overline{\mathbf{B}}}{\partial t} = \nabla\times\left(\overline{\mathbf{U}}\times\overline{\mathbf{B}} + \alpha\overline{\mathbf{B}}\right) + (\eta+\beta)\nabla^2\overline{\mathbf{B}} - \left(\gamma\nabla^2\overline{\mathbf{J}} - \zeta\nabla\times\nabla^2\overline{\mathbf{J}}\right) \tag{3.20a}$$

$$\frac{\partial\mathbf{b}}{\partial t} = \nabla\times\left(\overline{\mathbf{U}}\times\mathbf{b} + \mathbf{u}\times\mathbf{b} - \alpha\overline{\mathbf{B}} + \mathbf{u}\times\overline{\mathbf{B}}\right) - \beta\nabla^2\overline{\mathbf{B}} + \eta\nabla^2\mathbf{b} + \left(\gamma\nabla^2\overline{\mathbf{J}} - \zeta\nabla\times\nabla^2\overline{\mathbf{J}}\right), \tag{3.20b}$$

where we have also assumed that $\nabla\cdot\overline{\mathbf{J}} = 0$ and employ units of $\mu_0 = 1$. It appears that the inclusion of the high-order tensors γ_{ijkl} and ζ_{ijklm} introduces an additional type of hyper-diffusion involving the mean current density, $\overline{\mathbf{J}}$. This is similar to the result obtained in [104] where an additional "correction" to the non-linear component of the mean EMF was discussed.

Recasting the system (3.20) into the form

$$-\left(\gamma\nabla^2\overline{\mathbf{J}} - \zeta\nabla\times\nabla^2\overline{\mathbf{J}}\right) = \frac{\partial\overline{\mathbf{B}}}{\partial t} - \nabla\times\left(\overline{\mathbf{U}}\times\overline{\mathbf{B}} + \alpha\overline{\mathbf{B}}\right) - (\eta+\beta)\nabla^2\overline{\mathbf{B}} \tag{3.21a}$$

$$\left(\gamma\nabla^2\overline{\mathbf{J}} - \zeta\nabla\times\nabla^2\overline{\mathbf{J}}\right) = \frac{\partial\mathbf{b}}{\partial t} - \nabla\times\left(\overline{\mathbf{U}}\times\mathbf{b} + \mathbf{u}\times\mathbf{b} - \alpha\overline{\mathbf{B}} + \mathbf{u}\times\overline{\mathbf{B}}\right) + \beta\nabla^2\overline{\mathbf{B}} - \eta\nabla^2\mathbf{b}, \tag{3.21b}$$

and making the identification $\mathbf{F}(\mathbf{x},t) = \gamma\nabla^2\overline{\mathbf{J}} - \zeta\nabla\times\nabla^2\overline{\mathbf{J}}$, it can be seen that together γ_{ijkl} and ζ_{ijklm} can act as a "source" term to the "homogeneous" version of the equations in system (3.21) (that is, the equations without the presence of the terms introduced by the inclusion of γ_{ijkl} and ζ_{ijklm}):

$$\mathbf{0} = \frac{\partial\overline{\mathbf{B}}}{\partial t} - \nabla\times\left(\overline{\mathbf{U}}\times\overline{\mathbf{B}} + \alpha\overline{\mathbf{B}}\right) - (\eta+\beta)\nabla^2\overline{\mathbf{B}} \tag{3.22a}$$

$$\mathbf{0} = \frac{\partial\mathbf{b}}{\partial t} - \nabla\times\left(\overline{\mathbf{U}}\times\mathbf{b} + \mathbf{u}\times\mathbf{b} - \alpha\overline{\mathbf{B}} + \mathbf{u}\times\overline{\mathbf{B}}\right) + \beta\nabla^2\overline{\mathbf{B}} - \eta\nabla^2\mathbf{b}. \tag{3.22b}$$

It is possible to obtain solutions to both of the "homogeneous" equations in system (3.22) by using Green's functions. Similarly, system (3.21) can also be solved using the method of Green's functions, with the solution being a linear combination of the solution to the "homogeneous" system (3.22) as well as the particular solution to system (3.21) that takes into account the presence of the new "source" term, $\mathbf{F}(\mathbf{x},t)$. The integrals obtained using the Green's method will in general not be tractable, thus requiring the system (3.21) to be solved numerically, or particular forms of $\overline{\mathbf{U}}$ and $\mathbf{u}$ in order to obtain a closed-form analytical solution.

3.2.2 Determining the Tensors γ_{ijkl} and ζ_{ijklm}

Determining analytical forms for the tensors α_{ij}, β_{ijk}, γ_{ijkl} and ζ_{ijklm} are also of paramount importance if the behaviour of the mean EMF in the system is to be studied. Using Green's method, we have already presented integral forms for these tensors in expressions (3.15a) – (3.15d), but note that these integrals may not be analytically-soluble. Once more, we must rely on particular forms of $\overline{\mathbf{U}}$ and $\mathbf{u}$ if we wish to obtain closed-form expressions for these tensors.

Recall that the mean EMF, $\mathcal{E}$, is functionally-dependent on the fluctuating velocity field, $\mathbf{u}$, the mean velocity field, $\overline{\mathbf{U}}$ and the mean magnetic field, $\overline{\mathbf{B}}$. In order to simplify calculations, it is assumed that there is no motion from the mean velocity field, thus leaving $\overline{\mathbf{U}} = \mathbf{0}$ [67, 74, 83]. Together with this, $\overline{\mathbf{B}}$ is also assumed to be time-independent and uniform in space, while $\mathbf{u}$ is assumed to be a statistically-homogeneous, random fluctuating (i.e. turbulent) velocity field [67, 74, 83]. Solving for $\mathcal{E} = \overline{\mathbf{u}\times\mathbf{b}}$, then, also requires us to know what $\mathbf{b}$ is, having been given $\mathbf{u}$.

Using the assumptions stated above, we rewrite the time-evolution equations for $\mathbf{b}$ as:

$$\frac{\partial \mathbf{b}}{\partial t} = \nabla \times (\mathbf{u} \times \overline{\mathbf{B}}) + \nabla \times \mathcal{G} + \eta \nabla^2 \mathbf{b}, \tag{3.23}$$

where $\mathcal{G} = \mathbf{u} \times \mathbf{b} - \mathcal{E}$. The term $\nabla \times \mathcal{G}$ is a non-linear one, which makes obtaining a straightforward solution for $\mathbf{b}$ quite difficult. Eqns (3.23) are first simplified by taking into account properties of the fluctuating velocity field, $\mathbf{u}$. The first of these simplifications is known as the *first-order smoothing approximation* (FOSA), and takes into account the ratio of the non-linear term, $\nabla \times \mathcal{G}$, to that of the time derivative term in $\mathbf{b}$. We begin by expressing eqns (3.23) in terms of the scales that are involved with each of the quantities:

$$\frac{b_\star}{t_\star} = \frac{u_\star B_\star}{l_\star} + \frac{u_\star b_\star}{l_\star} + \frac{\eta b_\star}{{l_\star}^2}, \tag{3.24}$$

where $t_\star$ and $l_\star$ are the time- and length scales over which are typical to the fluctuating velocity field, $\mathbf{u}$, and $b_\star$ and $u_\star$ are typical rms values of the fluctuating magnetic and fluctuating velocity fields respectively.

In order to invoke the FOSA, we take the ratio of the magnitude of the non-linear term, $|\nabla \times \mathcal{G}|$, to that of the time derivative term, $|\partial \mathbf{b}/\partial t|$:

$$\begin{aligned} \frac{|\nabla \times \mathcal{G}|}{\left|\frac{\partial \mathbf{b}}{\partial t}\right|} &= \frac{\frac{u_\star b_\star}{l_\star}}{\frac{b_\star}{t_\star}} \\ &= \frac{u_\star t_\star}{l_\star}. \end{aligned}$$

Here, using $u_\star t_\star / l_\star$, we can distinguish between two distinct cases [67]:

1. For $u_\star t_\star / l_\star \ll 1$, we have random waves.
2. For $u_\star t_\star / l_\star \approx 1$, we have conventional turbulence.

The first case allows us to drop the $\nabla \times \mathcal{G}$ term from eqns (3.23) [67]. The second case asserts that while $|\nabla \times \mathcal{G}|$ and $|\partial \mathbf{b}/\partial t|$ may be of comparable magnitude, if both of these terms are

negligible when compared to the diffusive term, and $\mathrm{Re_M}^{(\mathbf{b})} = u_\star l_\star/\eta$, the magnetic Reynolds number associated with eqns (3.23), is much less than unity (i.e. $\mathrm{Re_M}^{(\mathbf{b})} \ll 1$), then both the $\nabla \times \mathcal{G}$ and $\partial \mathbf{b}/\partial t$ terms may be dropped from eqns (3.23) [67]. This leaves us with the following set of equations:

$$\frac{\partial \mathbf{b}}{\partial t} = \nabla \times (\mathbf{u} \times \overline{\mathbf{B}}) + \eta \nabla^2 \mathbf{b}, \tag{3.25a}$$

$$\mathbf{0} = \nabla \times (\mathbf{u} \times \overline{\mathbf{B}}) + \eta \nabla^2 \mathbf{b}, \tag{3.25b}$$

which correspond to the cases of random waves and conventional turbulence respectively.

Note that both equations in system (3.25) say that the fluctuating magnetic field, $\mathbf{b}$, is generated through the interaction of the fluctuating velocity field, $\mathbf{u}$, with the mean magnetic field, $\overline{\mathbf{B}}$. The generation of $\mathbf{b}$ is done automatically in eqns (3.25b) due to the large influence of diffusion, while in eqns (3.25a) this can depend largely on the behavioural history of $\mathbf{u}$ in past times [67]. It can be argued that the solutions to eqns (3.25a) could approximately solve eqns (3.25b), provided that $\mathrm{Re_M}^{(\mathbf{b})} \ll 1$ [67], thus allowing us to focus our attention on eqns (3.25a) in approximating the mean EMF.

The mean EMF may now be constructed through the use of the Fourier Transform. In general, eqns (3.25a) will be subjected to the Fourier Transform and solved for $\tilde{\mathbf{b}}$, the Fourier transform of $\mathbf{b}$.

Given that the Fourier transform of the fluctuating random turbulent velocity field, $\mathbf{u}$, is expressed as [67]:

$$\tilde{\mathbf{u}}(\mathbf{k}, \omega) = \frac{1}{(2\pi)^4} \iint \mathbf{u}(\mathbf{x}, t) e^{-i(\mathbf{k}\cdot\mathbf{x} - \omega t)} \mathrm{d}^3\mathbf{x}\, \mathrm{d}t, \tag{3.26}$$

and its inverse Fourier transform as [67]:

$$\mathbf{u}(\mathbf{x}, t) = \iint \tilde{\mathbf{u}}(\mathbf{k}, \omega) e^{i(\mathbf{k}\cdot\mathbf{x} - \omega t)} \mathrm{d}^3\mathbf{k}\, \mathrm{d}\omega, \tag{3.27}$$

the mean EMF may be constructed through solving

$$\begin{aligned}\mathcal{E} &= \overline{\mathbf{u}\times\mathbf{b}} \\ &= \iiiint \overline{\tilde{\mathbf{u}}(\mathbf{k},\omega)\times\tilde{\mathbf{b}}(\mathbf{k}',\omega')}e^{i(\mathbf{k}-\mathbf{k}')\cdot\mathbf{x}-i(\omega-\omega')t}\,\mathrm{d}^3\mathbf{k}\,\mathrm{d}^3\mathbf{k}'\,\mathrm{d}\omega\,\mathrm{d}\omega', \end{aligned} \tag{3.28}$$

the inverse Fourier transform integral for $\mathcal{E}$, where the form for $\tilde{\mathbf{b}}(\mathbf{k}',\omega')$ is given by the Fourier transform of eqns (3.25a). Using the assumptions and simplifications made this far, the integral (3.28) is written in a form corresponding to each of the terms in the Taylor expansion for $\mathcal{E}$ given in (3.14) after much simplification. It should also be noted that the form for $\tilde{\mathbf{b}}(\mathbf{k}',\omega')$ is dependent on which tensor in the expansion for $\mathcal{E}$ is being sought. Going back to eqns (3.25a), it can be seen that $\overline{\mathbf{B}} = \overline{\mathbf{B}}(\mathbf{x})$ (due to the assumptions of the field being time-independent and uniform) is the quantity that will influence the form of $\tilde{\mathbf{b}}(\mathbf{k}',\omega')$, due to it taking different forms depending on which tensor in the expansion is sought.

As an example, should we wish to determine β_{ijk}, $\overline{\mathbf{B}}(\mathbf{x})$ would be written as $\overline{B}_j(\mathbf{x}) = x_k\dfrac{\partial\overline{B}_j}{\partial x_k}$ [67]. Similarly, for γ_{ijkl} and ζ_{ijklm}, we would propose the forms $\overline{B}_j(\mathbf{x}) = x_kx_l\dfrac{\partial^2\overline{B}_j}{\partial x_kx_l}$ and $\overline{B}_j(\mathbf{x}) = x_kx_lx_m\dfrac{\partial^3\overline{B}_j}{\partial x_kx_lx_m}$ respectively.

Using these forms, it is possible to compute the curl term, $\nabla\times(\mathbf{u}\times\overline{\mathbf{B}})$, after which eqns (3.25a) are Fourier-transformed, solved for $\tilde{\mathbf{b}}(\mathbf{k}',\omega')$ and then substituted into the integral (3.28) in order to find the relevant tensor.

Another method of determining the tensors α_{ij}, β_{ijk}, γ_{ijkl} and ζ_{ijklm} under the FOSA is to make use of the Green's function in order to write a solution to eqns (3.25a) as is outlined in [74]. The tensors are then determined by construction from $\mathcal{E}$.

Using the Green's method, the solution to eqns (3.25a) may be written as [74]:

$$\begin{aligned} b_k(\mathbf{x},t) = &\int_\infty G(\mathbf{x}-\mathbf{x}',t-t_0)b_k(\mathbf{x}',t_0)\mathrm{d}^3x' \\ &+\varepsilon_{klm}\varepsilon_{mpq}\int_{t_0}^{t}\int_\infty G(\mathbf{x}-\mathbf{x}',t-t_0)\frac{\partial}{\partial x_l}\left(u_p'(\mathbf{x}',t')\overline{B}_q(\mathbf{x}',t')\right)\mathrm{d}^3x'\mathrm{d}t', \end{aligned} \tag{3.29}$$

with $\nabla \cdot \mathbf{b}(\mathbf{x}, t_0) = 0$ and $G(\mathbf{x} - \mathbf{x}', t - t_0)$ being a Green's function. Note that from the definition of the averages in expressions (3.2a) and (3.3a), we identify that $\mathbf{x} - \mathbf{x}' = \boldsymbol{\xi}$ and $t - t_0 = \tau$. Using these definitions, we change integration variables in expression (3.29) and are left with [74]:

$$b_k(\mathbf{x}, t) = \int_\infty G(\boldsymbol{\xi}, \tau) b_k(\mathbf{x} - \boldsymbol{\xi}, t_0) \mathrm{d}^3\xi + \varepsilon_{klm}\varepsilon_{mpq} \int_0^{t-t_0} \int_\infty \frac{1}{\xi} \frac{\partial G(\boldsymbol{\xi}, \tau)}{\partial \xi} \xi_l u'_p(\mathbf{x} - \boldsymbol{\xi}, t - \tau) \overline{B}_q(\mathbf{x} - \boldsymbol{\xi}, t - \tau) \mathrm{d}^3\xi \mathrm{d}\tau, \tag{3.30}$$

where the Green's function, $G(\boldsymbol{\xi}, \tau)$, is now solely a function of $\boldsymbol{\xi}$ and τ.

Having obtained an expression for $b_k(\mathbf{x}, t)$, recall that the mean EMF is given by $\mathcal{E}(\mathbf{x}, t) = \overline{\mathbf{u}(\mathbf{x}, t) \times \mathbf{b}(\mathbf{x}, t)}$. Substituting the expression for $b_k(\mathbf{x}, t)$ from (3.30) into the definition of $\mathcal{E}$, and reverting to indicial notation, we obtain the following:

$$\begin{aligned} \mathcal{E}_i(\mathbf{x}, t) &= \varepsilon_{ijk} \overline{u_j(\mathbf{x}, t) b_k(\mathbf{x}, t)} \\ &= \varepsilon_{ijk} \overline{u_j(\mathbf{x}, t) \left(\int_\infty G(\boldsymbol{\xi}, \tau) b_k(\mathbf{x} - \boldsymbol{\xi}, t_0) \mathrm{d}^3\xi \right.} \\ &\quad \left. + \varepsilon_{klm}\varepsilon_{mpq} \int_0^{t-t_0} \int_\infty \frac{1}{\xi} \frac{\partial G(\boldsymbol{\xi}, \tau)}{\partial \xi} \xi_l u'_p(\mathbf{x} - \boldsymbol{\xi}, t - \tau) \overline{B}_q(\mathbf{x} - \boldsymbol{\xi}, t - \tau) \mathrm{d}^3\xi \mathrm{d}\tau \right)}. \end{aligned} \tag{3.31}$$

Choosing to focus on times, t, which are much larger than the initial time, t_0, allows us to drop the first integral containing $b_k(\mathbf{x} - \boldsymbol{\xi}, t_0)$ as well as to send $t_0 \to -\infty$ in the upper limit of the second integral (3.31) due to the fact that there will no longer be any correlation between any quantities which are measured at these large times [74]. This leaves the mean EMF as:

$$\mathcal{E}_i(\mathbf{x}, t) = \varepsilon_{ijk} \overline{u_j(\mathbf{x}, t) \left(\varepsilon_{klm}\varepsilon_{mpq} \int_0^{\infty} \int_\infty \frac{1}{\xi} \frac{\partial G(\boldsymbol{\xi}, \tau)}{\partial \xi} \xi_l u'_p(\mathbf{x} - \boldsymbol{\xi}, t - \tau) \overline{B}_q(\mathbf{x} - \boldsymbol{\xi}, t - \tau) \mathrm{d}^3\xi \mathrm{d}\tau \right)}. \tag{3.32}$$

Further algebra allows the mean EMF to be expressed in the form given by expression (3.11) as [74]:

$$\mathcal{E}_i(\mathbf{x},t) = \int_0^\infty \int_\infty (\varepsilon_{ilm}\delta_{nj} - \varepsilon_{ilj}\delta_{mn})\frac{1}{\xi}\frac{\partial G(\boldsymbol{\xi},\tau)}{\partial \xi} Q_{lm}(\mathbf{x},t;-\boldsymbol{\xi},-\tau)\xi_n \overline{B}_j(\mathbf{x}-\boldsymbol{\xi},t-\tau)\mathrm{d}^3\xi\mathrm{d}\tau, \tag{3.33}$$

where we identify that:

$$K_{ij}(\mathbf{x},t;\boldsymbol{\xi},\tau) = (\varepsilon_{ilm}\delta_{nj} - \varepsilon_{ilj}\delta_{mn})\frac{1}{\xi}\frac{\partial G(\boldsymbol{\xi},\tau)}{\partial \xi} Q_{lm}(\mathbf{x},t;-\boldsymbol{\xi},-\tau)\xi_n \tag{3.34}$$

$$Q_{lm}(\mathbf{x},t;-\boldsymbol{\xi},-\tau) = \overline{u_l(\mathbf{x},t)u_m(\mathbf{x}+\boldsymbol{\xi},t+\tau)}. \tag{3.35}$$

Here, $K_{ij}(\mathbf{x},t;\boldsymbol{\xi},\tau)$ is the calculated form of the kernel which appeared in the integral representation for $\mathcal{E}(\mathbf{x},t)$ in expression (3.11) and $Q_{lm}(\mathbf{x},t;-\boldsymbol{\xi},-\tau)$ is the correlation tensor for the random turbulent field, $\mathbf{u}$.

The tensors α_{ij}, β_{ijk}, γ_{ijkl} and ζ_{ijklm}, whose integral forms are given by (3.15a) – (3.15d) are now finally expressed using the result from expression (3.33) as:

$$\alpha_{ij} = (\varepsilon_{ipq}\delta_{nj} - \varepsilon_{ipj}\delta_{qn})\int_0^\infty \int_\infty \frac{1}{\xi}\frac{\partial G(\boldsymbol{\xi},\tau)}{\partial \xi} Q_{pq}(\mathbf{x},t;-\boldsymbol{\xi},-\tau)\xi_n \mathrm{d}^3\xi\mathrm{d}\tau \tag{3.36a}$$

$$\beta_{ijk} = -(\varepsilon_{ipq}\delta_{nj} - \varepsilon_{ipj}\delta_{qn})\int_0^\infty \int_\infty \frac{1}{\xi}\frac{\partial G(\boldsymbol{\xi},\tau)}{\partial \xi} Q_{pq}(\mathbf{x},t;-\boldsymbol{\xi},-\tau)\xi_n\xi_k \mathrm{d}^3\xi\mathrm{d}\tau \tag{3.36b}$$

$$\gamma_{ijkl} = (\varepsilon_{ipq}\delta_{nj} - \varepsilon_{ipj}\delta_{qn})\int_0^\infty \int_\infty \frac{1}{\xi}\frac{\partial G(\boldsymbol{\xi},\tau)}{\partial \xi} Q_{pq}(\mathbf{x},t;-\boldsymbol{\xi},-\tau)\xi_n\xi_k\xi_l \mathrm{d}^3\xi\mathrm{d}\tau \tag{3.36c}$$

$$\zeta_{ijklm} = -(\varepsilon_{ipq}\delta_{nj} - \varepsilon_{ipj}\delta_{qn})\int_0^\infty \int_\infty \frac{1}{\xi}\frac{\partial G(\boldsymbol{\xi},\tau)}{\partial \xi} Q_{pq}(\mathbf{x},t;-\boldsymbol{\xi},-\tau)\xi_n\xi_k\xi_l\xi_m \mathrm{d}^3\xi\mathrm{d}\tau. \tag{3.36d}$$

These integrals may be evaluated further in order to obtain functional forms for the tensors α_{ij}, β_{ijk}, γ_{ijkl} and ζ_{ijklm}, where assumptions of the properties correlation tensor for the random,

turbulent fluctuating velocity field, $Q_{lm}(\mathbf{x}, t; -\boldsymbol{\xi}, -\tau)$, will need to be made in order to evaluate the integrals in order to obtain a functional form. In order to successfully calculate the functional forms for these tensors, the type of turbulence introduced by the field $\mathbf{u}$ must be known, and depending on this, could cause the integrals themselves to become analytically-insoluble.

As discussed in section 1.2, much work has been done on determining forms for the first two tensors, α_{ij} and β_{ijk} in different types of turbulence and is discussed in detail in works such as [24, 67, 74, 75, 78, 83, 104]. For our purposes, we present here only the integral forms for the higher-order tensors γ_{ijkl} and ζ_{ijklm} and note that they can be solved in order to obtain functional forms for these quantities.

3.2.3 Scale Analysis

Recall that in order to re-derive the Induction equations for $\overline{\mathbf{B}}$ and $\mathbf{b}$ including the terms for the tensors γ_{ijkl} and ζ_{ijklm} given by eqns (3.20a) and (3.20b), in addition to those already included due to the presence of α_{ij} and β_{ijk}, we assumed that γ_{ijkl} and ζ_{ijklm} were both isotropic, allowing the simple expressions of $\gamma_{ijkl} = \gamma\varepsilon_{ijkl}$ and $\zeta_{ijklm} = \zeta\varepsilon_{ijklm}$ for γ and ζ being scalars. Note that the assumption of isotropy also extended to α_{ij} and β_{ijk}, allowing them to be written in simple forms. The Induction equations involving the new terms for γ_{ijkl} and ζ_{ijklm} were found to be given by:

$$\begin{aligned}
\frac{\partial\overline{\mathbf{B}}}{\partial t} &= \nabla\times\left(\overline{\mathbf{U}}\times\overline{\mathbf{B}}+\alpha\overline{\mathbf{B}}\right)+(\eta+\beta)\nabla^2\overline{\mathbf{B}}-\left(\gamma\nabla^2\overline{\mathbf{J}}-\zeta\nabla\times\nabla^2\overline{\mathbf{J}}\right)\\
\frac{\partial\mathbf{b}}{\partial t} &= \nabla\times\left(\overline{\mathbf{U}}\times\mathbf{b}+\mathbf{u}\times\mathbf{b}-\alpha\overline{\mathbf{B}}+\mathbf{u}\times\overline{\mathbf{B}}\right)-\beta\nabla^2\overline{\mathbf{B}}+\eta\nabla^2\mathbf{b}+\left(\gamma\nabla^2\overline{\mathbf{J}}-\zeta\nabla\times\nabla^2\overline{\mathbf{J}}\right).
\end{aligned}$$

Due to the assumption of isotropy on γ_{ijkl} and ζ_{ijklm}, the new terms introduced by the inclusion of these tensors take on forms both involving $\nabla^2\overline{\mathbf{J}}$ and $\nabla\times\nabla^2\overline{\mathbf{J}}$ respectively, which appeared to describe a type of hyper-diffusion involving the mean current density, $\overline{\mathbf{J}}$. Noting that $\nabla\times\overline{\mathbf{B}}=\overline{\mathbf{J}}$ in units of $\mu_0 = 1$, re-expressing these terms in terms of $\overline{\mathbf{B}}$ would describe a type of *hyper-diffusion* involving $\overline{\mathbf{B}}$ due to the presence of a ∇^4 term.

The idea of hyper-diffusion in large- and small-scale dynamos is not a new one and has previously been studied and discussed in works such as [11, 13, 24, 104] and others. In [104], for

example, hyper-diffusion was studied in the context of non-linear effects within the flow itself, effectively adding a third component in the decomposition of $\mathbf{U}$: $\mathbf{U} = \overline{\mathbf{U}} + \mathbf{u} + \mathbf{v}$, where $\mathbf{v}$ is the non-linear component of the flow, satisfying its own equation of motion. In order to account for the contribution to the flow from the non-linear component, the mean EMF also picks up an additional component involving the cross product of the average of $\mathbf{v}$ and $\mathbf{b}$, to reflect that the non-linear component also interacts with the fluctuating magnetic field, $\mathbf{b}$.

On deriving the expression for the mean EMF, $\mathcal{E}$, taking into account the additional non-linear term for the flow, terms in $\nabla^4\overline{\mathbf{B}}$ appear in its functional form after taking the curl $\nabla \times \mathcal{E}$. The hyper-diffusive terms arising from the mean EMF, such as those discussed in [24, 104], play a role in understanding the saturation of small- and large-scale dynamos.

For the purposes of this work, the saturation of the small- and large-scale dynamos is not considered, but mention is made of this for the sake of completeness. In our case, we now perform a rudimentary scale analysis of the terms in γ and ζ in relation to the other terms in the Induction equations in order to determine bounds beyond which their contributions to the temporal evolution of the fields $\overline{\mathbf{B}}$ and $\mathbf{b}$ would become significant.

For this analysis, we make use of the length- and time scales $\xi_\star$ and $\tau_\star$, where we recall that these scales satisfy the inequalities $l_0 \ll \xi \ll L$ and $t_0 \ll \tau \ll T$ respectively. Here, l_0 and t_0 refer to the length- and time scales of the energy-containing eddies in the system, and L and T refer to the global length- and time scales over which the mean quantities vary. These scales are chosen in such a way that both eqns (3.20a) and (3.20b) apply simultaneously. That is, they act independently on the large- and small-scale magnetic fields that are present at these scales, where both of these fields have magnitudes that are non-negligible. In this way, we would be able to send, for example, $\tau_\star \to T$ or t_0 and $\xi_\star \to L$ or l_0 so that the corresponding set of Induction Equations (i.e. either eqns (3.20a) or (3.20b)) becomes fully relevant. Note that at the global scales L and T, the small-scale quantities may be regarded as negligible, whilst at the small scales l_0 and t_0, the large-scale quantities may be regarded as uniform.

Using the length- and time scales defined, eqns 3.20a and 3.20b are expressed as:

$$\frac{B_0}{\tau} = \frac{U_0 B_0}{\xi} + \frac{\alpha_\star B_0}{\xi} + \frac{(\eta + \beta_\star) B_0}{\xi^2} - \frac{\gamma_\star B_0}{\xi^3} + \frac{\zeta_\star B_0}{\xi^4} \tag{3.38a}$$

$$\frac{b_0}{\tau} = \frac{U_0 b_0}{\xi} + \frac{u_0 b_0}{\xi} - \frac{\alpha_\star B_0}{\xi} + \frac{\beta_\star B_0}{\xi^2} + \frac{\gamma_\star B_0}{\xi^3} - \frac{\zeta_\star B_0}{\xi^4} + \frac{u_0 B_0}{\xi} + \frac{\eta b_0}{\xi^2}, \tag{3.38b}$$

where U_0 and B_0 are the magnitudes of $\overline{\mathbf{U}}$ and $\overline{\mathbf{B}}$, and u_0 and b_0 the magnitudes of $\mathbf{u}$ and $\mathbf{b}$ (typically defined as rms values for these fields) respectively; all other symbols retain their usual meanings. Using the scale analysis, we wish to determine lower limits on the average values of γ and ζ, $\gamma_\star$ and $\zeta_\star$, above which, the terms they correspond to would make significant contributions to the evolution of both $\overline{\mathbf{B}}$ and $\mathbf{b}$ in their respective Induction equations. As was seen in the previous section, both γ_{ijkl} and ζ_{ijklm} are traditionally defined through the integral expressions (3.36c) and (3.36d) which are dependent on $\mathbf{u}$. Assuming that $\gamma_{ijkl} = \gamma\varepsilon_{ijkl}$ and $\zeta_{ijklm} = \zeta\varepsilon_{ijklm}$ then implies that both γ and ζ are themselves dependent on $\mathbf{u}$ as well, which requires the definition of the average values $\gamma_\star$ and $\zeta_\star$ which are defined though a suitable and well-defined averaging procedure. Note that $\alpha_\star$ and $\beta_\star$ are defined in a similar way, but are not discussed here.

In order to determine the lower limits on $\gamma_\star$ and $\zeta_\star$, we shall compare each of these terms' magnitudes to the magnitudes of both the inductive and diffusive terms (in η only) in eqns (3.20a) and (3.20b).

Beginning with eqns (3.20a), we require that for the terms in $\gamma_\star$ to become significant compared to the inductive and magnetic-diffusive terms (i.e. the diffusive terms in η), the following would have to hold:

$$\begin{aligned} \left|\gamma\nabla^2\overline{\mathbf{J}}\right| &\geq \left|\nabla\times(\overline{\mathbf{U}}\times\overline{\mathbf{B}})\right| \\ \Rightarrow \frac{\gamma_\star B_0}{{\xi_\star}^3} &\geq \frac{U_0 B_0}{\xi_\star} \\ \Rightarrow \gamma_\star &\geq U_0 {\xi_\star}^2 \end{aligned} \tag{3.39}$$

for the inductive term, and

$$\begin{aligned} \left|\gamma\nabla^2\overline{\mathbf{J}}\right| &\geq \left|\eta\nabla^2\overline{\mathbf{B}}\right| \\ \Rightarrow \frac{\gamma_\star B_0}{{\xi_\star}^3} &\geq \frac{\eta B_0}{{\xi_\star}^2} \end{aligned}$$

$$\Rightarrow \gamma_\star \geq \eta\xi \tag{3.40}$$

for the diffusive term. For $\zeta_\star$, the conditions are given by:

$$\begin{aligned}\left|\zeta\nabla\times\nabla^2\overline{\mathbf{J}}\right| &\geq \left|\nabla\times(\overline{\mathbf{U}}\times\overline{\mathbf{B}})\right| \\ \Rightarrow \frac{\zeta_\star B_0}{{\xi_\star}^4} &\geq \frac{U_0 B_0}{\xi_\star} \\ \Rightarrow \zeta_\star &\geq U_0 {\xi_\star}^3\end{aligned} \tag{3.41}$$

for the inductive term, and

$$\begin{aligned}\left|\zeta\nabla\times\nabla^2\overline{\mathbf{J}}\right| &\geq \left|\eta\nabla^2\overline{\mathbf{B}}\right| \\ \Rightarrow \frac{\zeta_\star B_0}{{\xi_\star}^4} &\geq \frac{\eta B_0}{{\xi_\star}^2} \\ \Rightarrow \zeta_\star &\geq \eta {\xi_\star}^2.\end{aligned} \tag{3.42}$$

Turning now to eqns (3.20b), we find that the conditions on $\gamma_\star$ for the inductive and magnetic-diffusive terms are given by:

$$\begin{aligned}\left|\gamma\nabla^2\overline{\mathbf{J}}\right| &\geq \left|\nabla\times(\overline{\mathbf{U}}\times\mathbf{b}+\mathbf{u}\times\mathbf{b}+\mathbf{u}\times\overline{\mathbf{B}})\right| \\ \Rightarrow \frac{\gamma_\star B_0}{{\xi_\star}^3} &\geq \frac{U_0 b_0 + u_0 b_0 + u_0 B_0}{\xi_\star} \\ \Rightarrow \gamma_\star &\geq \frac{(U_0 b_0 + u_0 b_0 + u_0 B_0){\xi_\star}^2}{B_0}\end{aligned} \tag{3.43}$$

and

$$\begin{aligned}\left|\gamma\nabla^2\overline{\mathbf{J}}\right| &\geq \left|\eta\nabla^2\mathbf{b}\right| \\ \Rightarrow \frac{\gamma_\star B_0}{{\xi_\star}^3} &\geq \frac{\eta b_0}{{\xi_\star}^2} \\ \Rightarrow \gamma_\star &\geq \frac{\eta b_0 \xi}{B_0}\end{aligned} \tag{3.44}$$

respectively, while for $\zeta_\star$, the conditions for significance in comparison to the inductive and magnetic-diffusive terms are given by are given by:

$$\begin{aligned}\left|\zeta\nabla\times\nabla^2\overline{\mathbf{J}}\right| &\geq \left|\nabla\times(\overline{\mathbf{U}}\times\mathbf{b}+\mathbf{u}\times\mathbf{b}+\mathbf{u}\times\overline{\mathbf{B}})\right| \\ \Rightarrow \frac{\zeta_\star B_0}{{\xi_\star}^4} &\geq \frac{U_0 b_0 + u_0 b_0 + u_0 B_0}{\xi_\star} \\ \Rightarrow \zeta_\star &\geq \frac{(U_0 b_0 + u_0 b_0 + u_0 B_0){\xi_\star}^3}{B_0}\end{aligned} \tag{3.45}$$

and

$$\begin{aligned}\left|\zeta\nabla\times\nabla^2\overline{\mathbf{J}}\right| &\geq \left|\eta\nabla^2\mathbf{b}\right| \\ \Rightarrow \frac{\zeta_\star B_0}{{\xi_\star}^4} &\geq \frac{\eta b_0}{{\xi_\star}^2} \\ \Rightarrow \zeta_\star &\geq \frac{\eta b_0 {\xi_\star}^2}{B_0}\end{aligned} \tag{3.46}$$

respectively.

Note that if we were to assume that both γ and ζ are independent of position and time, they would be able to replaced by scalar values that would control the strength of the hyper-diffusivities to which they are attached in a similar way to what is done with the magnetic diffusivity, η, which controls the strength of the diffusive terms to which it is attached.

Another way of observing the effects of these quantities on the temporal evolution of the fields $\overline{\mathbf{B}}$ and $\mathbf{b}$ would be to, as a simple approximation, drop the terms in α and β in eqns (3.20a) and (3.20b) and then solve the resulting equations either analytically through Green's method, or numerically using a suitable computer code. In addition to dropping the terms in α and β, γ and ζ may also initially be assumed to be independent of position and time, admitting representation as pure scalar quantities.

Now that we have determined lower limits on $\gamma_\star$ and $\zeta_\star$, above which their corresponding terms in γ and ζ would become significant in the time evolution of the large- and small-scale magnetic fields, we finally turn to a brief discussion of the application of the theory of analogies to Mean-Field Electrodynamics.

3.3 The Analogy Between the Reynolds Stress Tensor and the Mean EMF

In order to obtain the evolution equations for the large-scale magnetic field given in (3.20a), an averaging operator was applied to the Induction equations for the total magnetic field, given in (3.5), while the evolution equations for the small-scale magnetic field were obtained by noting that since $\mathbf{b} = \mathbf{B} = \overline{\mathbf{B}}$, eqns (3.20b) could be obtained by taking the difference between eqns (3.5) and (3.20a).

In turbulent Fluid Dynamics, it is also common to decompose the total velocity field, $\mathbf{U}$, into its mean and fluctuating parts using the decomposition given by expression (3.1b). In this way, the time evolution equations for the respective large- and small scale component fields, $\overline{\mathbf{U}}$ and $\mathbf{u}$, must also be considered. The total velocity field, $\mathbf{U}$, evolves according to the Navier-Stokes or *momentum* equations, given here in indicial notation as [73]:

$$\rho \frac{\mathrm{D}U_j}{\mathrm{D}t} = \nu \nabla^2 U_j \partial x_i \partial x_j - \frac{\partial p}{\partial x_j}, \tag{3.47}$$

where we identify the Lagrangian derivative, $\dfrac{\mathrm{D}U_j}{\mathrm{D}t} = \dfrac{\partial U_j}{\partial t} + \dfrac{\partial U_i U_j}{\partial x_i}$ and all other symbols retain their usual meanings. Taking the mean of eqns (3.47) is straightforward, but becomes more involved when looking at the mean Lagrangian derivative, which is given by:

$$\begin{aligned}
\overline{\frac{\mathrm{D}U_j}{\mathrm{D}t}} &= \overline{\frac{\partial U_j}{\partial t} + \frac{\partial U_i U_j}{\partial x_i}} \\
&= \frac{\partial \overline{U_j}}{\partial t} + \frac{\partial \overline{U_i U_j}}{\partial x_i} \\
&= \frac{\partial \overline{U_j}}{\partial t} + \frac{\partial \overline{U_i}\,\overline{U_j}}{\partial x_i} + \frac{\partial \overline{u_i u_j}}{\partial x_i},
\end{aligned}$$

after using the Reynolds averaging rules given by expressions (3.4a) – (3.4h). The averaged or mean momentum equations for the time evolution of $\overline{\mathbf{U}}$ are then given by:

$$\frac{\mathrm{D}\overline{U_j}}{\mathrm{D}t} = -\frac{\partial p}{\partial x_j} + \nu \nabla^2 U_j \partial x_i \partial x_j - \frac{\partial \overline{u_i u_j}}{\partial x_i}, \tag{3.48}$$

where the quantity $\overline{u_i u_j}$ is identified as the *Reynolds stress tensor* [67,73] or *two-point, second-order turbulent velocity correlation tensor* [24, 74] and $\dfrac{\mathrm{D}\overline{U_j}}{\mathrm{D}t} = \dfrac{\partial \overline{U_j}}{\partial t} + \dfrac{\partial \overline{U_i}\,\overline{U_j}}{\partial x_i}$ is the mean Lagrangian derivative for U_j [73].

It is known that the Reynolds stress tensor, $\overline{u_i u_j}$, is the fluid counterpart of the mean EMF, $\mathcal{E}_i = \varepsilon_{ijk}\overline{u_j b_k}$, however, there is not yet any satisfactory theory in that allows this tensor to be expressed in terms of the mean velocity field, $\overline{\mathbf{U}}$ [67], unlike the theory that allows the mean EMF to be expressed in terms of the mean velocity and magnetic fields, $\overline{\mathbf{U}}$ and $\overline{\mathbf{B}}$, as well as the fluctuating, turbulent velocity field, $\mathbf{u}$.

In the work [32], under the assumption that the mean velocity field is incompressible (i.e. $\nabla \cdot \overline{\mathbf{U}} = 0$), uniform and constant, and weak, Reynolds the stress tensor is assumed to be a functional of $\overline{\mathbf{U}}$ and is expanded in a Taylor series as:

$$\overline{u_i u_j} = \overline{{u_i}^{(0)} {u_j}^{(0)}} + \overline{U}_l \left[\frac{\partial \overline{u_i u_j}}{\partial \overline{U}_l} \right]_{\overline{U}=0} + \mathcal{O}\left(\overline{U}^2\right), \tag{3.49}$$

where ${u_i}^{(0)}$ is a "basic (small-scale) flow" that is driven by a time-dependent forcing function that is also periodic in both time and space, satisfying the incompressible Navier-Stokes equations [32], and the term $\alpha_{ijl} = \left[\dfrac{\partial \overline{u_i u_j}}{\partial \overline{U}_l} \right]_{\overline{U}=0}$ is identified as the kinematic counterpart of the MHD α-tensor, α_{ij}. They note also that the tensor α_{ijl} can vanish in many cases which include the following cases [32]:

1. A parity-invariant basic flow causing α_{ijl} to vanish due to $\alpha_{ijl} = \left[\dfrac{\partial \overline{u_i u_j}}{\partial \overline{U}_l} \right]_{\overline{U}=0}$ having an odd number of velocities.
2. α_{ijl} vanishing in a random isotropic flow due to it being symmetrical in i and j by construction. All third-order isotropic tensors possessing this type of symmetry vanish.
3. A basic flow that is time-independent can cause α_{ijl} to vanish to leading order when it is calculated perturbatively in powers of the fluid Reynolds number, Re.
4. A basic flow that is random and δ-correlated in time.
5. Flows of the ABC-type can also cause α_{ijl} to vanish, as was noted in [29, 32].

The authors of [32] then go on to study the effects of α_{ijl} using a full three-dimensional simulation of the Navier-Stokes equations for an anisotropic flow that lacks parity-invariance and note that an instability at large scales is observed in the flow itself, which is consistent with the α-effect in MHD and dynamo theory. The authors refer to this phenomenon as the AKA. Nonlinear behaviour in the AKA is also observed and discussed briefly by the authors of [32], but is further explored and expanded on in [33] and [109]. In particular, the authors of [33] also observe a transfer of kinetic energy from small scales to large scales, consistent with the inverse cascade phenomenon seen in MHD.

For the case of $\overline{\mathbf{U}}$ being a compressible flow (i.e. $\nabla \cdot \overline{\mathbf{U}} \neq 0$), the possibility of a kinetic α-effect is also explored in [68] analytically, and through the use of simulation. They find that perturbation seed eddies are magnified through the presence of helical turbulence, which once more leads to instability in the flow as well as the appearance of large-scale structures. Again, this is seen as consistent with the MHD α-effect. In addition to the appearance of large-scale structures and instability within the flow, the inverse cascade of kinetic energy is also observed once more. This is also further discussed in [60].

In the work [21], the AKA is further explored though simulation and its relevance in the astrophysical context is considered. Once more, it is found that the AKA produces a large-scale flow pattern in the velocity field when the fluid Reynolds number, Re, is small. Furthermore, its components are found to be independent of Re in this case. However, as the value of Re increases, the components of the kinetic α-tensor are found to fall away. A magnetic field is also introduced into the simulation in order to assess the relevance of the AKA in astrophysical settings, but once more it is found that the presence of the magnetic field suppresses the AKA, likely implying that it may play no great role in an astrophysical environment.

More recently, the work [79] explores the similarity of the behaviour exhibited by cross-helically forced flows to that of kinetically-forced flows. The test-field method is used to determine the coefficients of turbulent transport in this case, and mean-field effects that appear to depend on the cross-correlation between the magnetic and velocity fluctuations are found.

3.4 Conclusion

In this chapter, we set out to investigate higher-order terms which appear in the Taylor expansion of the mean EMF, $\mathcal{E}$, which arises naturally from the mean-field Induction equations as a result of the decomposition of the total magnetic and velocity fields into mean and fluctuating components, and represents the interaction between the fluctuating velocity and magnetic fields, $\mathbf{u}$ and $\mathbf{b}$.

We discussed the averaging procedures that were used to obtain the the mean velocity and magnetic fields, $\overline{\mathbf{U}}$ and $\overline{\mathbf{B}}$, as well as the Reynolds averaging rules which these mean quantities were expected to obey. By averaging the Induction equations for the total magnetic field, $\mathbf{B}$, the Induction equations for $\overline{\mathbf{B}}$ were obtained. Furthermore, by noting that the total magnetic field was a linear combination of the mean- and fluctuating magnetic fields, $\mathbf{B} = \overline{\mathbf{B}} + \mathbf{b}$, the Induction equations for $\mathbf{b}$ were obtained. As the mean EMF represents the interaction between the fluctuating velocity and magnetic fields, the identification $\mathcal{E} = \overline{\mathbf{u} \times \mathbf{b}}$ was made.

In order to determine a form for $\mathcal{E}$, we assumed that it could be written in an integral form using the product of a Green's function or kernel, and the mean magnetic field, $\overline{\mathbf{B}}$, where the kernel would be determined later. By assuming that the time and space variation of $\overline{\mathbf{B}}$ is small, it was replaced by a Taylor expansion up to the third order about the points $\boldsymbol{\xi}$ and τ, which are the length- and time scales on which the averaging that defines the mean quantities is done. Further algebra in the integral for $\mathcal{E}$ yielded the integral forms for the tensors α_{ij}, β_{ijk}, γ_{ijkl} and ζ_{ijklm}. We noted that the tensors α_{ij} and β_{ijk} corresponded to the α- and β-effects studied widely MHD; the focus of this chapter was to be on the higher-order tensors, γ_{ijkl} and ζ_{ijklm}.

Under the assumptions of isotropy and homogeneity, the tensors γ_{ijkl} and ζ_{ijklm} permitted the simple forms $\gamma_{ijkl} = \gamma\varepsilon_{ijkl}$ and $\zeta_{ijklm} = \zeta\varepsilon_{ijklm}$, with γ and ζ being scalars, and the Induction equations incorporating these new tensors were derived. It was noted in these Induction equations that the new terms involving the simple forms of γ_{ijkl} and ζ_{ijklm} appeared to be hyper-diffusive terms that involved the mean current density, $\overline{\mathbf{J}}$. Returning to the method outlined in [74], integral forms for γ_{ijkl} and ζ_{ijklm} were obtained.

The Induction equations involving the terms in γ and ζ were once more considered in a brief scale analysis in order to determine lower limits, above which, the terms in γ and ζ would become significant when compared to the inductive and magnetic-diffusive terms. To this end, due to γ

and ζ being determined by $\mathbf{u}$, we defined the quantities $\gamma_\star$ and $\zeta_\star$ for the scale analysis, which were taken to be average values for γ and ζ that were defined through an appropriate averaging process. It was noted that the Induction equations incorporating these terms could be solved through the use of Green's method in order to obtain an analytical solution, or numerically, in order to observe the effects of these new terms on the evolution of the magnetic fields $\overline{\mathbf{B}}$ and $\mathbf{b}$. The tensors γ_{ijkl} and ζ_{ijklm} could also be analysed further using their integral forms in order to determine their structure and obtain a better idea of their effects on the mean- and small-scale magnetic fields.

The analogy between the mean EMF, $\mathcal{E}$, and the Reynolds stress tensor, $\overline{u_i u_j}$ was discussed in closing. Noting that the same averaging done for the Induction equations for $\mathbf{B}$ could be applied to the Navier-Stokes equations for $\mathbf{U}$, the averaged Navier-Stokes equations were obtained. Here, the Reynolds stress tensor, like the mean EMF, arose naturally from the averaging of the Lagrangian derivative for $\mathbf{U}$ in the Navier-Stokes equations. By assuming that the mean velocity field, $\overline{\mathbf{U}}$, is weak, it was found in [32] that the Reynolds stress tensor could also be expanded in a Taylor series, similar to that of the mean EMF, from whence the tensor α_{ijl} arose as a first-order term. It was found that the tensor, α_{ijl} behaved as the kinematic counterpart of the α-effect from MHD, and was called the AKA by the authors of [32]. We noted that many authors described that the AKA could only exist under specific conditions of the mean flow, $\overline{\mathbf{U}}$, one of them being that the mean flow itself had to be anisotropic and parity-invariant. The relevance of the AKA in astrophysical contexts was also briefly discussed, and was found that due to the presence of a magnetic field, the AKA would be suppressed, thus likely causing the AKA to be of little to no relevance in an astrophysical context.

Chapter 4

Conclusion

4.1 Final Closing Points

In this thesis we set out to study problems in the theory of Analogue Magnetism and Mean-Field Electrodynamics.

For Analogue Magnetism, we sought to explore the possibility of an analogy between a charged and non-conducting fluid by comparing the behaviour of the magnetic field, to that of the vorticity in an analogous system of equations consisting of the Induction equations and the vorticity evolution equations, both without the presence of source terms. Similar behaviour observed between these two quantities would serve as evidence for an analogy between the two fluids.

For Mean-Field Electrodynamics, we sought to determine integral forms for two higher-order tensors occurring in the Taylor series expansion for the mean EMF. These tensors multiplied the second- and third-order spatial derivatives of $\overline{\mathbf{B}}$ in the aforementioned expansion, and were called γ_{ijkl} and ζ_{ijklm}. Assuming simple forms for these tensors, we wished to re-derive Ohm's law and the Induction equations for $\overline{\mathbf{B}}$ and $\mathbf{b}$ in order to determine what effect these new tensors' terms would have on the evolution of the two magnetic fields. Using a scale analysis, we wished to determine what the lower limits were on the new terms in comparison to the inductive and magnetic-diffusive terms, above which, the new terms would become comparable to the inductive

and magnetic-diffusive terms. Lastly, we wished to discuss the analogy between the mean EMF and the Reynolds stress tensor from Fluid Dynamics.

Note that notation presented in each of the following sections pertains to the notation used in the relevant chapter.

4.1.1 Analogue Magnetism

After reviewing the relevant theory and determining that we wished to compare the behaviour of a conducting fluid to that of a non-conducting fluid, the analogous system consisting of the Induction equations for a conducting fluid and the vorticity evolution equations for a non-conducting fluid, both without source terms was stated. We noted that in the analyses that were to follow were different from what is normally considered in literature, where instead the vorticity of the conducting fluid is often compared to the magnetic field of the same conducting fluid when the analogy between the magnetic field and vorticity is studied.

Since the Induction and vorticity evolution equations appeared to be structurally-similar, we expected that we should be able to see similar behaviour between the magnetic and vorticity field, thus implying an analogy between the charged and non-charged fluids. The analogous system was simulated using the PENCIL CODE.

Similar behaviour between $\mathbf{B}$ and $\boldsymbol{\omega}$ was observed for the hydrodynamical case of $\nu_{\mathrm{VF}} = \eta = 10^{-2}$, where $\nu_{\mathrm{VF}} = 10^{-2}$ was the viscosity of the non-conducting fluid corresponding to water at 20°C, giving evidence of an analogy between the charged and non-charged fluids at this value of the parameters. Plotting B_{rms} versus ω_{rms} produced a straight line relationship. The result was expected due to the structural similarity between the evolution equations for $\mathbf{B}$ and $\boldsymbol{\omega}$, as well as for the fact that $\nu_{\mathrm{VF}} = \eta$.

For the cases of $\nu_{\mathrm{VF}} \neq \eta$, similar behaviour between $\mathbf{B}$ and $\boldsymbol{\omega}$ was no longer observed due to the plots of B_{rms} versus ω_{rms} becoming curves instead of straight lines. This implied that there was no analogy between the charged and non-charged fluids for values of $\nu_{\mathrm{VF}} \neq \eta$. Once more, this result was expected due to the diffusive terms in the Induction and vorticity evolution equations operating at different rates.

Source terms were then introduced into the analogous system and simulations were performed once more. No fields were grown from zero initial conditions – in call cases, as before, seed fields of small magnitude were used. As before, pairs of $\nu_{\rm VF} \neq \eta$ and $\nu_{\rm VF} = \eta$ were simulated and B_{rms} versus ω_{rms} plotted. For the case of $\nu_{\rm VF} \neq \eta$, the plots reflecting B_{rms} versus ω_{rms} were again not straight lines, being curves instead. Once more, this result was expected due to the diffusive terms in the both evolution equations operating at different rates. The curved-line plots for B_{rms} versus ω_{rms} persisted even for $\nu_{\rm VF} = \eta < 10^{-6}$. For values of $\nu_{\rm VF} = \eta \geq 10^{-6}$, the plots for B_{rms} versus ω_{rms} displayed straight lines once more, suggesting that similar behaviour between $\mathbf{B}$ and $\boldsymbol{\omega}$, and hence an analogy between the charged and non-charged fluids, could be obtained for high values of dissipation.

Finally, evidence of a battery-aided dynamo was also observed on examining growths of $B_{rms,123}$ and $B_{rms,12}$ against time, corresponding to the B_{rms} produced by the Induction equations with and without a source term respectively, for the case of $\nu_{\rm VF} = \eta = 10^{-10}$. This case was initially investigated due to the display of a curved-line relationship for B_{rms} versus ω_{rms}.

After determining that the curved-line relationship observed for B_{rms} versus ω_{rms} was not due to any systemic effects within the code, $B_{rms,123}$ and $B_{rms,12}$ were both plotted against time for $\nu_{\rm VF} = \eta = 10^{-10}$ in order to determine whether the Induction equations with the source term present produced a stronger magnetic field than those without it present. It was found initially that $B_{rms,123} > B_{rms,12}$, implying the operation of a battery-aided dynamo, which would be an amendment to the standard dynamo theory. The reason for $B_{rms,123} > B_{rms,12}$ was due to the changing velocity field in both equations causing the strengths of both fields to be amplified through the standard dynamo effect, however, the presence of the source term also made a positive contribution to $B_{rms,123}$, thus helping it to grow faster. This effect did not last for long, however, as the rate of the growth of $B_{rms,12}$ soon increased, causing $B_{rms,12} > B_{rms,123}$ for the remainder of the run. It was reasoned that this change in strength was due to the contribution from the battery term remaining constant in time and not being big enough to counteract the losses due to the presence of the pressure term in the Navier-Stokes equations, which feed into the induction term through the changing velocity. Due to this, the field $B_{rms,12}$ grew stronger than the field $B_{rms,123}$, and also experiencing a bigger growth rate for the remainder of the run.

4.1.2 Mean-Field Electrodynamics

The Taylor expansion of the mean EMF was considered and taken up to the second and third order, introducing two new tensors, γ_{ijkl} and ζ_{ijklm}, in addition to the usual tensors α_{ij} and β_{ijk} which are usually only considered in the expansion. Writing the mean EMF as the product of an undetermined kernel, $K_{ij}(\mathbf{x}, t; \boldsymbol{\xi}, \tau)$, and the mean magnetic field, $B_j\mathbf{x}, t$ using Green's method, integral expressions for the tensors γ_{ijkl} and ζ_{ijklm} were written down. Assuming that these new tensors were isotropic and homogeneous permitted them to be rewritten as a scalar multiple of the Levi-Civita symbol: $\gamma_{ijkl} = \gamma\varepsilon ijkl$ and $\zeta_{ijklm} = \zeta\varepsilon_{ijklm}$. Ohm's law and the Induction equations for $\overline{\mathbf{B}}$ and $\mathbf{b}$ including these new terms were re-derived and their effects on the evolution of the magnetic fields were examined. In the simple forms $\gamma_{ijkl} = \gamma\varepsilon ijkl$ and $\zeta_{ijklm} = \zeta\varepsilon_{ijklm}$, the terms in γ and ζ in the Induction equations appeared to describe a hyper-diffusion in terms of the mean current density, $\overline{\mathbf{J}}$. A scale analysis was performed on the Induction equations for $\overline{\mathbf{B}}$ and $\mathbf{b}$ in order to determine lower limits on average values of γ and ζ, $\gamma_\star$ and $\zeta_\star$, new hyper-diffusive terms in γ and ζ would become comparable to the inductive and magnetic-diffusive terms in the respective Induction equations for $\overline{\mathbf{B}}$ and $\mathbf{b}$. The use of Green's method was also briefly discussed in obtaining a solution to the Induction equations for $\overline{\mathbf{B}}$ and $\mathbf{b}$ that incorporated the new terms. By writing the Induction equations for $\overline{\mathbf{B}}$ and $\mathbf{b}$ as equal to the new terms in γ and ζ, we argued that a solution could be obtained using the Green's method to obtain a solution for the "homogeneous" versions of the respective Induction equations (i.e. the equations only involving terms up to possibly those given by the presence of α_{ij} and β_{ijk} in the mean EMF expansion), and then adding to that the particular solution taking into account the new "source terms" involving γ and ζ.

In order to properly determine their effects on the evolution of the magnetic fields, we noted that analytical forms for γ_{ijkl} and ζ_{ijklm} would be required. Using the FOSA to eliminate the non-linear term in the Induction equations for $\mathbf{b}$, an integral solution was written down for these equations using Green's method. By calculating the mean EMF as $\mathcal{E}_i = \varepsilon_{ijk}\overline{\mathbf{u} \times \mathbf{b}}$ and substituting the integral expression obtained for $\mathbf{b}$, an expression for the previously-unknown kernel, $K_{ij}(\mathbf{x}, t; \boldsymbol{\xi}, \tau)$ described before was found, allowing us to at last write down the functional forms for γ_{ijkl} and ζ_{ijklm} as an integral expression with a known kernel. In order to further obtain functional forms for γ_{ijkl} and ζ_{ijklm}, we noted that these integrals would have to be solved, given information about the fluctuating velocity field, $\mathbf{u}$.

In closing, we discussed briefly the possibility of applying the theory of analogues in order to better study the Reynolds stress tensor, as it is known to be the fluid analogue of the mean EMF studied in this chapter. We noted that a kinetic α-effect, called the anisotropic kinetic alpha effect, was known to exist under specific conditions on the properties of the mean velocity field, $\overline{\mathbf{U}}$, and was found to be analogous to the MHD α-effect. Brief mention was made on the possibility of studying a conducting fluid with similar properties to a non-conducting fluid in which the AKA is known to exist in order to determine whether the AKA could exist under more conditions and if, like the MHD β-effect, higher-order effects could possibly be found from the Reynolds stress tensor. It was noted in closing that a study of this analogy would require further simulation work to be done.

4.2 Extensions to Future Work

The fields of Analogue Magnetism and MFEM and Mean-field MHD remain open for further study.

As noted in our study of Analogue Magnetism, fluids can exhibit different behaviours and kinetic viscosities at different temperatures. Thus, the effects of temperature, and thus entropy, need also be considered in the study of finding an analogue between charged and non-charged fluids. Study in this area would require further simulations of the charged and non-charged fluids, and can further aid in studying magnetic fields in extreme or inaccessible environments such as within the interiors of stars or those present in plasma jets observed in active galactic nuclei, as well as the magnetic fields present within large-scale cosmological structures at high redshifts.

Where source terms are present in the analogous system that was studied, further simulation may also be done on generating the magnetic and vorticity fields from zero initial conditions. This would involve the addition of numerical forcing into the system, which would correspond to the addition of energy into a given physical system. With the addition of numerical forcing, any phenomena observed in the behaviours of the magnetic and vorticity fields would need to be studied carefully so as to ascertain that what is observed is physical behaviour, and not simply due to the presence of a numerical forcing term. We note that this too could lead to a study of the non-linear dynamics of the analogous system in the sense of the study of dynamical systems. It

should also be noted that different types of forcing terms would also introduce different types of dynamics into the system. Thus, before attempting to study any similar behaviour between the charged and non-charged fluids, a thorough study of the effects of the forcing term in the system would need to be conducted first.

In this work, we also introduced two higher-order tensors in the Taylor expansion of the mean EMF. It was noted that the integral forms given for these terms can be further solved, depending on the given fluctuating, turbulent velocity field, in order to determine functional forms for these tensors. The forms for these tensors were obtained using the FOSA of the evolution equations for the fluctuating magnetic field. Thus, other approximations discussed in literature such as the minimal-τ approximation can also be used in order to determine forms for these higher-order tensors from the mean EMF [24, 74, 78]. These higher-order tensors can also be studied using MHD simulation, and functional forms can be determined this way too. These would involve using techniques such as the test-field method, which involves calculating the mean EMF after applying a series of test fields that have different directions and different directions as is outlined in [24, 75, 78, 91].

Due to the known analogue between the Reynolds stress tensor and mean EMF, as well as the analogue between the anisotropic kinetic alpha effect and the MHD α-effect, further study and simulation can also be done in order to determine whether the higher-order effects, such as the MHD β-effect, could also be observed in non-charged fluids and, if so, under what conditions these effects would exist. The conditions for such higher-order effects from the Reynolds stress tensor would have to be determined analytically first, and then confirmed through the use of computer simulation. In this way, it would also be possible to use charged fluids to study the behaviour of non-charged fluids in the context of turbulence, where mean- and fluctuating fields are important.

4.3 Acknowledgements

I firstly wish to acknowledge my supervisor, Dr Bob Osano, for his unfailing support, advice and patience with me for the duration of my doctoral studies – I could not have asked for a better mentor. I would also like to acknowledge the funding support, in the form of scholarships, from

the National Research Foundation (NRF) of South Africa, as well as the University of Cape Town, all administered by the Postgraduate Funding Office of the University of Cape Town.

★

Bibliography

[1] ABRAMENKO, V. I., CARBONE, V., YURCHYSHYN, V., GOODE, P. R., STEIN, R. F., LEPRETI, F., CAPPARELLI, V., AND VECCHIO, A. Turbulent Diffusion in the Photosphere as Derived from Photospheric Bright Point Motion. *The Astrophysical Journal* (2011).

[2] ABRAMENKO, V. I., AND LONGCOPE, D. W. Distribution of the Magnetic Flux in Elements of the Magnetic Field in Active Regions. *The Astrophysical Journal* (2005).

[3] AHARONOV, Y., AND BOHM, D. Significance of Electromagnetic Potentials in the Quantum Theory. *Physical Review* (1959).

[4] AMARI, T., LUCIANI, J.-F., AND ALY, J.-J. Small-scale dynamo magnetism as the driver for heating the solar atmosphere. *Nature* (2015).

[5] ARBAB, A. I. The analogy between electromagnetism and hydrodynamics. *Physics Essays 24* (2011), 254.

[6] BABCOCK, H. W. The Topology of the Sun's Magnetic Field and the 22-Year Cycle. *The Astrophysical Journal 133* (1961).

[7] BAO, S. D., ZHANG, H. Q., AI, G. X., AND ZHANG, M. A survey of flares and current helicity in active regions. *Astronomy and Astrophysics, Supplement* (1999).

[8] BATCHELOR, G. K. On the Spontaneous Magnetic Field in a Conducting Liquid in Turbulent Motion. *Proceedings of the Royal Society of London Series A* (1950).

[9] BENÍTEZ-LLAMBAY, P., AND MASSET, F. S. FARGO3D: A New GPU-oriented MHD Code. *The Astrophysical Journal Supplement* (2016).

[10] BHAT, P., SUBRAMANIAN, K., AND BRANDENBURG, A. A unified large/small-scale dynamo in helical turbulence. *Monthly Notices of the Royal Astronomical Society* (2016).

[11] BHATTACHARJEE, A., AND YUAN, Y. Self-Consistency Constraints on the Dynamo Mechanism. *The Astrophysical Journal* (1995).

[12] BIERMANN, L. Über den Ursprung der Magnetfelder auf Sternen und im interstellaren Raum. *Zeitschrift Naturforschung Teil A 5* (1950).

[13] BISKAMP, D. *Nonlinear Magnetohydrodynamics*. 1997.

[14] BORRERO, J. M., JAFARZADEH, S., SCHÜSSLER, M., AND SOLANKI, S. K. Solar Magnetoconvection and Small-Scale Dynamo - Recent Developments in Observation and Simulation. *Space Science Reviews* (2015).

[15] BRANDENBURG, A. *Computational Aspects of Astrophysical MHD and Turbulence*. 2003.

[16] BRANDENBURG, A., AND DOBLER, W. Hydromagnetic turbulence in computer simulations. *Computer Physics Communications* (2002).

[17] BRANDENBURG, A., DOBLER, W., ET AL. The Turbulent Dynamo: A Translation of a Series of Papers by F. Krause, K.-H Rädler, and M. Steenbeck. Obtained at the following URL: http://www.nordita.org/pencil-code/doc/manual.pdf, 1971.

[18] BRANDENBURG, A., ENQVIST, K., AND OLESEN, P. Large-scale magnetic fields from hydromagnetic turbulence in the very early universe. Phys. Rev. D*54* (July 1996), 1291–1300.

[19] BRANDENBURG, A., KÄPYLÄ, P. J., AND MOHAMMED, A. Non-Fickian diffusion and tau approximation from numerical turbulence. *Physics of Fluids 16* (Apr. 2004), 1020–1027.

[20] BRANDENBURG, A., RÄDLER, K.-H., AND SCHRINNER, M. Scale dependence of alpha effect and turbulent diffusivity. A&A*482* (May 2008), 739–746.

[21] BRANDENBURG, A., AND REKOWSKI, B. V. Astrophysical significance of the anisotropic kinetic alpha effect. *Astronomy and Astrophysics* (2001).

[22] BRANDENBURG, A., SCHOBER, J., AND ROGACHEVSKII, I. The contribution of kinetic helicity to turbulent magnetic diffusivity. *ArXiv e-prints* (June 2017).

[23] BRANDENBURG, A., SOKOLOFF, D., AND SUBRAMANIAN, K. Current Status of Turbulent Dynamo Theory. From Large-Scale to Small-Scale Dynamos. Space Sci. Rev. (2012).

[24] BRANDENBURG, A., AND SUBRAMANIAN, K. Astrophysical Magnetic Fields and Nonlinear Dynamo Theory. *Physics Reports 417* (2005).

[25] BROWN, M. R., CANFIELD, R. C., AND PEVTSOV, A. A. Magnetic Helicity in Space and Laboratory Plasmas. *Washington DC American Geophysical Union Geophysical Monograph Series 111* (1999).

[26] CONTOPOULOS, I., KAZANAS, D., AND CHRISTODOULOU, D. M. The Cosmic Battery Revisited. *The Astrophysical Journal 652* (2006). arXiv:astro-ph/0608701.

[27] COOK, R. J., FEARN, H., AND MILONNI, P. W. Fizeau's experiment and the Aharonov-Bohm effect. *American Journal of Physics* (1995).

[28] DEVLEN, E., BRANDENBURG, A., AND MITRA, D. A mean field dynamo from negative eddy diffusivity. MNRAS*432* (June 2013), 1651–1657.

[29] DOMBRE, T., FRISCH, U., HENON, M., GREENE, J. M., AND SOWARD, A. M. Chaotic streamlines in the ABC flows. *Journal of Fluid Mechanics* (1986).

[30] D'SILVA, S., AND CHOUDHURI, A. R. A theoretical model for tilts of bipolar magnetic regions. *Astronomy and Astrophysics* (1993).

[31] FRISCH, U. *Turbulence. The legacy of A. N. Kolmogorov.* 1995.

[32] FRISCH, U., SHE, Z. S., AND SULEM, P. L. Large-scale flow driven by the anisotropic kinetic alpha effect. *Physica D Nonlinear Phenomena* (1987).

[33] GALANTI, B., AND SULEM, P.-L. Inverse cascades in three-dimensional anisotropic flows lacking parity invariance. *Physics of Fluids* (1991).

[34] GALLOWAY, D. J., AND WEISS, N. O. Convection and magnetic fields in stars. *The Astrophysical Journal* (1981).

[35] GOEDBLOED, J. P., AND POEDTS, S. *Principles of Magnetohydrodynamics, with Applications to Laboratory and Astrophysical Plasmas*. Cambridge University Press, 2004, ch. 1-4.

[36] HALE, G. E. On the Probable Existence of a Magnetic Field in Sun-Spots. *The Astrophysical Journal* (1908).

[37] HAUGEN, N. E., BRANDENBURG, A., AND DOBLER, W. Simulations of nonhelical hydromagnetic turbulence. *Physics Review E* (2004).

[38] HAUGEN, N. E. L., BRANDENBURG, A., AND DOBLER, W. Is Nonhelical Hydromagnetic Turbulence Peaked at Small Scales? *The Astrophysical Journal Letters* (2003).

[39] HERZENBERG, A. Geomagnetic Dynamos. *Royal Society of London Philosophical Transactions Series A 250* (1958).

[40] HUBBARD, A., AND BRANDENBURG, A. Memory Effects in Turbulent Transport. ApJ*706* (Nov. 2009), 712–726.

[41] IGOR, K. A new GPU-accelerated hydrodynamical code for numerical simulation of interacting galaxies. *ArXiv e-prints* (2013).

[42] KAZANTSEV, A. P. Enhancement of a Magnetic Field by a Conducting Fluid. *Soviet Journal of Experimental and Theoretical Physics 26* (1968).

[43] KESTENER, P., CHÂTEAU, F., AND TEYSSIER, R. *Accelerating Euler Equations Numerical Solver on Graphics Processing Units*. Springer Berlin Heidelberg, Berlin, Heidelberg, 2010, pp. 281–288.

[44] KHOMENKO, G. A., MOISEEV, S. S., AND TUR, A. V. The hydrodynamical alpha-effect in a compressible medium. *Journal of Fluid Mechanics 225* (1991), 355369.

[45] KIPPENHAHN, R., AND WEIGERT, A. *Stellar Structure and Evolution*. 1990.

[46] KLEEORIN, N., AND ROGACHEVSKII, I. Growth rate of small-scale dynamo at low magnetic Prandtl numbers. *Physica Scripta* (2012).

[47] KLEEORIN, N. I., RUZMAIKIN, A. A., AND SOKOLOFF, D. D. Correlative properties of self-exciting fluctuative magnetic fields. In *Plasma Astrophysics* (1986), T. D. Guyenne and L. M. Zeleny, Eds., vol. 251 of *ESA Special Publication*.

[48] KLIAKHANDLER, I., AND SIVASHINSKY, G. Kinetic alpha effect in viscosity stratified creeping flows. *Physics of Fluids 7*, 8 (1995), 1866–1871.

[49] KOLMOGOROV, A. On degeneration (decay) of isotropic turbulence in an incompressible viscous liquid. *Akademiia Nauk SSSR Doklady 31* (1941), 538–540.

[50] KOLMOGOROV, A. The Local Structure of Turbulence in Incompressible Viscous Fluid for Very Large Reynolds' Numbers. *Akademiia Nauk SSSR Doklady 30* (1941), 301–305.

[51] KOLMOGOROV, A. N. Dissipation of Energy in Locally Isotropic Turbulence. *Akademiia Nauk SSSR Doklady* (1941).

[52] KOLMOGOROV, A. N. A refinement of previous hypotheses concerning the local structure of turbulence in a viscous incompressible fluid at high Reynolds number. *Journal of Fluid Mechanics 13* (1962), 82–85.

[53] KOLMOGOROV, A. N. Dissipation of Energy in the Locally Isotropic Turbulence. *Proceedings of the Royal Society of London Series A* (1991).

[54] KOLMOGOROV, A. N. The local structure of turbulence in incompressible viscous fluid for very large Reynolds numbers. *Proceedings of the Royal Society of London Series A* (1991).

[55] KRAUSE, F., AND RAEDLER, K.-H. *Mean-field magnetohydrodynamics and dynamo theory*. 1980.

[56] KULSRUD, R. M., CEN, R., OSTRIKER, J. P., AND RYU, D. The protogalactic origin for cosmic magnetic fields. *The Astrophysical Journal 480* (1997). arXiv:astro-ph/9607141.

[57] LANDAU, L. D., AND LIFSHITZ, E. M. *Fluid Mechanics, Second Edition: Volume 6 (Course of Theoretical Physics)*, 2 ed. Course of theoretical physics by L. D. Landau and E. M. Lifshitz, Vol. 6. Butterworth-Heinemann, 1987.

[58] LEIGHTON, R. B. A Magneto-Kinematic Model of the Solar Cycle. *The Astrophysical Journal 156* (1969).

[59] LELE, S. K. Compact Finite Difference Schemes with Spectral-like Resolution. *Journal of Computational Physics 103* (1992).

[60] LEVINA, G., MOISEEV, S. S., AND RUTKEVICH, P. B. *Hydrodynamic Alpha-Effect in a Convective System*, vol. 2 of *Advances in Fluid Mechanics*. WIT Press, 2000, ch. 4, pp. 110–161.

[61] MARMANIS, H. On the analogy between electromagnetism and turbulent hydrodynamics. *ArXiv High Energy Physics - Theory e-prints* (1996).

[62] MARMANIS, H. Analogy between the Navier-Stokes equations and Maxwell's equations: Application to turbulence. *Physics of Fluids* (1998).

[63] MARTINS, A. A. Fluidic Electrodynamics: On parallels between electromagnetic and fluidic inertia. *ArXiv e-prints* (2012).

[64] MARTINS, A. A., AND PINHEIRO, M. J. Fluidic electrodynamics: Approach to electromagnetic propulsion. *Physics of Fluids* (2009).

[65] MAXWELL, J. C. On Physical Lines of Force, Part I: The theory of molecular vortices applied to magnetic phenomena. *Philosophical Magazine and Journal of Science 21*, 139 (1861).

[66] MESTEL, L., AND ROXBURGH, I. W. On the Thermal Generation of Toroidal Magnetic Fields in Rotating Stars. *The Astrophysical Journal 136* (1962).

[67] MOFFATT, H. K. *Magnetic field generation in electrically conducting fluids*. 1978.

[68] MOISEEV, S. S., SAGDEEV, R. Z., TUR, A. V., KHOMENKO, G. A., AND IANOVSKII, V. V. Theory of the origin of large-scale structures in hydrodynamic turbulence. *Journal of Experimental and Theoretical Physics*.

[69] PARKER, E. N. Hydromagnetic Dynamo Models. *The Astrophysical Journal* (1955).

[70] PEVTSOV, A. A., CANFIELD, R. C., AND METCALF, T. R. Latitudinal variation of helicity of photospheric magnetic fields. *The Astrophysical Journal, Letters* (1995).

[71] PEVTSOV, A. A., AND LATUSHKO, S. M. Current Helicity of the Large-Scale Photospheric Magnetic Field. *The Astrophysical Journal* (2000).

[72] PONTY, Y., POLITANO, H., AND PINTON, J.-F. Simulation of Induction at Low Magnetic Prandtl Number. *Physical Review Letters* (2004).

[73] POPE, S. B. *Turbulent Flows*. 2000.

[74] RÄDLER, K.-H. The Generation of Cosmic Magnetic Fields. In *From the Sun to the Great Attractor* (2000), D. Page and J. G. Hirsch, Eds., vol. 556 of *Lecture Notes in Physics, Berlin Springer Verlag*, p. 101.

[75] RÄDLER, K.-H. Mean-field dynamos: the old concept and some recent developments. *ArXiv e-prints* (2014).

[76] RÄDLER, K.-H., AND BRANDENBURG, A. Mean-field effects in the Galloway-Proctor flow. MNRAS*393* (Feb. 2009), 113–125.

[77] RÄDLER, K.-H., BRANDENBURG, A., DEL SORDO, F., AND RHEINHARDT, M. Mean-field diffusivities in passive scalar and magnetic transport in irrotational flows. Phys. Rev. E*84*, 4 (Oct. 2011), 046321.

[78] RÄDLER, K.-H., AND RHEINHARDT, M. Mean-field electrodynamics: critical analysis of various analytical approaches to the mean electromotive force. *Geophysical and Astrophysical Fluid Dynamics* (2007).

[79] RHEINHARDT, M., AND BRANDENBURG, A. Test-field method for mean-field coefficients with MHD background. A&A*520* (Sept. 2010), A28.

[80] RHEINHARDT, M., AND BRANDENBURG, A. Modeling spatio-temporal nonlocality in mean-field dynamos. *Astronomische Nachrichten 333* (Jan. 2012), 71–77.

[81] RHEINHARDT, M., DEVLEN, E., RÄDLER, K.-H., AND BRANDENBURG, A. Mean-field dynamo action from delayed transport. MNRAS*441* (June 2014), 116–126.

[82] RICHARDSON, L. F. Weather prediction by numerical process. *Quarterly Journal of the Royal Meteorological Society 48*, 203 (1922), 282–284.

[83] ROBERTS, P. H., AND STIX, M. The Turbulent Dynamo, 1971.

[84] RUZMAIKIN, A. A., AND SOKOLOV, D. D. The magnetic field in mirror-invariant turbulence. *Pisma v Astronomicheskii Zhurnal* (1981).

[85] SCHEKOCHIHIN, A., COWLEY, S., MARON, J., AND MALYSHKIN, L. Structure of small-scale magnetic fields in the kinematic dynamo theory. *Physical Review E* (2002).

[86] SCHEKOCHIHIN, A. A., BOLDYREV, S. A., AND KULSRUD, R. M. Spectra and Growth Rates of Fluctuating Magnetic Fields in the Kinematic Dynamo Theory with Large Magnetic Prandtl Numbers. ApJ (2002).

[87] SCHEKOCHIHIN, A. A., COWLEY, S. C., MARON, J. L., AND MCWILLIAMS, J. C. Critical Magnetic Prandtl Number for Small-Scale Dynamo. *Physical Review Letters* (2004).

[88] SCHEKOCHIHIN, A. A., COWLEY, S. C., TAYLOR, S. F., MARON, J. L., AND MCWILLIAMS, J. C. Simulations of the Small-Scale Turbulent Dynamo. *The Astrophysical Journal* (2004).

[89] SCHOBER, J., SCHLEICHER, D., BOVINO, S., AND KLESSEN, R. S. Small-scale dynamo at low magnetic Prandtl numbers. *Physical Review E* (2012).

[90] SCHRINNER, M., RÄDLER, K.-H., SCHMITT, D., RHEINHARDT, M., AND CHRISTENSEN, U. Mean-field view on rotating magnetoconvection and a geodynamo model. *Astronomische Nachrichten* (2005).

[91] SCHRINNER, M., RÄDLER, K.-H., SCHMITT, D., RHEINHARDT, M., AND CHRISTENSEN, U. R. Mean-field concept and direct numerical simulations of rotating magnetoconvection and the geodynamo. *Geophysical and Astrophysical Fluid Dynamics* (2007).

[92] SEEHAFER, N. Electric current helicity in the solar atmosphere. *Solar Physics* (1990).

[93] SIEGEL, D. M. *Innovation in Maxwell's electromagnetic theory: Molecular vortices, displacement current, and light*. Cambridge University Press, 2002.

[94] SPITZER, L. *The Physics of Fully Ionized Gases*. Interscience Publishers, Inc., 1956, ch. 2.

[95] SPRUIT, H. C., AND VAN BALLEGOOIJEN, A. A. Stability of toroidal flux tubes in stars. *Astronomy and Astrophysics* (1982).

[96] STEENBECK, M., KRAUSE, F., AND RÄDLER, K.-H. Berechnung der mittleren LORENTZ-Feldstärke $\overline{\mathbf{u} \times \mathbf{b}}$ für ein elektrisch leitendes Medium in turbulenter, durch CORIOLIS-Kräfte beeinflußter Bewegung. *Zeitschrift Naturforschung Teil A* (1966).

[97] STENFLO, J. O. Global wave patterns in the sun's magnetic field. *Astrophysics and Space Science* (1988).

[98] STENFLO, J. O. Cycle patterns of the axisymmetric magnetic field. In *NATO Advanced Science Institutes (ASI) Series C* (1994), R. J. Rutten and C. J. Schrijver, Eds., vol. 433 of *NATO Advanced Science Institutes (ASI) Series C*, p. 365.

[99] STONE, J. M., MIHALAS, D., AND NORMAN, M. L. ZEUS-2D: A radiation magnetohydrodynamics code for astrophysical flows in two space dimensions. III - The radiation hydrodynamic algorithms and tests. *The Astrophysical Journal Supplement* (1992).

[100] STONE, J. M., AND NORMAN, M. L. ZEUS-2D: A radiation magnetohydrodynamics code for astrophysical flows in two space dimensions. I - The hydrodynamic algorithms and tests. *The Astrophysical Journal Supplement* (1992).

[101] STONE, J. M., AND NORMAN, M. L. ZEUS-2D: A Radiation Magnetohydrodynamics Code for Astrophysical Flows in Two Space Dimensions. II. The Magnetohydrodynamic Algorithms and Tests. *The Astrophysical Journal Supplement* (1992).

[102] SUBRAMANIAN, K. Dynamics of fluctuating magnetic fields in turbulent dynamos incorporating ambipolar drifts. *ArXiv Astrophysics e-prints* (1997).

[103] SUBRAMANIAN, K. Can the turbulent galactic dynamo generate large-scale magnetic fields? MNRAS (1998).

[104] SUBRAMANIAN, K. Hyperdiffusion in Nonlinear Large- and Small-Scale Turbulent Dynamos. *Physical Review Letters* (2003).

[105] SUBRAMANIAN, K. Magnetizing the universe. *ArXiv e-prints* (2008).

[106] SUBRAMANIAN, K. The origin, evolution and signatures of primordial magnetic fields. *Reports on Progress in Physics* (2016).

[107] SUBRAMANIAN, K., AND BRANDENBURG, A. Traces of large-scale dynamo action in the kinematic stage. *Monthly Notices of the Royal Astronomical Society 445*, 3 (2014), 2930.

[108] SUBRAMANIAN, K., NARASIMHA, D., AND CHITRE, S. M. Thermal generation of cosmological seed magnetic fields in ionization fronts. *Monthly Notices of the Royal Astronomical Society* (1994).

[109] SULEM, P. L., SHE, Z. S., SCHOLL, H., AND FRISCH, U. Generation of Large-Scale Structures in Three-Dimensional Flows Lacking Parity Invariance. *Journal of Fluid Mechanics 205* (1989).

[110] SUR, S., BRANDENBURG, A., AND SUBRAMANIAN, K. Kinematic α-effect in isotropic turbulence simulations. *Monthly Notices of the Royal Astronomical Society* (2008).

[111] TEYSSIER, R. Cosmological hydrodynamics with adaptive mesh refinement. A new high resolution code called RAMSES. *Astronomy and Astrophysics* (2002).

[112] VAINSHTEIN, S. I., AND ZEL'DOVICH, YA. B. Origin of Magnetic Fields in Astrophysics (Turbulent "Dynamo" Mechanisms). *Physics-Uspekhi 15*, 2 (1972).

[113] WIDROW, L. M. Origin of Galactic and Extragalactic Magnetic Fields. *Reviews of Modern Physics 74* (2002). arXiv:astro-ph/0207240.

[114] WILLIAMSON, J. H. Low-Storage Runge-Kutta Schemes. *Journal of Computational Physics 35* (1980).

List of Figures

List of Tables